THE UNIVERSITY OF MICHIGAN
COLLEGE OF LITERATURE, SCIENCE, AND THE ARTS
Department of Physics

Technical Report

SELF-INTERACTION OF ACOUSTIC WAVES IN CADMIUM SULFIDE

John H. Gibson

ORA Project 04941

under contract with:

U. S. ATOMIC ENERGY COMMISSION
CHICAGO OPERATIONS OFFICE
CONTRACT NO. AT(11-1)-1112
ARGONNE, ILLINOIS

administered through:

OFFICE OF RESEARCH ADMINISTRATION ANN ARBOR

May 1968

ACKNOWLEDGMENTS

I wish to express my sincere gratitude and appreciation to Professor Gabriel Weinreich for his interest, guidance, and constant encouragement during the course of the experiment.

I am deeply indebted to Dr. Victor E. Henrich for his help with all aspects of the problem and for many favors, without which the experiment would not have been possible. I wish also to thank Dr. William H. Wing for many interesting discussions on electronics and experimental technique.

Thanks are also due Dr. Benjamin Tell for providing the cadium sulfide crystal used in the experiment.

The partial support of this research by the United States Atomic Energy Commission under Contract No. AT(11-1)-1112 is gratefully acknowledged.

TABLE OF CONTENTS

TABLE OF CONTENTS (Concluded)

LIST OF FIGURES

LIST OF FIGURES (Continued)

LIST OF FIGURES (Concluded)

ABSTRACT

In a piezoelectric crystal acoustic waves of certain modes and propagation directions are accompanied by electric fields. If the crystal also contains free electrons, and if there is a sink (for example, the lattice) to which they may dump their energy, then the electric fields will do work on the electrons, thereby dissipating the energy of the wave. As the wave surrenders its energy to the electrons, so must it also give up its momentum to the same absorber. The result is the production of a direct current along the wave propagation vector. This acoustoelectric current is a primary source of information on local electronic conditions encountered by the wave. For example, conservation of momentum for the interaction requires that the current be proportional to the rate of dissipation of energy from the wave (the Weinreich relation), so the acoustoelectric current pulse produced as a short acoustic wave packet traverses the crystal gives directly the acoustic dissipation rate at each instant of time during the trip, a result not obtainable by observation of the transmitted sound alone.

This thesis reports a study of the acoustoelectric self-interaction of a 30 Mc ultrasonic wave packet propagating in a cadmium sulfide single crystal. This self-interaction results from the fact that the acoustic attenuation rate may be modified by imparting a drift velocity to the electrons, and such a drift velocity is in turn produced by the acoustoelectric current resulting from acoustic attenuation. The effect of the self-interaction may be computed by substituting the acoustoelectric current for the drift current in the small-signal theory. We have done this in order to compute the influence of the self-interaction on the detailed shape of the acoustoelectric current pulses generated as short acoustic wave packets traverse the crystal. These predicted pulses have been compared directly with experimental results. Upon comparison it is seen that the observed effect of the self-interaction is larger than the computed effect, and the predictions are more accurate at high crystal resistivity than at low. This is in part explained as a failure of the calculation to account for the influence of the second harmonic component of the acoustoelectric current on the local attenuation rate.

INTRODUCTION

The acoustoelectric effect is a wave-particle drag phenomenon and refers specifically to the appearance of a direct current along the direction of propagation of a decaying acoustic wave in a medium containing mobile charge carriers. The effect occurs whenever there is a possibility of energy and momentum exchange between the wave and the charges, providing there exists a sink (such as the crystal lattice) to which the charges may dump their energy. The interaction causes the charges to drain energy and momentum from the wave, and the absorbed momentum propels them in the direction of the wave propagation vector. The result is attenuation of the wave accompanied by a direct current along its direction of propagation.

In 1956 Weinreich[1] published a definitive theoretical treatment of the acoustoelectric effect in a semiconductor in which both holes and electrons are simultaneously involved. About a year later Weinreich and White[2] detected a weak acoustoelectric effect in n-type germanium, and in 1959 Weinreich, Sanders, and White[3] reported they had used the acoustoelectric effect to measure the intervalley scattering rate of electrons in arsenic-doped germanium.

In 1960 cadmium sulfide was discovered to be more strongly piezoelectric then quartz.[4] This property, in combination with the crystal's easily-controlled and wide-ranging photoconductivity, made it an ideal material for the further investigation of electronically induced acoustic attenuation, and a thorough theoretical treatment of this possibility was published in 1962 by Hutson and

White.[5] This theory is based on a small-signal analysis of the electron-wave interaction derived from the piezoelectric equations of state for a conducting medium.

Weinreich had proven in 1956 that, by application of a dc electric field along the direction of propagation, it should be possible to use the acousto-electric interaction to achieve traveling wave amplification of sound.[1] In 1961 this was attempted in CdS by Hutson, McFee, and White.[6] They succeeded in demonstrating acoustic amplification, and this phenomenon[7-9] and the related effect of current saturation[10-12] have received the lion's share of attention on the subject ever since. Reference 9 contains an extensive bibliography of recent work on these effects.

The study of the less glamorous basic acoustoelectric effect in CdS in the absence of an applied electric field has consequently been neglected, even though it offers much in the way of experimental simplification. Nonamplifying experiments do not require the fast rise time, high voltage apparatus needed for amplification work,[6,12] and they avoid the instabilities and current saturation effects[6,10-12] which have come to be associated with CdS under amplifying conditions. That there is a wealth of information to be had from nonamplifying experiments was demonstrated by Henrich,[13] when he analyzed acoustoelectric current pulse shapes to verify the attenuation predictions of the small-signal theory of Hutson and White and also to compute electron trapping parameters in several CdS samples.

The work presented here is also based on an experimental study of cadmium sulfide under nonamplifying conditions. It is primarily concerned with large-

signal acoustoelectric effects in CdS, the analysis of which falls outside the immediate province of the small-signal theory of Hutson and White, but which nonetheless may be treated by perturbation calculations on that theory. By this approach we shall show that under large-signal conditions the propagating acoustic wave interacts with itself, and that it is possible to make computer-calculated predictions of the acoustoelectric currents generated by acoustic waves of large (but not too large) amplitude.

CHAPTER I

ACOUSTOELECTRIC CURRENT WAVEFORMS

We shall begin this chapter by presenting the basic experimental evidence for the acoustoelectric effect in cadmium sulfide, placing particular emphasis on the shape of the observed acoustoelectric current waveforms. We shall then introduce the Weinreich relation,[14] the fundamental energy-momentum conservation relation which underlies all acoustoelectric phenomena, and use this relation to explain and predict the detailed shape of the current waveforms. This approach is possible because much of what we observe in CdS is true of any acoustoelectric interaction and is unaffected by details of the electron-wave coupling for a particular material or a special experimental situation.

1.1 THE OBSERVED ACOUSTOELECTRIC EFFECT

Consider the experimental arrangement pictured in Figs. 1 and 2. A cadmium sulfide crystal, cut as a cube 7 mm on a side, is clamped between two pieces of fused silica. These fused silica pieces are called "buffers" (their function will be explained in Chapter IV), and each is a cylinder 1/2 in. in diameter and 1 in. long. Quartz transducers, cut for half-wave resonance at 30 Mc, are attached to the outside circular faces of these buffers, and all of these elements are solidly cemented together to form an acoustic assembly. If we electrically excite one of these transducers with a brief burst of 30 Mc rf, the acoustic wave generated will propagate through the assembly and be detected at the opposite transducer. Shear waves for example will traverse this system in about 17 μsec.

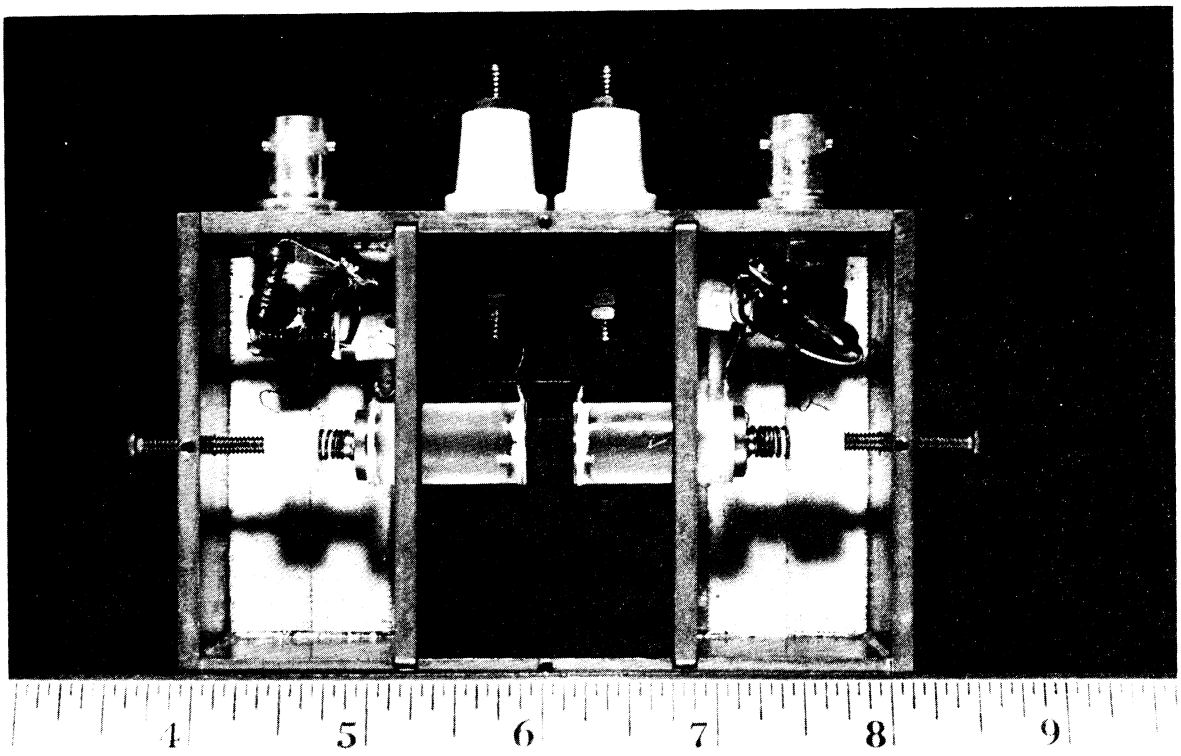

Fig. 1. Photograph of the acoustic assembly in the sample holder.

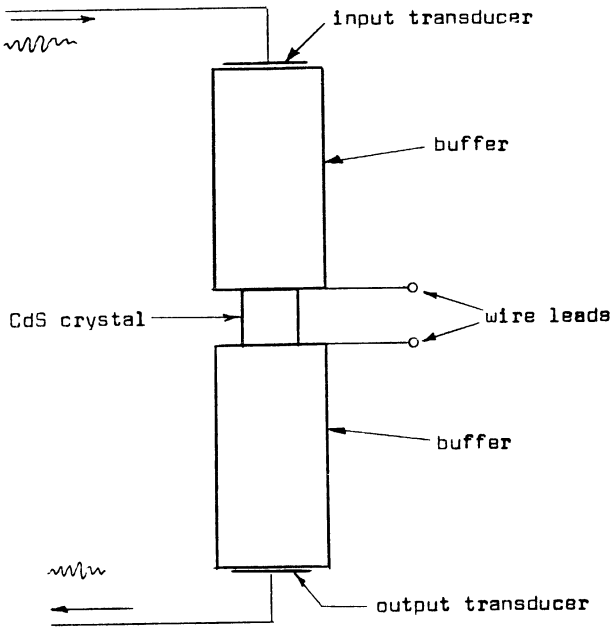

Fig. 2. Diagram of the acoustic assembly.

We said in the introduction that cadmium sulfide is both piezoelectric and photoconductive. The acoustoelectric effect in CdS is a consequence of the interaction between the piezoelectric fields accompanying a propagating acoustic wave and the photoconduction electrons in the crystal. We therefore choose a crystal orientation in the acoustic assembly which causes the acoustic wave to be accompanied by strong piezoelectric fields. In Chapter II we shall show that it is impossible to have strong transverse piezoelectric fields accompany a propagating acoustic plane wave. We are therefore limited to crystal orientations and acoustic modes which together generate strong longitudinal piezoelectric fields.

In the system thus far described an acoustic wave packet will propagate through all elements of the assembly, suffering some attenuation or reflection at the bonded interfaces between components of the system, but experiencing negligible losses in either the buffers or the CdS crystal—providing the crystal is kept in the dark. But if we now illuminate the crystal, we will discover that it is possible to cause the propagating acoustic wave to be strongly attenuated, the severity of the attenuation being a function of the light intensity and varying from a maximum greater than 40 db for a certain optimum brightness to near zero in the dark.

There is a simple explanation for this phenomenon. We know the propagating wave packet is accompanied by piezoelectric fields, and we also know that the CdS crystal is an insulator in the dark but becomes a conductor when illuminated. It therefore is reasonable that the piezoelectric fields of the

traveling wave do work on the free electrons produced by the illumination, and that the energy thus dissipated by the piezoelectric fields must be drawn from the propagating acoustic wave, thus producing attenuation.

If this explanation is correct, then we may further expect to find a crystal conductivity for which the $E \cdot J$ dissipation of the photoconduction electrons is a maximum. The argument goes as follows: It is obvious that $E \cdot J$ losses must vanish in the dark when the crystal is an insulator, i.e., when $J = 0$. At the opposite extreme of very intense illumination we might look for a diminished rate of dissipation as the electric field goes to zero, short-circuited by the very high photoconductivity. In between these two extremes there must be a maximum. This prediction would be borne out by experimentation on the system we have described. We would observe a maximum acoustic attenuation in excess of 40 db at a crystal resistivity of about 6500 ohm-cm.

Let us now consider an extension of the experiment. Imagine the end faces of the CdS crystal (the faces in contact with the buffers) to be coated with a metal film to allow broad, ohmic contact to the crystal, and let these contacts be made externally accessible through wire leads (see Fig. 2). These leads might have been used to measure the crystal's photoconductivity in the preceding experiment, but they will also serve to show us another interesting phenomenon.

Suppose these wire leads are joined through a small resistor, and an oscilloscope is connected across the resistor to monitor any current which may flow in this circuit (see Fig. 3). If the CdS crystal is now illuminated and

repeated bursts of electrical excitation are supplied to the input transducer, then an oscilloscope trace of the type shown in Fig. 4 will be observed each time an acoustic wave packet traverses the crystal.

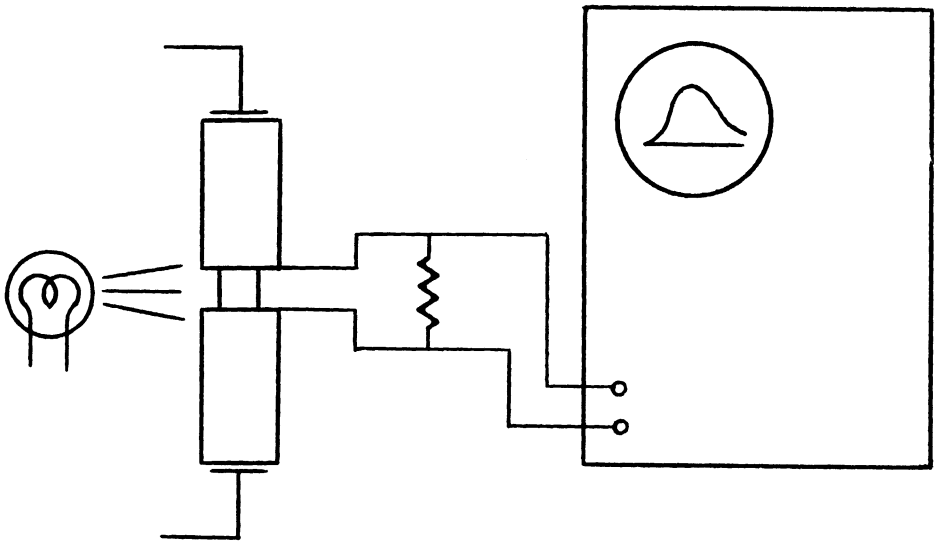

Fig. 3. Basic experimental arrangement.

This phenomenon of direct current production ("direct current" in the sense that it is slowly varying compared to the 30 Mc frequency of the acoustic wave) is called the acoustoelectric effect, and the current thus generated is called the acoustoelectric current.

Let us examine the oscilloscope trace in detail. The acoustic wave packet used was that of Fig. 5. The acoustoelectric current (Fig. 4) begins to rise just as the wave packet enters the crystal; it reaches a maximum just after the peak enters and then dies away. The oscillations which appear on the rising portion of the trace are generated as the traveling wave crosses the input face of the crystal. They will be discussed in Section 1.3.

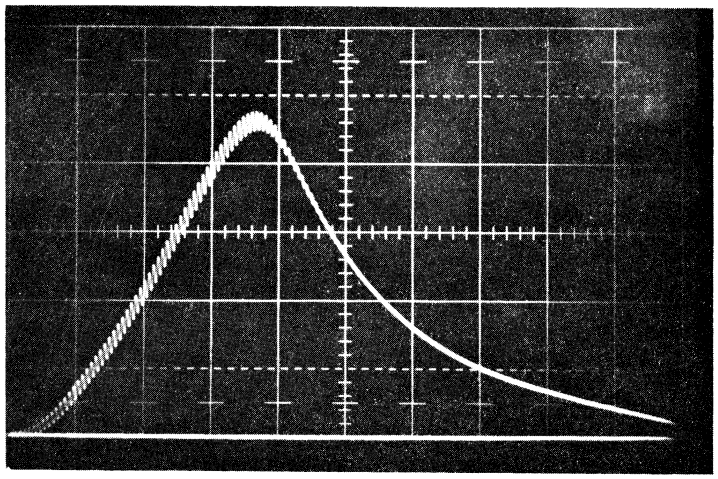

Fig. 4. Representative acoustoelectric current trace produced by the input wave of Fig. 5. The current was measured in terms of the voltage drop across an external 2000 ohm resistor. Crystal resistivity = 3.7×10^4 ohm-cm. Vertical scale = .001 v/cm. Time base = .5 μsec/cm.

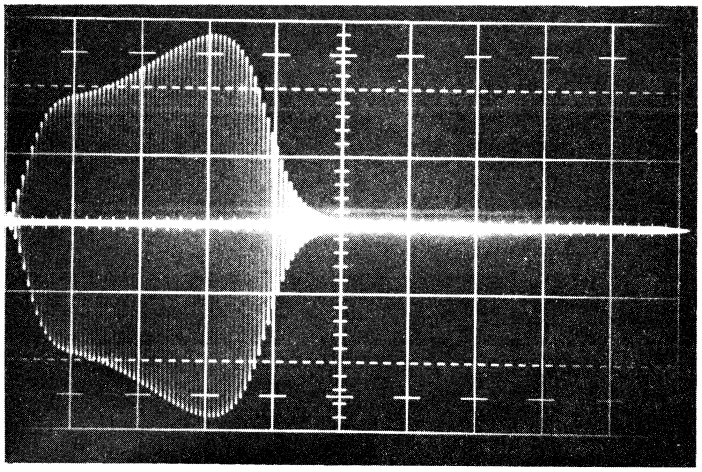

Fig. 5. 30 Mc excitation applied to the input transducer to produce the acoustoelectric current trace of Fig. 4. Time base = .5 μsec/cm.

Let us concentrate our attention upon the falling portion of the trace. The input acoustic wave had a length of 2.5 μsec, and the transit time through the 7 mm crystal is 4.0 μsec. Thus that portion of the current trace recorded between 2.5 and 4.0 μsec occurred while the wave packet was entirely within the crystal.

This portion of the trace is a falling exponential. Were we to change the amplitude of the input wave (by use of a precision attenuator so as not to change the envelope shape), we would observe the height of the current trace (but not the shape) to change in direct proportion to the square of the input acoustic amplitude, i.e., to vary as the input acoustic energy. The effect is illustrated in Fig. 6.

Study of oscilloscope traces recorded during experimentation at other photoresistivities (see Fig. 7) would further reveal that the time constant τ_e describing the exponentially falling tail of the current trace is in each case the same time constant that would be needed to predict the attenuation suffered by the acoustic wave packet in traversing the crystal; i.e., if the decaying tail of the current trace is described by

$$I = I_o e^{-t/\tau_e} \qquad (1.1)$$

and if the attenuation experienced by the acoustic wave packet is given by

$$W_{out} = W_{in} e^{-\alpha L} , \qquad (1.2)$$

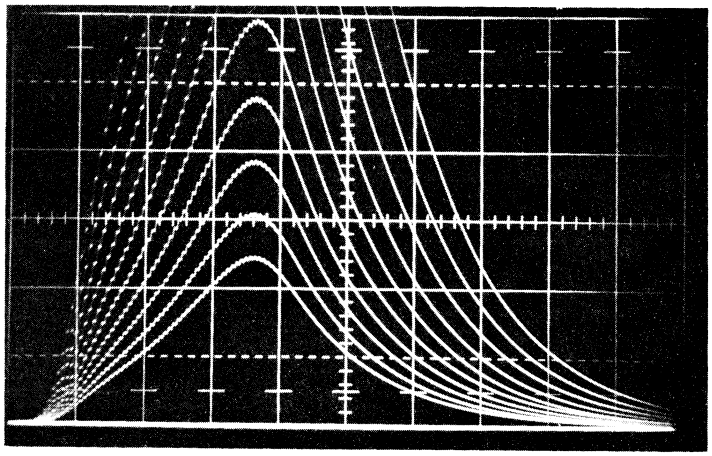

(a) Acoustoelectric current traces produced by varying the input attenuator in 1 db steps. Vertical scale = .1 v/cm.

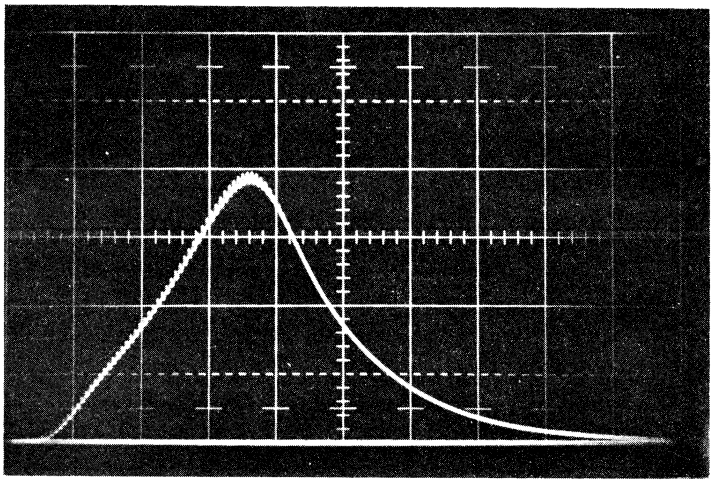

(b) Acoustoelectric current traces produced for two settings of the attenuator with compensating changes in the oscilloscope vertical sensitivity switch. The traces overlap exactly.

Attenuator	Vertical Scale
-10 db	.1 v/cm
-20 db	.01 v/cm

Fig. 6. Illustration of the linear relationship between the acoustoelectric current and the input acoustic power (at small signal levels). Input acoustic power was adjusted with a precision attenuator controlling excitation of the input transducer. Crystal resisitivity = 1.57×10^4 ohm-cm. Time base = .5 μsec/cm.

where Eq. (1.2) may be considered the defining equation for the attenuation coefficient α, then

$$1/\tau_e = \alpha v_s \quad , \tag{1.3}$$

where

W = energy density of the acoustic wave packet

L = crystal length

v_s = propagation velocity of the acoustic wave.

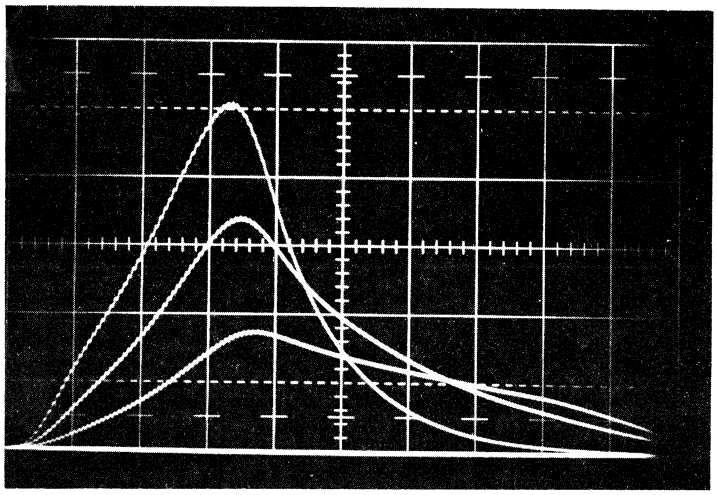

Fig. 7. Acoustoelectric current traces produced for constant input power and changing crystal resistivity. Input attenuator set at -10 db. Time base = .5 μsec/cm. Listed according to peak height, the traces are:

Trace	Crystal Resistivity	Acoustic Attenuation Rate
Top	9.5×10^3 ohm-cm	60 db/cm
Center	3.5×10^4 ohm-cm	23 db/cm
Bottom	1.1×10^5 ohm-cm	8 db/cm

The implication of these observations is that the instantaneous value of the observed acoustoelectric current is directly proportional to the energy of the acoustic wave packet which decays exponentially as it traverses the crystal. That this is indeed the case (at least for the idealized experiment we have been describing) will be shown in the section which follows.

1.2 THE WEINREICH RELATION

We have not yet studied in detail the interaction between the piezoelectric fields of the propagating acoustic wave and the photoconduction electrons in the crystal, but such information is not necessary to an understanding of the relationship between acoustic attenuation and the acoustoelectric current. This was shown by Weinreich[14] in 1957 when he proved that the energy and momentum surrendered by the decaying acoustic wave are given over entirely to driving a direct current down the crystal, with the result that the ratio of the attenuation coefficient to the current is determined entirely by wave dynamics and is independent of the detailed mechanism of the acoustoelectric interaction. (The application at that time was to the prediction of the weak acoustoelectric currents produced in multi-valley semiconductors as a consequence of the drag exerted on a traveling wave by free carriers.) The derivation goes as follows:

(1) Momentum relation for the electrons: The force on the free electrons is given by

$$dp_e/dt = -nqE \qquad (1.4)$$

where

n = density of electrons

p_e = momentum density carried by the electrons

q = absolute magnitude of the electronic charge

E = an effective acoustoelectric field acting on the electron to produce the acoustoelectric current (E is defined to be positive when it points along the propagation vector of the wave).

(2) Energy-momentum relation for waves:

$$W = v_s p_s \quad , \tag{1.5}$$

where

W = energy density carried by the wave

p_s = momentum density carried by the wave.

Therefore

$$\frac{dW}{dx} = v_s \frac{dp_s}{dx} = \frac{dp_s}{dt} \quad . \tag{1.6}$$

(3) Conservation of momentum for the interaction requires that

$$\frac{dp_s}{dt} + \frac{dp_e}{dt} = 0 \, . \tag{1.7}$$

Substitution of Eqs. (1.4) and (1.6) into Eq. (1.7) gives the Weinreich relation:

$$nqE = \frac{dW}{dx} \tag{1.8}$$

If the acoustic attenuation is describable by an attenuation coefficient, that is, if

$$- dW/dx = \alpha W ,$$

then the Weinreich relation becomes

$$E = - 1/nq \, \alpha W . \tag{1.9}$$

We would like an expression involving the acoustoelectric current density This must be given by $j = \sigma E$ or

$$j = - \alpha W \tag{1.10}$$

where μ = electron mobility in the crystal

The Weinreich relation can serve as a powerful tool for the study of acoustic attenuation in CdS. Equation (1.10) tells us that the local rate of acoustoelectric current generation is directly proportional to local acoustic energy density. If the traveling acoustic wave is well localized ($T \ll \tau_e$, where T is the length of the wave packet, and τ_e is defined by Eq. (1.3)), then Eq. (1.10) allows us to measure the energy of the wave packet at any point along its traverse of the crystal, assuming both μ and α are known.

For a wave packet which is not well localized the relationship is more complicated. In Chapter III we shall prove that the current flowing in the external circuit is given by

$$J(t) = \frac{1}{L} \int_0^L j(x,t) \, dx , \tag{1.11}$$

where L is the length of the crystal, and $j(x,t)$ is the rate of acoustoelectric current generation at each point on the wave. Equation (1.11) may also be

developed from a simple equivalent-circuit model of the crystal. Let us conceptually divide the crystal into N segments, each segment being of length $\delta x = \frac{L}{N}$. Within each segment let us represent the local rate of acoustoelectric current generation by an ideal current generator

$$j_i(t) = -\mu\alpha W_i(t) \tag{1.12}$$

working across the local crystal resistance $R = r\delta x$ as in Fig. 8.

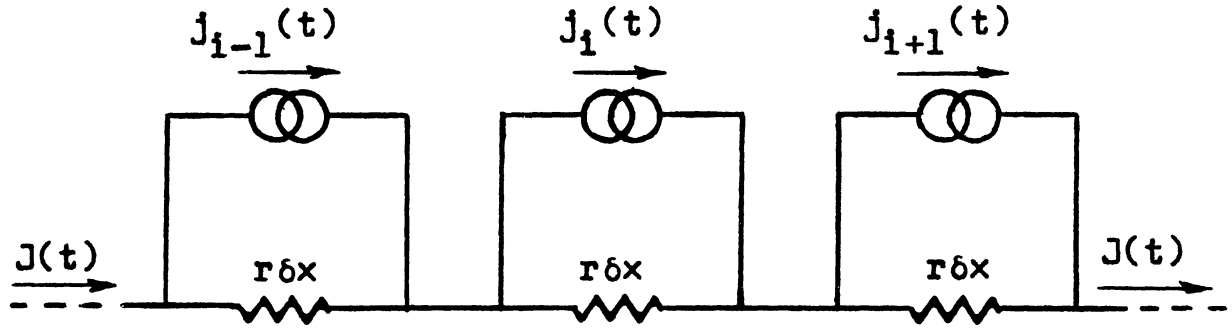

Fig. 8. Elementary equivalent circuit model of the crystal.

We should pause here to clarify our sign convention. All flow quantities (currents and velocities) are taken as positive when they point in the direction of the acoustic propagation vector. We have just shown that for acoustic attenuation produced by mobile charge carriers, the recoil of the absorber must cause

a net drift of the carriers in the direction of the wave. For negative carriers (as in CdS) conventional current flow is opposite in direction to the carrier drift, so $j(t)$ becomes a negative number as in Eq. (10). Because of our sign convention, equivalent circuit representations like that of Fig. 8 show generating elements which appear to produce a conventional current in the direction of the wave, but we must remember that it is the carrier velocity which is always with the wave, and the sign of the current carriers determines the sign of $j(t)$.

Flowing through all N crystal segments and in the external circuit is the circulating current $J(t)$. The voltage drop across the ith segment is

$$V_i = R(J - j_i) . \tag{1.13}$$

If we require as a boundary condition that the ends of the crystal be short-circuited, then we must have

$$\sum_{i=1}^{N} V_i = R(NJ - \sum_{i=1}^{N} j_i) = 0 . \tag{1.14}$$

The solution for the circulating current is therefore

$$J(t) = \frac{1}{L} \sum_{i=1}^{N} j_i(t)\, \delta x . \tag{1.15}$$

In the limit of N becoming infinite, this passes to the integral form

$$J(t) = \frac{1}{L} \int^{L} j(x,t)\, dx , \tag{1.16}$$

which is the same as Eq. (11).

Because the integration need not be carried past the leading edge of the propagating wave packet, the upper limit may be changed to $x = v_s t$ (for

$v_s t < L$). If we substitute Eq. (1.10) for $j(x,t)$, then Eq. (1.16) becomes

$$J(t) = -\mu\alpha \frac{1}{L} \int_o^{v_s t} W(x,t)\, dx \quad . \tag{1.17}$$

Within the crystal $W(x,t)$ may be expressed in terms of the acoustic energy density at the input face. For the case of uniform acoustic attenuation we have

$$W(x,t) = e^{-\alpha x} W(0,\ t - \frac{x}{v_s}) \quad , \tag{1.18}$$

so that

$$J(t) = -\mu\alpha \frac{1}{L} \int_o^{v_s t} e^{-\alpha x} W(0,\ t - \frac{x}{v_s})\, dx \quad . \tag{1.19}$$

Using Eq. (1.19) we may explicitly display the exponentially decaying character of the acoustoelectric current when the acoustic wave packet is entirely within the crystal. Let us first introduce a change of integration variables

$$t'' = t - \frac{x}{v_s} \tag{1.20}$$

with the result that

$$J(t) = -\mu\alpha v_s \frac{1}{L} e^{-\alpha v_s t} \int_o^t e^{\alpha v_s t''} W(0,t'')\, dt'' \quad . \tag{1.21}$$

This may be rewritten as

$$\frac{1}{\alpha v_s} J(t)\, e^{\alpha v_s t} = -\frac{\mu}{L} \int_o^t e^{\alpha v_s t''} W(0,t'')\, dt'' \quad .$$

If we now differentiate both sides with respect to t and then divide throughout by $e^{\alpha v_s t}$, we obtain

$$\frac{1}{\alpha v_s}\frac{dJ}{dt} + J(t) = -\frac{\mu}{L} W(0,t) \quad . \tag{1.22}$$

Now the usual specification for the input energy density will be of the form

$$\begin{aligned} W(0,t) &= A^2(t) \ , \quad t \leq T \\ &= 0 \quad , \quad t > T \ , \end{aligned} \tag{1.23}$$

where T is the length of the acoustic wave packet whose amplitude is A(t). For $t > T$ (the wave packet entirely within the crystal) the right side of Eq. (1.22) vanishes, and the remaining homogeneous equation has the solution

$$J(t) = J(T)\, e^{-\alpha v_s (t-T)} \ , \tag{1.24}$$

which is the exponentially decaying result that we sought. Equation (1.24) may be compared with Eqs. (1.1) and (1.3).

1.3 CURRENT RIPPLE DUE TO THE BOUNDARY CONDITION

The small oscillations superposed upon the larger acoustoelectric current trace (Figs. 4-7) are generated as the acoustic wave train crosses the input face of the crystal. Their frequency is the same as that of the traveling wave, and their envelope closely resembles the envelope of the traveling wave before it enters the crystal. They are <u>not</u> the result of capacitive feed-through of the excitation voltage applied to the input transducer; the 6.4 μsec transit time of the first buffer assures us of that. What they are may be understood as follows:

While inside the CdS crystal the traveling acoustic wave generates longitudinal piezoelectric fields. Local intensity of the resultant electric

fields is approximately proportional to local mechanical strain (the exact relationship will be derived in Chapter II). The net voltage available to drive a current around the external circuit may be computed by integrating this electric field over the crystal length. This voltage divided by the total circuit resistance is then the circulating current.

The input face of the crystal is one of the limits of the integration. The integral may therefore contain a fraction of a cycle at the input face plus a number of whole cycles already in the crystal. To the extent that the traveling wave is symmetric about zero we may expect the average contribution of whole cycles already inside the crystal to be small, whereas the cycle crossing the input face contributes an amount

$$V_1(t) = \int_{x=v_s t}^{x=0} E_s(x-v_s t)\, dx \quad , \tag{1.25}$$

where t is the time since the leading edge (i.e., zero) of this cycle crossed the input face. Equation (1.25) may be rewritten as

$$V_1(t) = E_1(t) \int_{x=v_s t}^{x=0} \sin k(x-v_s t)\, dx = \frac{\lambda}{2\pi} E_1(t)\,(1 - \cos \omega t) \quad , \tag{1.26}$$

where $E_1(t)$ represents the envelope of the piezoelectric field generated by the traveling wave as it crosses the input face. The current ripple is therefore given by

$$I_1(t) = \frac{\lambda}{2\pi} \frac{E_1(t)}{R} (1 - \cos \omega t) \quad , \tag{1.27}$$

where R is the total circuit resistance (crystal resistance plus the external resistor).

The observed amplitude of the current ripple is smaller than that predicted by Eq. (1.27). A possible explanation is that $I_1(t)$ is reduced because the acoustic wavefront does not arrive exactly parallel to the input face of the crystal. The probability of this occuring may be estimated by noting that for an acoustic wavelength λ = .06 mm (30 Mc shear waves in CdS) and a crystal 7 mm wide, a deviation of 0.5° could cause complete cancellation of the 30 Mc component of the circulating current. Such small deviations are unavoidable in the assembly of the acoustic system; e.g., the end faces of the buffers are only guaranteed parallel within .25°, and there is no way of measuring to such close tolerances the thickness uniformity of the bonds in the assembled acoustic system.

Thus there appears little hope for quantitative use of the 30 Mc component. For this reason no attempt was made to extend the bandwidth of the measuring equipment (described in Section 4.2) to accurately reproduce it.

1.4 THE SHAPE OF THE ACOUSTOELECTRIC CURRENT TRACE

We are now ready to predict and explain the detailed shape of the acoustoelectric current trace. We shall do this with the aid of Eq. (1.22), which may write as

$$\tau_e \frac{dJ}{dt} + J(t) = -\frac{\mu}{l} W(0,t) , \qquad (1.28)$$

where

$$\tau_e = \frac{1}{\alpha v_s} \quad . \tag{1.29}$$

The behavior of J(t) in Eq. (1.28) is most easily visualized with the help of the mathematically equivalent circuit of Fig. 9(a). In this representation the forcing function $-\frac{\mu}{L} W(0,t)$ appears as an ideal current generator working across a parallel RC circuit, J(t) is the current flowing in the resistive branch of the load, and R_e and C_a may take any value, providing they together satisfy

$$R_e C_a = \tau_e = \frac{1}{\alpha v_s} \quad . \tag{1.30}$$

R_e and C_a form a low pass filter at the output of the ideal current generator, thereby restricting the speed with which the observed current J(t) is able to follow changes in the generator current. The problem of predicting the detailed shape of the acoustoelectric current trace (produced by a uniformly attenuated acoustic wave) has therefore been reduced to the problem of analyzing the response of a simple low pass filter to the input wave $-\frac{\mu}{L} W(0,t)$.

Let us first examine the effect of the filter for the extreme cases of either very large or very small values of the attenuation coefficient. When α is very large ($\tau_e \ll T$), the influence of the filter is negligible. "Resistor" R_e effectively swamps "capacitor" C_a, and the observed current is a faithful record of the acoustic energy density at the input face of the crystal:

$$J(t) = -\frac{\mu}{L} W(0,t) \quad . \tag{1.31}$$

The peak of the observed current therefore coincides with the peak of the input wave and is independent of α. Physically this is the case where the acoustic

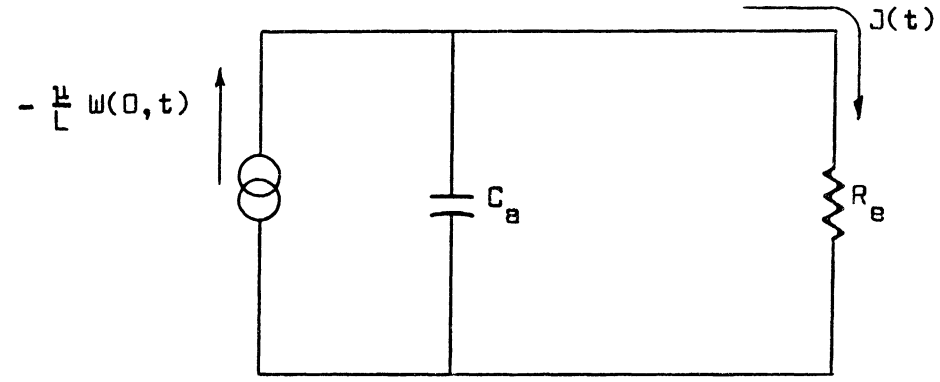

(a) Equivalent circuit representation of Eq. (1.28) showing how the acoustoelectric current trace produced by a uniformly attenuated acoustic wave may be synthesized by a constant current generator working into a low pass filter.

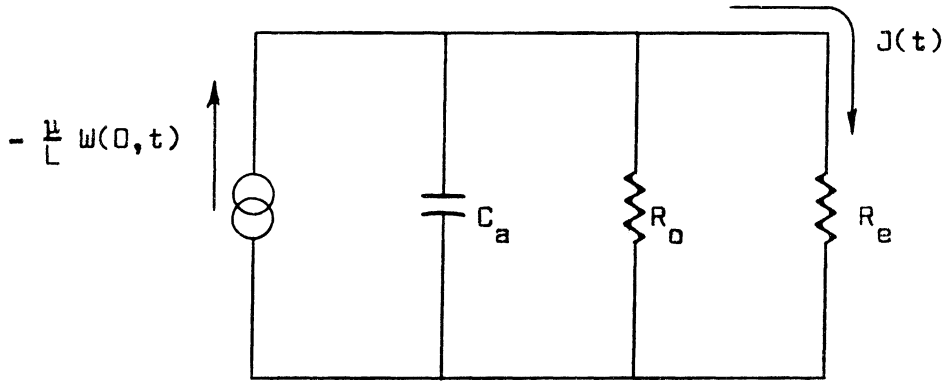

(b) Equivalent circuit representation of Eq. (1.35) showing the influence of nonelectronic losses.

Fig. 9. Equivalent circuit for synthesizing acoustoelectric waveforms generated by a uniformly attenuated acoustic wave.

attenuation is so rapid that only that part of the wave which has just crossed the input face has enough energy to contribute significantly to the circulating current J(t), i.e., the crystal has an acoustic skin depth of $1/\alpha$.

When α is very small ($\tau_e \gg T$), the response of the filter is sluggish compared to the duration of the wave, and the output of the current generator goes wholly into charging C_a. C_a integrates the generator output, and the "leakage current" through R_e is

$$J(t) = \frac{1}{\tau} \int_o^t [-\frac{\mu}{L} W(0,t")] \, dt", \quad t < T . \tag{1.32}$$

The observed current therefore rises for as long as the wave crosses the input face of the crystal. Thus we see that J(t) maximum occurs at t = T and is proportional to α. Physically this is the case where the attenuation is so slow that all portions of the wave inside the crystal are essentially undiminished and contribute accordingly to the circulating current. We therefore expect to see the observed current rise for as long as we inject acoustic energy into the system.

Before discussing intermediate cases we wish to add one more observation. From the representation of Fig. 9(a), it appears that the entire output of the ideal current generator must eventually flow through R_e, i.e., for a given input wave the integrated area under all possible acoustoelectric current traces must be the same, regardless of the filter time constant:

$$\int_o^\infty J(t) \, dt = \int_o^T [-\frac{\mu}{L} W(0,t)] \, dt \tag{1.33}$$

This useful identity helps us maintain some perspective on the relative heights of the acoustoelectric current traces generated for different values of the attenuation coefficient. Of course the left-hand integration (over the time to infinity) can have no physical meaning for a real crystal, since the circuit representation of Fig. 9(a) ceases to be valid as soon as the wave reaches the opposite crystal face (see Eq. (1.17)), where it either propagates out of the crystal, suffers reflection, or experiences some combination of these effects. But this deficiency in no way impairs the utility of Eq. (1.33) in comparing different acoustoelectric current traces. Although the tails of real traces will depart from the ideal decaying exponential form after $t = \frac{L}{v_s}$, that portion of the traces recorded up to this time is correctly given by Eq. (1.28) and therefore by the circuit of Fig. 9(a).

What may we now say about the intermediate case? Of course we already have the exact solution through Eq. (1.21). The question we wish answered here is: What will the comparison be between two acoustoelectric current traces generated by the same input wave but for different values of the attenuation coefficient?

Based on our study of the low pass filter response, we conclude the following: For a very large value of α we know that the observed current is a faithful record of the input wave (Eq. (1.31)), and that the peak of the current coincides with the peak of the wave and is independent of α. By comparison with this case, diminshing values of the attenuation coefficient will cause the peak of the observed current to be reduced in amplitude and delayed in time, and will slow the decay of the current following the peak. These

phenomena are all clearly illustrated in the experimental record of Fig. 7. We emphasize these relationships because they will be useful to us in Chapter V when we study the way acoustic attenuation rates can change under large-signal conditions.

1.5 REPRESENTATION OF NONELECTRONIC LOSSES

We have not yet mentioned that there may be acoustic attenuation for reasons other than the absorption of the wave momentum by the free electrons. These nonelectronic losses may be grouped under the general heading of "transfer of momentum to the lattice" and are independent of the concentration of free carriers in the crystal. We may account for them by observing that the α of the Weinreich relation (Eq. (1.10)) is due to the electronic losses alone, whereas Eq. (1.18) for the acoustic attenuation should be written

$$W(x,t) = e^{-(\alpha+\alpha_o)x} W(0,t - \frac{x}{v_s}) , \tag{1.34}$$

where α_o is an attenuation coefficient representing the nonelectronic losses. Equation (1.22) therefore becomes

$$\frac{1}{\alpha v_s} \frac{dJ}{dt} + (1 + \frac{\alpha_o}{\alpha}) J(t) = - \frac{\mu}{L} W(0,t) . \tag{1.35}$$

A modified equivalent circuit representation which includes these nonelectronic losses is that shown in Fig. 9(b), where C_a is arbitrarily chosen, and R_e and R_o must then satisfy

$$R_e = \frac{\tau_e}{C_a} = \frac{1}{\alpha v_s C_a} \tag{1.36}$$

$$R_o = \frac{\tau_o}{C_a} = \frac{1}{\alpha_o v_s C_a} \tag{1.37}$$

When the wave packet is entirely inside the crystal, the homogeneous Eq. (1.35) has the solution

$$J(t) = J(T)\, e^{-(\alpha+\alpha_o)v_s(t-T)}, \tag{1.38}$$

or, in terms of the decay time constants,

$$J(t) = J(T)^{-(\frac{1}{\tau}+\frac{1}{\tau_o})(t-T)} \tag{1.39}$$

In Section 1.1 we argued that the acoustoelectric attenuation rate should go to zero in low light as the CdS crystal approaches an insulating condition. Because the nonelectronic losses are independent of the density of free carriers, any remaining slope to the tail of the acoustoelectric current trace as the crystal conductivity is reduced to zero must be due entirely to α_o. This gives us an easy experimental check on the nonelectronic losses in the crystal. We need only see whether an experimental plot of attenuation vs conductivity tends to some value α_o rather than zero in the high resistivity limit ($\omega\tau \to \infty$). Such a plot will be presented at the beginning of Chapter V. For the moment we shall merely say that the nonelectronic losses in the crystal are small enough (less than 1 db/cm) that they are not a cause for worry, and they will be disregarded in the theoretical development of the next two chapters.

CHAPTER II

THE SMALL-SIGNAL THEORY

In this chapter we shall investigate the mechanism of the acoustoelectric interaction between the electrons and a propagating wave in a piezoelectric crystal. Our goal is to develop a small-signal theory for the prediction of acoustic attenuation and acoustoelectric current generation. The work presented here is a rederivation of the original small-signal theory of Hutson and White[5] and its later extension by White[7] to cover the case of acoustic gain. We have chosen a somewhat different approach to the problem with a consequent change in emphasis of some of the results.

The theory will be developed as follows: In Section 2.1 we shall use the piezoelectric equations of state to demonstrate the Weinreich relation for the acoustoelectric interaction in a conducting piezoelectric crystal, indicating the phase relationships between electrical and mechanical components of the wave necessary to the production of acoustic attenuation and acoustoelectric current. In Section 2.2 we shall introduce a simple equivalent circuit model of the interaction and show how it gives directly these relationships along with the dissipation rate. Sections 2.3 and 2.4 will be devoted to the development of formulae for acoustic attenuation and acoustoelectric current production. In Section 2.5 we shall discuss modifications of the theory needed to account for the effect of diffusion of the electrons. Finally, in Section 2.6 we shall list some of the problems associated with the experimental study of acoustic gain.

The acoustoelectric effect in CdS follows from the strong piezoelectric coupling which may exist between a propagating sound wave and the free electrons. To study this interaction for all interesting directions of polarization and propagation of the acoustic wave would appear to require that we undertake a three-dimensional analysis of the system. In fact it is a problem in only one dimension, that being along the propagation vector of the wave.

Consider an acoustic plane wave of either longitudinal or shear mode propagating in an insulating piezoelectric crystal. On the basis of our understanding of the static case it would seem that the sound wave could be accompanied by longitudinal and transverse electric fields, with the strength of a particular electric field component essentially unchanged from that produced by an equivalent static strain. In 1949 Kyame[15] showed that such a description is correct for the longitudinal electric field, which is essentially electrostatic in nature, but that the transverse electric field (and consequent magnetic field) behaves like an electromagnetic wave constrained to move at the velocity of sound and is therefore reduced in amplitude compared to the expected electrostatic value by a factor $(v/c)^2$, where v is the velocity of sound and c the velocity of light in the crystal. In 1954 Kyame[16] expanded his theory to include conductive crystals, but there was no change in his earlier result about the magnitudes of the electric fields accompanying the wave (our Appendix contains a partial rederivation of this result for conductive piezoelectric crystals). Because of their extremely small amplitude the transverse electric fields are of no consequence to us in our study of the acoustoelectric effect in CdS, and our analysis does become a one-dimensional problem along the propagation vector of the wave.

We may effect a further simplification by restricting the directions of propagation and displacement of the acoustic wave to lie along the crystallographic axes, thereby avoiding the task of recomputing the crystal's anisotropic properties in a rotated coordinate frame. Cadmium sulfide is a hexagonal crystal belonging to crystal class C_{6v}. The existence of a sixfold symmetry axis imposes a high degree of degeneracy upon the crystal's anisotropic physical properties.[17] The nonzero elements of the dielectric constant are

$$\epsilon_{11} = \epsilon_{22}, \quad \epsilon_{33},$$

and those of the piezoelectric coefficient are

$$e_{311} = e_{322}, \quad e_{333}, \quad e_{113} = e_{223},$$

where the 3-axis is the axis of hexagonal symmetry.

As a consequence of this degeneracy only certain electric field polarizations may be associated with a given acoustic plane wave. For acoustic propagation along the hexagonal axis longitudinal waves (e_{333}) are accompanied only by longitudinal electric fields, but shear waves ($e_{113} = e_{223}$) have only transverse field components. For propagation at right angles to the hexagonal axis, shear waves with displacement along the hexagonal axis ($e_{113} = e_{223}$) are accompanied only by longitudinal electric fields, but those with displacement at right angles to the hexagonal axis see no piezoelectric effect. Longitudinal waves propagating at right angles to the hexagonal axis ($e_{311} = e_{322}$) are accompanied only by transverse electric fields.

Therefore, the only acoustic propagation modes of interest to us are (1) the shear mode with propagation vector at right angles to the hexagonal axis and displacement along the hexagonal axis ($e_{113} = e_{223}$), and (2) the longitudinal mode with propagation along the hexagonal axis (e_{333}).

2.1 WEINREICH RELATION IN A PIEZOELECTRIC PHOTOCONDUCTING CRYSTAL

Consider an acoustic wave propagating in the x-direction in a piezoelectric photoconducting medium and define a strain S, a stress T, and a displacement u such that

$$S = \frac{\partial u}{\partial x} \quad \text{and} \quad \frac{\partial T}{\partial x} = m \frac{\partial^2 u}{\partial t^2} ,$$

where m is the mass density. Further, assume that the medium is characterized by a piezoelectric coefficient e such that S produces an electric field in the x-direction. Under adiabatic conditions the piezoelectric equations of state corresponding to the one-dimensional problem are

$$T = cS - eE \tag{2.1}$$

$$D = eS + \epsilon E, \tag{2.2}$$

where

T = stress

S = strain

E = electric field

D = electric displacement

$$c = \left.\frac{\partial T}{\partial S}\right)_{E} = \text{adiabatic short-circuit elastic constant}$$

$$\epsilon = \left.\frac{\partial D}{\partial E}\right)_{S} = \text{adiabatic clamped dielectric constant}$$

$$e = \left.\frac{\partial D}{\partial S}\right)_{E} = -\left.\frac{\partial T}{\partial E}\right)_{S} = \text{adiabatic piezoelectric coupling coefficient.}$$

In the absence of the piezoelectric coupling we recognize these equations as being simply:

(1) Hooke's Law

(2) The usual relation for D and E.

The piezoelectric equations of state tell us that, in the presence of piezoelectric coupling, the propagating pattern of mechanical stresses and strains which characterize the traveling acoustic wave will be accompanied by proportional E and D fields. The fact that the piezoelectric coefficients e in the two equations of state are identical may be proven by a thermodynamic argument that the electric enthalpy of the system must be a total differential.[18]

A propagating wave packet may be mathematically represented as the product of an envelope function and an oscillating function. In particular, for a dispersionless medium we may represent the strain associated with an acoustic plane wave of frequency ω by:

$$S(x,t) = \mathrm{Re}\left[S_1\left(\frac{x}{v_s} - t\right) e^{i(kx-\omega t)}\right], \qquad (2.3)$$

where

$$k = \frac{\omega}{v_s} \qquad (2.4)$$

and v_s is the propagation velocity. The envelope function $S_1(x-v_st)$ then represents the local amplitude of the propagating wave and can be said to modulate the oscillatory component. But how can such a description have any application to a medium where there is attenuation and dispersion?

In the preceding chapter we stated that the maximum acoustic attenuation we shall encounter with our particular experimental sample is about 65 db/cm. Although this would seem to be a very large rate of attenuation, it is still small compared to a wavelength of sound; e.g., for a 30 Mc wave the attenuation is less than 0.1 db/radian. Therefore, although the attenuation should be explicitly displayed in a complex propagation constant as

$$k = \frac{\omega}{v_s} + i\frac{\alpha}{2} \quad , \tag{2.5}$$

our approach will be to treat the attenuation over one wavelength of the sound as being so small that for the purpose of computing local relationships among the components T, S, D, and E of the traveling wave we are justified in taking the propagation vector k as being entirely real. To this approximation, the strain associated with the traveling acoustic wave may be represented by

$$S(x,t) = \mathrm{Re}\left[S_1\left(\frac{x}{v_s} - t\right) e^{i\omega\left(\frac{x}{v_s} - t\right)}\right] \quad . \tag{2.6}$$

If we assume similar representations for T, E, and D and substitute these expressions into the piezoelectric equations of state, then the oscillatory components will cancel, leaving the following relationships among the amplitudes:

$$T_1 = cS_1 - eE_1 \tag{2.7}$$

$$D_1 = eS_1 + \epsilon E_1 \ . \tag{2.8}$$

These amplitudes may be complex in order that they properly represent possible differences in phase between the components of the traveling wave. However, the physical constants c, e, and ϵ will all be real, because the ultrasonic frequency (30 Mc) is small compared to a typical lattice vibration frequency ($\sim 10^{12}$ sec^{-1}).

If the acoustic wave is attenuated in its passage through the crystal, then the local rate of acoustic energy dissipation is

$$-\frac{dW}{dt} = \frac{1}{2\pi}\int_0^{2\pi} T\,\frac{dS}{dt}\,d\Phi \ , \tag{2.9}$$

where the phase

$$\Phi = \omega\left(\frac{x}{v_s} - t\right) \ . \tag{2.10}$$

If we assume the envelope of the wave is slowly varying compared to the frequency ω, then we may replace the derivative by

$$\frac{dS}{dt} = -i\omega S \ , \tag{2.11}$$

so that Eq. (2.9) becomes

$$-\frac{dW}{dt} = \frac{1}{2\pi}\int_0^{2\pi} T\,(-i\omega S)\,d\Phi \tag{2.12}$$

$$= \frac{1}{2}\,\mathrm{Re}[T_1^*(-i\omega S_1)] \ , \tag{2.13}$$

where the asterisk indicates complex conjugation. Thus the acoustic energy dissipation is given by

$$-\frac{dW}{dt} = \frac{\omega}{2} \mathrm{Im}[T_1^* S_1] \quad . \tag{2.14}$$

The local rate of acoustic energy dissipation is therefore different from zero only when there is a phase difference between the amplitudes T_1 and S_1. This we expect, since the condition that the stress and strain of a propagating wave be in phase requires that they be linked only by an effective elastic constant which is entirely real and therefore dissipationless. From Eq. (2.7) we see that any phase difference between T_1 and S_1 must come from E_1 being out of phase with S_1. By substituting Eq. (2.7) into Eq. (2.14), we may display directly this relationship between the acoustic dissipation rate and the relative phase of the electric field and the strain. We obtain:

$$-\frac{dW}{dt} = \frac{\omega}{2} \mathrm{Im}[-eE_1^* S_1] \quad . \tag{2.15}$$

We normally think of the piezoelectric effect as describing a linear dependence of electric field upon mechanical strain. On this basis we should expect the electric field to be exactly proportional to the strain everywhere on the traveling wave, thus making E_1 in phase with S_1. But it is apparent from Eq. (2.15) that there must be a phase difference between these quantities for acoustic dissipation. The second equation of state (Eq. (2.8)) reveals that this phase difference is directly traceable to D_1. This is where the photoconduction electrons enter the picture.

It is instructive first to study the case of the insulating crystal. In the absence of illumination the crystal is an insulator, a condition of charge neutrality exists throughout, and $\frac{dD}{dx}$ is therefore everywhere zero. Thus we must have $D_1 = 0$, and Eq. (2.8) becomes:

$$E_1 = -\frac{e}{\epsilon} S_1 , \tag{2.16}$$

giving E_1 in phase with S_1. If we substitute this expression into Eq. (2.7), we get

$$T_1 = cS_1 + \frac{e^2}{\epsilon} S_1 \tag{2.17}$$

$$= c(1 + \frac{e^2}{\epsilon c}) S_1 . \tag{2.18}$$

We may define a new elastic constant

$$c_D = \frac{\partial T}{\partial S}\Big)_D = c(1 + \frac{e^2}{\epsilon c}) , \tag{2.19}$$

so that

$$T_1 = c_D S_1 . \tag{2.20}$$

We shall later have use for the electromechanical coupling coefficient K^2, which is usually defined by

$$K^2 = \frac{c_D - c}{c_D} = \frac{\frac{e^2}{\epsilon c}}{1 + \frac{e^2}{\epsilon c}} . \tag{2.21}$$

Equations (2.18) and (2.20) may therefore be written as

$$T_1 = \frac{c}{1 - K^2} S_1 . \tag{2.22}$$

Thus, in an insulating crystal, the effect of the piezoelectric coupling is to stiffen the elastic constant. Typically K^2 has a value of about .036 in CdS[5], so the effect is small.

Let us now return to the general case of the piezoelectric crystal with free conduction electrons. In the quiescent crystal there will be a condition of charge neutrality with $\frac{dD}{dx} = 0$ and therefore $D_1 = 0$. But in the presence of the wave we may expect the piezoelectric field accompanying the wave to upset local charge equilibrium conditons. In particular, since the piezoelectric field reverses sign every half wavelength along the wave, we may expect <u>periodic bunching</u> of the electrons by the wave.

If we let n_s represent the local density of electrons in excess of that required for charge neutrality, then D must reflect the bunching through Gauss' law

$$\frac{dD}{dx} = -qn_s \quad , \tag{2.23}$$

where q is the absolute magnitude of the electronic charge. The amplitude of D is assumed to be slowly varying compared to the frequency of the wave, so we may write Eq. (2.23) as

$$\frac{i\omega}{v_s} D = -qn_s \quad . \tag{2.24}$$

The charge bunching n_s has the periodicity of the wave and may also be represented as the product of an amplitude and an oscillatory component:

$$n_s(x,t) = \mathrm{Re}[n_1(\frac{x}{v_s} - t)\, e^{i\omega(\frac{x}{v_s} - t)}] \quad , \tag{2.25}$$

so that Eq. (2.24) may be written in terms of the amplitudes alone:

$$\frac{i\omega}{v_s} D_1 = -qn_1 \quad . \tag{2.26}$$

In discussing Eq. (2.15) we observed that there can be attenuation only if there is a relative phase difference between E_1 and S_1 and that this phase difference is directly traceable to D_1. This dependence of the acoustic dissipation on D_1 may be explicitly shown by using Eq. (2.8) to eliminate E_1 in Eq. (2.15), with the result that

$$-\frac{dW}{dt} = \frac{\omega}{2} \text{Im}\left[-\frac{e}{\epsilon} D_1^* S_1\right]$$

$$= \frac{\omega}{2} \text{Im}\left[D_1^*\left(-\frac{e}{\epsilon} S_1\right)\right] \quad . \tag{2.27}$$

We recognize $-\frac{e}{\epsilon} S_1$ as just the piezoelectric field which would accompany the acoustic wave in the absence of the conduction electrons (see Eq. (2.16)). Let us replace this quantity by an equivalent <u>piezoelectromotive</u> field $\mathcal{E}$ given by

$$\mathcal{E}(x,t) = -\frac{e}{\epsilon} S(x,t) \quad ; \tag{2.28}$$

or, in terms of the amplitudes

$$\mathcal{E}_1\left(\frac{x}{v_s} - t\right) = -\frac{e}{\epsilon} S_1\left(\frac{x}{v_s} - t\right) \quad . \tag{2.29}$$

This is tantamount to writing the second piezoelectric equation of state (Eq. (2.8)) as

$$E_1 = \mathcal{E}_1 + \frac{1}{\epsilon} D_1 \quad . \tag{2.30}$$

If we substitute Eq. (2.29) into Eq. (2.27), the expression for the rate of acoustic energy dissipation becomes

$$-\frac{dW}{dt} = \frac{\omega}{2}\,\mathrm{Im}[D_1^{*}\,\mathcal{E}_1] \quad . \tag{2.31}$$

But we know D_1 in terms of the charge bunching amplitude n_1. We therefore substitute Eq. (2.26) into Eq. (2.31) and obtain after some manipulation

$$-\frac{dW}{dt} = \frac{v_s}{2}\,\mathrm{Re}[(-qn_1)^{*}\mathcal{E}_1] \quad . \tag{2.32}$$

We shall later wish to compute an attenuation coefficient. For this we need $-\frac{dW}{dx}$ rather than $-\frac{dW}{dt}$. The relation between the two is simply

$$-\frac{dW}{dx} = -\frac{1}{v_s}\frac{dW}{dt} \quad , \tag{2.33}$$

so that

$$-\frac{dW}{dx} = \frac{1}{2}\,\mathrm{Re}[(-qn_1)^{*}\mathcal{E}_1] \quad . \tag{2.34}$$

Thus we see, as we expected, that the energy of the acoustic wave is dissipated through work done on the conduction electrons by the piezoelectric field which accompanies the wave. What perhaps was not intuitively apparent was that the piezoelectric field would cause periodic bunching of the electrons, and that the attenuation suffered by the wave would be strongly dependent on the relative phase between the charge bunching and the piezoelectric field. Had we been looking for the charge bunching, we might have expected the distribution of electric fields and conduction electrons illustrated in Fig. 10(a); i.e., we might have looked for symmetric bunching around electric field minima. But this symmetric condition unfortunately gives

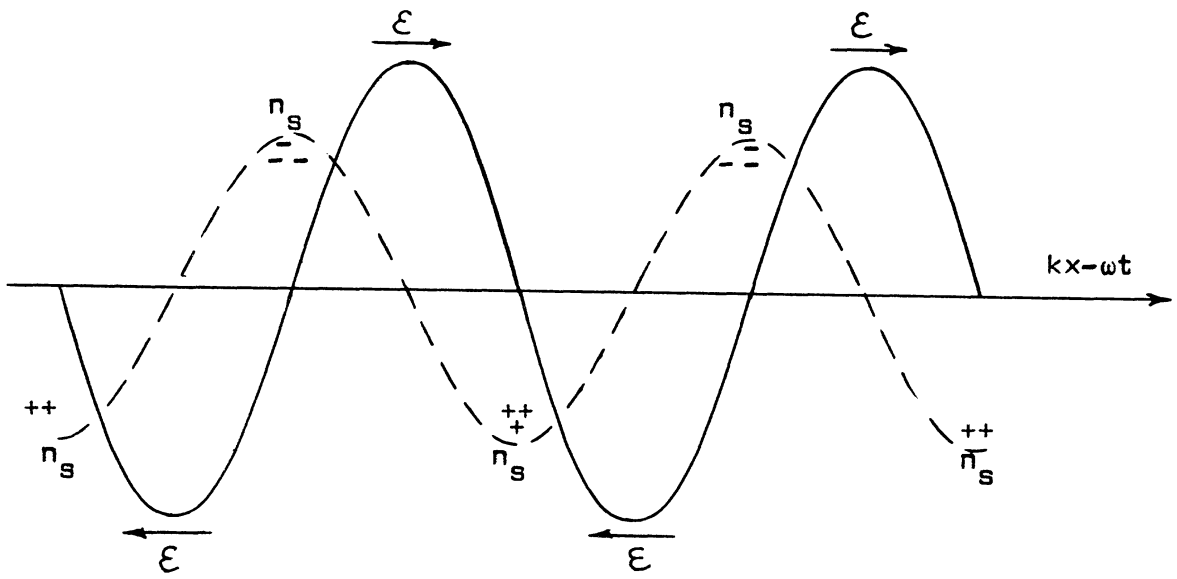

Fig. 10(a). Illustration of the phase relationships needed for acoustic attenuation. Phase condition for the static case. The electrons are symmetrically bunched around the zeros of the piezoelectric field. This phase condition cannot produce acoustic attenuation.

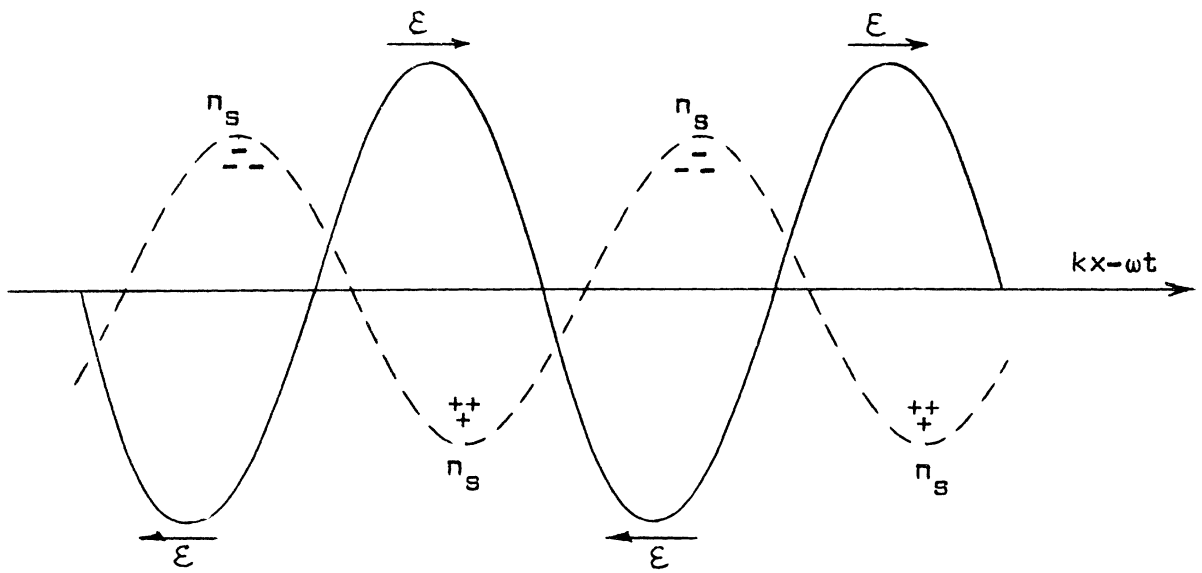

Fig. 10(b). Illustration of the phase relationships needed for acoustic attenuation. Phase condition needed for acoustic attenuation. The electron bunching lags the zeros of the piezoelectric field.

$$\mathrm{Re}[(-qn_1)^{*}\mathcal{E}_1] = 0$$

and therefore no attenuation. We shall later show that this condition also delivers no net direct current down the crystal. It is the relative phase lag of the charge bunching which produces acoustic attenuation and acoustoelectric current generation.

We may guess that a phase lag occurs because the electrons' finite mobility makes them sluggish in response to the rapidly oscillating local piezoelectric field induced by the passing wave. If this is the case, then we see that there are two ways we might expect to influence the rate of acoustic attenuation:

(1) By adjustment of the illumination we may change the rate of generation of free electrons, thus regulating the density of carriers available for bunching by the acoustic wave. This technique is effective, as will be shown in Section 2.3.

(2) A more interesting possibility is that by application of an external dc field E_o to the crystal we may be able to adjust the relative phase by which the electron bunching lags the acoustic wave. An external dc field would impart an average drift velocity $v_d = -\mu E_o$ to the free electrons, and that particular value of E_o which gives $v_d = v_s$ should produce no phase lag and therefore no attenuation. The logical extension of this speculation is that the application of even larger drift fields may cause the electron bunching to lead in phase, thereby reversing the direction of momentum exchange between the electrons and the wave, i.e., we should be able to acheive acoustic gain. This point will be considered further in Section 2.3, and some of the problems associated with the experimental study of acoustic gain will be discussed in Section 2.6.

To finish our proof of the Weinreich relation in a piezoelectric crystal we need an expression for the acoustoelectric current to compare with Eq. (2.34) for the acoustic attenuation. If there is a net flow of direct current (i.e., current slowly varying compared to the ultrasonic frequency of the acoustic wave) down the crystal, then the local production of the current must be given by

$$j = \frac{1}{2\pi}\int_0^{2\pi}(qn)(\mu E)d\Phi \tag{2.35}$$

$$= \frac{1}{2}\,\mathrm{Re}[(qn_1)^*\,\mu E_1] \,. \tag{2.36}$$

To eliminate E_1 from Eq. (2.36) we first combine Eq. (2.30) with Eq. (2.26), obtaining

$$E_1 = \mathcal{E}_1 + \frac{v_s}{-i\omega}\,qn_1 \,. \tag{2.37}$$

This expression may then be substituted into Eq. (2.36), with the result

$$j = \mu\,\frac{1}{2}\,\mathrm{Re}\,[(qn_1)^*\mathcal{E}_1]. \tag{2.38}$$

Our proof is finished. Upon comparing Eq. (2.38) with Eq. (2.34) we see that we have indeed demonstrated the Weinreich relation for a piezoelectric conducting crystal:

$$\frac{1}{\mu}\,j = \frac{dW}{dx} \,. \tag{2.39}$$

2.2 EQUIVALENT CIRCUIT MODEL OF THE INTERACTION

Working from the piezoelectric equations of state and Gauss' law we have succeeded in demonstrating the Weinreich relation in a piezoelectric photoconducting crystal, and we have also obtained some insight into the conditions necessary to the production of acoustic attenuation. So far we have not independently predicted either the attenuation or the acoustoelectric current; we have only proven that each could be computed in terms of the other through the Weinreich relation.

To be able to predict the attenuation and acoustoelectric current at a given crystal conductivity for a particular input acoustic wave packet, we must first understand the mechanism which causes the charge bunching to lag in phase behind the zeros of the piezoelectric field. We begin by writing the expression for the electron current in the crystal.

Under illumination cadmium sulfide behaves like a n-type extrinsic semiconductor. At the maximum available light intensity our experimental sample has a photoconductivity of 10^{-3} $(\text{ohm-cm})^{-1}$. For an electron mobility of 315 $\frac{\text{cm/sec}}{\text{V/cm}}$, we may compute the maximum density of free electrons at $2 \times 10^{13}/\text{cm}^3$. At such low concentrations the electrons may be regarded as classical particles whose behavior is described by Maxwell-Boltzman statistics. For a short mean free path the electron current may be written as the sum of drift and diffusion currents:

$$J = \underbrace{qn_c\mu E}_{\text{drift}} + \underbrace{\mu kT \frac{dn_c}{dx}}_{\text{diffusion}}, \qquad (2.40)$$

where n_c = density of electrons in the conduction band. The coefficient of the diffusion term follows from the Einstein relation.

In most circumstances the contribution of the diffusion term is small, and presentation of the theory is clearer if this term is omitted. In the theoretical development which follows we shall first derive results without this term; then in Section 2.5 we shall show how the theoretical results must be modified to include the influence of diffusion.

Continuing with our small-signal approach to the problem, let us separate the variables on the right hand side of Eq. (2.40) into their dc and first order oscillatory components:

$$n_c = n_o + n_s \tag{2.41}$$

$$E = E_o + E_s \ . \tag{2.42}$$

where

n_o = steady-state (quiescent) density of electrons in the conduction band. The crystal's dc photoconductivity is given by $\sigma = n_o q\mu$.

n_s = Re $[n_1 e^{i\omega(\frac{x}{v_s} - t)}]$ represents the acoustic charge bunching.

E_o = any externally applied dc drift field.

E_s = Re $[E_1 e^{i\omega(\frac{x}{v_s} - t)}]$ is the oscillatory component of the local electric field.

After this separation (and dropping the diffusion term) Eq. (2.40) becomes

$$J = qn_o\mu E_o + qn_s\mu E_s + qn_s\mu E_o + qn_o\mu E_s \ . \tag{2.43}$$

We may effect a similar separation of J into dc and first order parts:

$$J = J_o + J_s \ . \tag{2.44}$$

If we then collect first order (oscillatory) terms only, we will have

$$J_s = \sigma E_s + qn_s\mu E_o \ . \tag{2.45}$$

We recognize that the intermodulation term $qn_s\mu E_s$ in Eq. (2.43) has dc and second order oscillatory components only. Hence it will contribute to J_o but not to J_s.

In terms of amplitudes Eq. (2.45) is

$$J_1 = \sigma E_1 + qn_1\mu E_o \quad . \tag{2.46}$$

We may use the continuity equation

$$\frac{dJ}{dx} = \frac{d}{dt}(qn_c) \tag{2.47}$$

to eliminate n_1 from Eq. (2.46). If we make our usual assumption about amplitudes varying slowly compared to the frequency of the wave, then the continuity equation may be written as

$$i\frac{\omega}{v_s}J_s = -i\omega\, qn_s \tag{2.48}$$

or, in terms of the amplitudes

$$qn_1 = -\frac{1}{v_s}J_1 \quad . \tag{2.49}$$

Substitution of Eq. (2.49) into Eq. (2.45) then gives

$$\left(1 + \frac{\mu E_o}{v_s}\right)J_1 = \sigma E_1 \tag{2.50}$$

or

$$E_1 = \gamma\, r\, J_1 \quad , \tag{2.51}$$

where $r = \frac{1}{\sigma}$, and

$$\gamma = 1 + \frac{\mu E_o}{v_s} \quad . \tag{2.52}$$

The externally applied drift field imparts a drift velocity

$$v_d = -\mu E_o$$

to the conduction electrons. Thus the factor γ may also be written

$$\gamma = 1 - \frac{v_d}{v_s} \quad . \tag{2.53}$$

We demonstrated earlier (Eq. (2.32)) that the traveling acoustic wave gives up its energy by doing work on the conduction electrons. Thus the rate of dissipation of energy from the wave must be given by

$$-\frac{dW}{dt} = \frac{1}{2} \text{Re} \left[E_1^* J_1 \right] \quad , \tag{2.54}$$

(this expression may also be derived by manipulation of Eq. (2.32)). From Eq. (2.51) we see that the product $E_1^* J_1$ is entirely real and is positive for γ positive ($v_d < v_s$), negative for γ negative ($v_d > v_s$), and zero when the drift velocity of the electrons is matched to the propagation velocity of the wave. Equation (2.54) clearly shows how the direction of energy transfer between the wave and the electrons may be reversed to produce acoustic gain.

Knowing E_1 in terms of J_1 is not particularly useful. We would rather know both E_1 and J_1 in terms of ξ_1, to which we have access through Eq. (2.37):

$$E_1 = \xi_1 + \frac{v_s}{-i\omega} q n_1 \quad . \tag{2.55}$$

We may combine this with the continuity Eq. (2.49) to obtain

$$\mathcal{E}_1 = E_1 + \frac{1}{-i\omega\epsilon} J_1 \ . \tag{2.56}$$

If we further substitute Eq. (2.51) to eliminate E_1, we have

$$\mathcal{E}_1 = (\gamma r + \frac{1}{-i\omega\epsilon}) J_1 \ . \tag{2.57}$$

The relationships among $\mathcal{E}_S$, E_S, and J_S may be neatly summarized in an equivalent circuit diagram (Fig. 11). The corresponding equations for the dependence of the amplitudes E_1 and J_1 upon $\mathcal{E}_1$ are[20]

$$J_1 = \frac{\mathcal{E}_1}{\gamma r + \frac{1}{-i\omega\epsilon}} = \frac{1}{\gamma + \frac{1}{-i\omega\tau}} \frac{\mathcal{E}_1}{r} \tag{2.58}$$

$$E_1 = \frac{\gamma r \mathcal{E}_1}{\gamma r + \frac{1}{-i\omega\epsilon}} = \frac{\gamma}{\gamma + \frac{1}{-i\omega\tau}} \mathcal{E}_1 \tag{2.59}$$

where $\tau = r\epsilon$ is the dielectric relaxation time.

These relationships are also displayed in the phase diagram of Fig. 11(b). If we define θ as the relative phase angle by which the electron bunching n_1 lags the zeros of the piezoelectric field $\mathcal{E}_1$ (our time convention makes a phase lag appear as a counterclockwise rotation), then

$$\theta = \arctan \frac{\gamma r}{1/\omega\epsilon} = \arctan \gamma\omega\tau \ .$$

The angle θ may take any value between $-\pi/2$ and $+\pi/2$, with the negative values (phase lead) representing acoustic gain. Equation (2.51) requires that E_1 be colinear with J_1, and Eqs. (2.30) and (2.59) are satisfied only if the tip of E_1 is constrained to lie on the circle shown in the diagram. The lower semi-circle is the region of acoustic attenuation, and the upper semi-circle is the

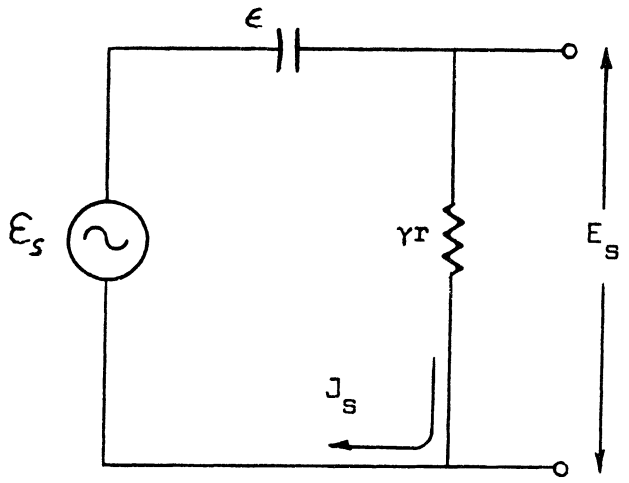

$$\mathcal{E}_s = -\frac{e}{\epsilon} S; \quad \gamma = 1 - \frac{v_d}{v_s} = 1 + \frac{\mu E_o}{v_s}$$

(a) Equivalent circuit.

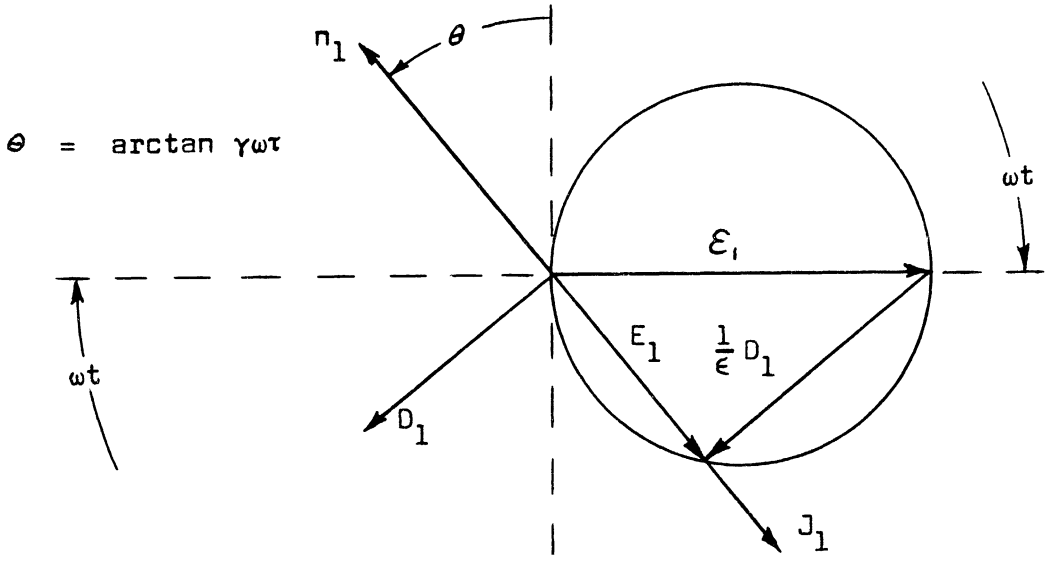

(b) Phase diagram.

Fig. 11. Equivalent circuit and phase diagram for the acoustoelectric interaction (without diffusion).

region of acoustic gain. E_1 reverses sigh when θ goes through zero, so E_1 and J_1 are parallel in the region of acoustic attenuation and anti-parallel in the region of acoustic gain. Maximum acoustic gain or attenuation occurs at $\theta = \pm \frac{\pi}{4}$.

We make the following observations:

(1) The electric field E_1 vanishes when $\gamma = 0$, that is, when the drift velocity of the electrons is matched to the propagation velocity of the traveling wave. For this case the wave is stationary in a reference frame "fixed" with respect to the average drift velocity of the electrons. Thus the electrons have "enough time" to completely neutralize the piezoelectric field of the acoustic wave.

(2) The current J_1 and therefore charge bunching n_1 are largest at $\gamma = 0$. This is also consistent with the concept of "enough time." Also notice that J_1 and n_1 are exactly 90° out of phase with $\mathcal{E}_1$ at $\gamma = 0$, this being the phase condition which we earlier showed could give no attenuation and no net direct current.

(3) The equivalent circuit model clearly displays the conditions needed for maximum attenuation, i.e., maximum dissipation in γr. Maximum transfer of power to "load resistor" γr occurs when it is matched to the equivalent generator impedance $1/-i\omega\varepsilon$. For a given crystal resistivity this condition occurs when

$$\gamma = \pm \frac{1}{\omega\tau} \qquad (2.60)$$

with the minus sign representing the condition of acoustic gain. Alternatively if $\gamma = 1$ (no external drift field available) then maximum dissipation will occur for

$$r = \frac{1}{\omega\epsilon} \quad . \tag{2.61}$$

2.3 THE ATTENUATION COEFFICIENT

We may now compute an attenuation coefficient. From Eq. (2.34) the decay rate of the wave is given by

$$-\frac{dW}{dx} = \frac{1}{2} \mathrm{Re}\,[(-qn_1)^* \mathcal{E}_1] \quad . \tag{2.62}$$

To eliminate $-qn_1$ from Eq. (2.62), we combine the continuity Eq. (2.49) with Eq. (2.59)

$$-qn_1 = \frac{1}{v_s} J_1 = \frac{1}{v_s} \frac{\mathcal{E}_1}{r} \frac{1}{\gamma + \frac{1}{-i\omega\tau}} \tag{2.63}$$

and substitute the result into Eq. (2.62), obtaining

$$-\frac{dW}{dx} = \frac{1}{v_s} \frac{|\mathcal{E}_1|^2}{2r} \mathrm{Re}\left[\frac{1}{\gamma + \frac{1}{-i\omega\tau}}\right] \tag{2.64}$$

$$= \frac{1}{v_s} \frac{|\mathcal{E}_1|^2}{2r} \frac{\mathrm{Re}[\gamma]}{\left|\gamma + \frac{1}{-i\omega\tau}\right|^2} \tag{2.65}$$

(Our reason for writing $\mathrm{Re}[\gamma]$ instead of just γ will become apparent when we discuss the influence of diffusion in Section 2.5.) Alternatively, Eq. (2.65) may also be derived directly from the equivalent circuit model. The dissipation in "resistor" γr is

$$-\frac{dW}{dt} = \frac{1}{2} \mathrm{Re}[E_1^* J_1] \quad . \tag{2.66}$$

We may use Eqs. (2.58) and (2.59) to replace E_1 and J_1, obtaining:

$$-\frac{dW}{dt} = \frac{|\mathcal{E}_1|^2}{2r} \frac{\mathrm{Re}[\gamma]}{\left|\gamma + \frac{1}{-i\omega\tau}\right|^2} \quad . \tag{2.67}$$

Multiplication throughout by $1/v_s$ will again give Eq. (2.65).

To compute an attenuation coefficient we would like - dW/dx in terms of the strain S_1 rather than the equivalent piezoelectromotive field $\mathcal{E}_1$. From Eq. (2.29) we may write

$$\frac{|\mathcal{E}_1|^2}{2r} = \frac{1}{2r} \frac{e^2}{\epsilon^2} S_1^2 = \frac{1}{r\epsilon} \frac{e^2}{\epsilon c} \frac{cS_1^2}{2} \quad . \tag{2.68}$$

We may combine this with Eqs. (2.19) and (2.21), with the result

$$\frac{|\mathcal{E}_1|^2}{2r} = \frac{1}{\tau} \frac{K^2}{1 - K^2} \frac{cS_1^2}{2} = \frac{K^2}{\tau} \frac{1}{2} c_D S_1^2 \quad . \tag{2.69}$$

Thus

$$-\frac{dW}{dx} = \frac{K^2}{v_s \tau} \frac{1}{2} c_D S_1^2 \frac{\mathrm{Re}[\gamma]}{\left|\gamma + \frac{1}{-i\omega\tau}\right|^2} \quad . \tag{2.70}$$

The attenuation coefficient α is defined by

$$\alpha = -\frac{1}{W} \frac{dW}{dx} \quad . \tag{2.71}$$

If we approximate W by the energy density of a traveling acoustic wave in an insulating crystal

$$W = \frac{1}{2} c_D S_1^2 \quad , \tag{2.72}$$

then our final expression for the attenuation coefficient is

$$\alpha = \frac{K^2}{v_s \tau} \frac{\mathrm{Re}[\gamma]}{\left|\gamma + \frac{1}{-i\omega\tau}\right|^2} \quad . \tag{2.73}$$

Figure 12 is a plot of α vs. v_d. The plot is antisymmetric about $\gamma = 0$ ($v_d = v_s$), and the peaks of maximum attenuation and maximum gain are displaced from $\gamma = 0$ by an amount

$$\gamma = \pm \frac{1}{\omega\tau} \quad . \tag{2.74}$$

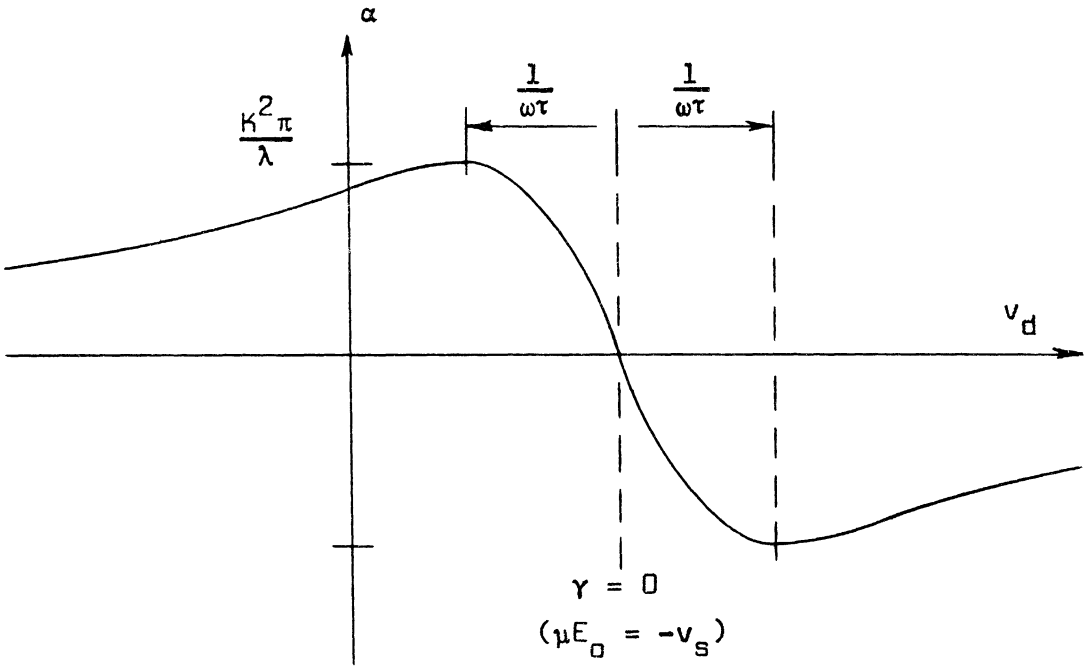

Fig. 12. Plot of α vs. v_d (without diffusion).

These maxima therefore occur at

$$\gamma r = \pm \frac{1}{\omega\epsilon} \tag{2.75}$$

and correspond to values of externally applied drift field and crystal resistance for which the charge bunching n_1 lags or leads the zeros of $\mathcal{E}_1$ by a relative phase of 45°. These maximum and minimum values of α are

$$\alpha = \pm \frac{K^2}{v_s \tau} \cdot \frac{\omega\tau}{2}$$

$$= \frac{K^2}{2} \cdot \frac{2\pi}{\lambda} \quad . \tag{2.76}$$

For 30 Mc shear waves propagating in CdS the length of a radian is[5]

$$\frac{\lambda}{2\pi} = \frac{v_s}{\omega} = \frac{1.75 \times 10^5 \text{ cm/sec}}{2\pi \times 30 \times 10^6/\text{sec}} = .93 \times 10^{-3} \text{ cm}$$

In our particular experimental sample the electromechanical coupling coefficient has the value[13]

$$K^2 = .0284 \quad .$$

The maximum value of α is therefore

$$\alpha = 15.0 \text{ cm}^{-1} = 65.2 \text{ db/cm} \quad .$$

This is attenuation so large that it nearly deserves to be called annihilation. One might fairly ask whether we have violated our criterion that $\alpha/2$ be small compared with ω/v_s (see Eq. (2.5)), but this is not the case, since

$$\frac{\alpha/2}{\omega/v_s} = \frac{(15.0 \text{ cm}^{-1})(.93 \times 10^{-3} \text{ cm})}{2} = .007 \quad .$$

If we wish to observe this much attenuation with no externally applied drift field, then we shall have to set $\gamma = 1$ and choose the crystal resistivity to satisfy Eq. (2.75). For the shear mode the crystal capacitivity ϵ_{22} is [19]

$$\epsilon_{22} = .8 \times 10^{-12} \text{ farads/cm} \quad ,$$

so the required crystal resistivity is

$$r = 6650 \text{ ohm-cm} \quad .$$

This is the particular crystal resistivity for which the separation between peaks of maximum and minimum α (Eq. (2.74)) is given by $\gamma = \pm 1$, thus centering the positive peak on the vertical axis. Values of crystal resistivity different from this amount must therefore produce diminished acoustic attenuation at zero drift field.

This last statement is illustrated in Fig. 13, where we see a plot of α as a function of crystal resistivity for the case of no applied drift field. We have taken $\omega\tau$ (assuming ω constant) rather than the resistivity as the independent variable, and we have chosen to make the horizontal axis a logarithmic scale. When plotted this way the curve is symmetric about its maximum at $\omega\tau = 1$.

The simple analytic function describing the shape of the curve may be derived as follows: If there is no externally applied drift field, then $\gamma = 1$, and Eq. (2.73) becomes

$$\alpha = \frac{K^2}{v_s \tau} \frac{1}{1 + \left(\frac{1}{\omega\tau}\right)^2} \quad , \tag{2.77}$$

which reduces to

$$\alpha = \frac{K^2 \pi}{\lambda} \frac{2}{\omega\tau + \frac{1}{\omega\tau}} \quad . \tag{2.78}$$

Here the symmetry about $\omega\tau = 1$ on a logarithmic scale is clearly apparent. We may find the exact shape of the curve by defining

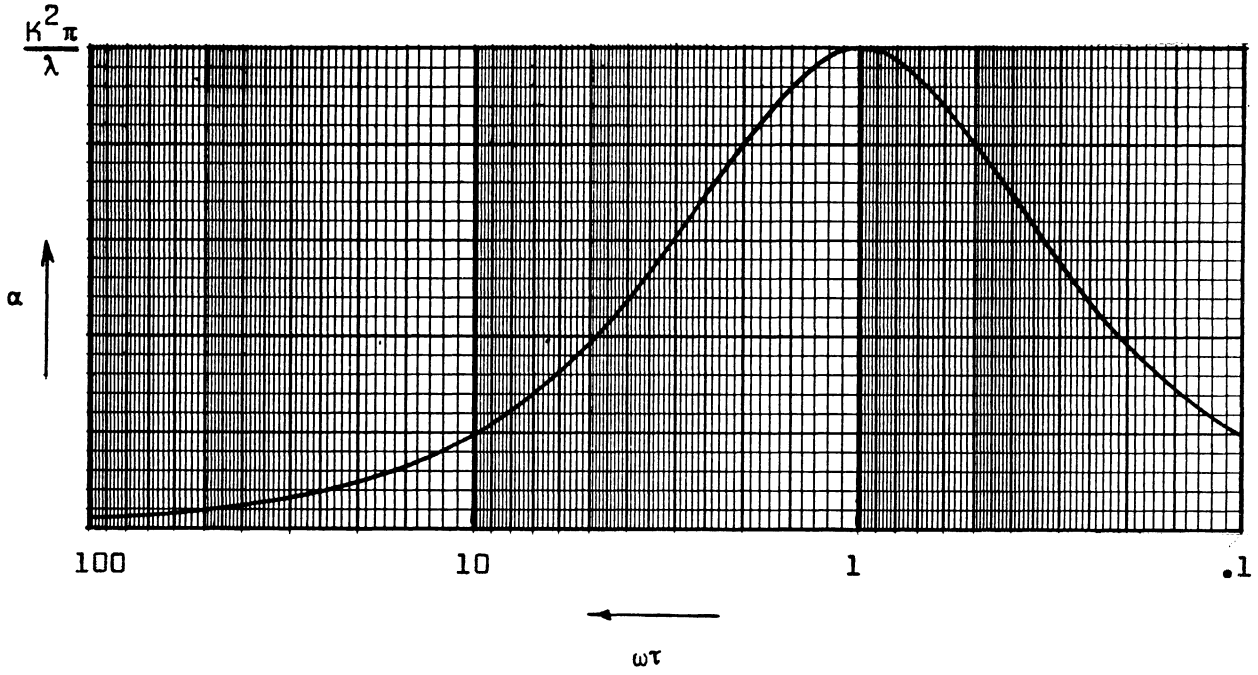

Fig. 13. Plot of α vs. $\omega\tau$ for the case of no applied drift field (without diffusion).

$$a = \log_e \omega\tau \quad , \tag{2.79}$$

so that

$$\alpha = \frac{K^2\pi}{\lambda} \frac{2}{e^a + e^{-a}} \tag{2.80}$$

$$= \frac{K^2\pi}{\lambda} \operatorname{sech} a \quad . \tag{2.81}$$

The shape of the curve is therefore simply that of the hyperbolic secant:

$$\alpha = \frac{K^2\pi}{\lambda} \operatorname{sech}(\log_e \omega\tau) \quad . \tag{2.82}$$

2.4 THE ACOUSTOELECTRIC CURRENT

In the last section we computed an attenuation coefficient by collecting the first order oscillatory terms from Eq. (2.43) and using these terms to

calculate the rate of dissipation of energy from the wave. We wish now to compute the acoustoelectric current. If we return to Eq. (2.43) and collect the dc terms, we will have

$$J_o = qn_o\mu E_o + \frac{1}{2\pi}\int_o^{2\pi} qn_s\mu E_s \, d\phi \tag{2.83}$$

$$= qn_o\mu E_o + \frac{1}{2}\,\mathrm{Re}\,[(qn_1)^*\,\mu E_1] \quad . \tag{2.84}$$

We identify the acoustoelectric current j as

$$j = \frac{1}{2}\,\mathrm{Re}\,[(qn_1)^*\,\mu E_1] \quad . \tag{2.85}$$

The product $qn_s\mu E_s$ also has an oscillating component whose frequency is 2ω and whose amplitude is equal to that of the dc term.[21] The relationship between these intermodulation products and the initial interaction term is simply that of the trigonometric identity

$$\cos^2\phi = \frac{1}{2}\,(1 + \cos 2\phi) \quad . \tag{2.86}$$

We are unable to observe this oscillatory component of the acoustoelectric current. There are two reasons: (1) The observed current is physically integrated over the entire crystal length, so any ripples are "smoothed out" by the action of the "low pass filter" discussed in Section 1.4; (2) The requirement of parallelism between the acoustic wavefront and the crystal end faces is twice as severe as that for observation of the ripple due to the boundary condition (Section 1.3). For these reasons we have made no attempt to extend the bandwidth of our measuring equipment to 60 Mc where these oscillations occur.

Following a procedure similar to that used in developing Eq. (2.73) for the attenuation coefficient, we use Eqs. (2.59) and (2.63) to eliminate qn_1 and μE_1 from Eq. (2.85), obtaining

$$j = -\frac{\mu}{v_s}\frac{|\mathcal{E}_1|^2}{2r}\frac{\mathrm{Re}[\gamma]}{\left|\gamma + \frac{1}{-i\omega\tau}\right|^2} \quad .$$

Substitution of Eq. (2.69) and further manipulation then gives

$$j = -\mu W \frac{K^2}{v_s \tau}\frac{\mathrm{Re}[\gamma]}{\left|\gamma + \frac{1}{-i\omega\tau}\right|^2} \quad . \tag{2.87}$$

Comparison of Eq. (2.87) with Eq. (2.73) for the attenuation coefficient again illustrates the Weinreich relation

$$j = -\mu\alpha W \quad . \tag{2.88}$$

At the beginning of the introduction we characterized the acoustoelectric effect as a wave-particle drag phenomenon. We think of the wave and the electrons as exerting a drag on each other, the drag being the result of a momentum exchange which attempts to equalize their velocities. In the absence of an externally applied drift field the electrons are initially "at rest" with respect to the crystal lattice, and the momentum exchange results in attenuation of the wave and the production of a net acoustoelectric direct current.

From the Weinreich relation and from the work of this section we know that the acoustoelectric current is proportional to the acoustic attenuation and that the current must reverse direction when the attenuation coefficient changes sign. An amplifying drift field propels the electrons at a velocity higher

than that of the acoustic wave, and the retarding drag on these carriers by the wave causes a reduction of the drift current, the amount of this reduction then being the reverse acoustoelectric current associated with acoustic gain.

2.5 INCLUSION OF THE DIFFUSION TERM

Let us now return to Eq. (2.40) and make the corrections needed to account for the influence of diffusion. The expression for the current was

$$J = \underbrace{qn_c\mu E}_{\text{drift}} + \underbrace{\mu kT \frac{dn_c}{dx}}_{\text{diffusion}} .$$

The gradient in n_c must be the result of charge bunching; i.e.,

$$\frac{dn_c}{dx} = \frac{dn_s}{dx} = \frac{i\omega}{v_s} n_s \quad . \tag{2.89}$$

We see that the diffusion term will contribute only to J_1 (no dc contribution). Equation (2.46) for the amplitudes therefore becomes

$$J_1 = \sigma E_1 + (\mu E_o + \frac{i\omega}{v_s} \cdot \frac{\mu kT}{q}) qn_1 \quad . \tag{2.90}$$

If we use the continuity Eq. (2.49) to eliminate qn_1 from Eq. (2.90), we obtain

$$(1 + \frac{\mu E_o}{v_s} + \frac{i\omega}{v_s^2} \cdot \frac{\mu kT}{q}) J_1 = \sigma E_1 \tag{2.91}$$

or, after multiplying through by r and substituting $\gamma = 1 + \frac{\mu E_o}{v_s}$,

$$(\gamma r + \frac{i\omega}{v_s^2} \cdot \frac{\mu kT}{q} r) J_1 = E_1 \quad . \tag{2.92}$$

If we now introduce the diffusion frequency ω_D:

$$\frac{i}{\omega_D} = \frac{1}{v_s^2} \cdot \frac{\mu k T}{q} , \tag{2.93}$$

then Eq. (2.92) may be reduced to

$$(\gamma + \frac{1}{-i} \frac{\omega}{\omega_D}) \, r J_1 = E_1 . \tag{2.94}$$

By comparison with Eq. (2.51) we see that all of the formulae we derived in Sections 2.2 - 2.4 will be preserved if we everywhere replace γ by the new quantity Γ, where

$$\Gamma = \gamma + \frac{1}{-i} \frac{\omega}{\omega_D} . \tag{2.95}$$

For 30 Mc shear waves propagating in CdS (at 300°K) $\frac{\omega}{\omega_D}$ has an approximate numerical value of

$$\frac{\omega}{\omega_D} = \frac{1}{25} ,$$

so we see that in the absence of an amplifying drift field (i.e., for $\gamma = 1$) the influence of the diffusion term is indeed small.

Equations (2.58) and (2.59) now become

$$J_1 = \frac{\mathcal{E}_1}{\Gamma r + \frac{1}{-i\omega\epsilon}} , \tag{2.96}$$

$$E_1 = \frac{1}{\Gamma + \frac{1}{-i\omega\tau}} \mathcal{E}_1 . \tag{2.97}$$

We may include the influence of the diffusion term in the equivalent circuit model. The factor -i in the denominator of Eq. (2.94) fixes the phase and dictates that proper representation must be as a capacitive impedance[20]

$$X_D = \frac{1}{-i}\left(\frac{\omega}{\omega_D}\right) r \quad . \tag{2.98}$$

At the risk of concealing its dependence upon the frequency and the conductivity, we can make the diffusion term appear like a capacitor. We do this by returning to Eq. (2.92) and substituting

$$\frac{L_D^2}{\epsilon} = \frac{kT}{n_o q^2} = \frac{\mu kT}{q} r \quad , \tag{2.99}$$

where L_D is the Debye screening length. After some manipulation Eq. (2.92) becomes

$$\left(\gamma r + \frac{1}{-i\omega\epsilon_D}\right) J_1 = E_1 \quad , \tag{2.100}$$

where the effective dielectric permitivity due to diffusion is defined by

$$\epsilon_D(r,\omega) = \left(\frac{\lambda/2\pi}{L_D}\right)^2 \epsilon \quad , \tag{2.101}$$

and the equivalent circuit representation of the interaction takes the form of Fig. 14(a).

If we substitute Eq. (2.95) into Eqs. (2.96) and (2.97), the expressions for local current density and electric field intensity become

$$J_1 = \frac{\mathcal{E}_1}{\gamma r + \frac{1}{-i}\left(\frac{1}{\omega\epsilon} + \frac{\omega}{\omega_D} r\right)} \tag{2.102}$$

$$E_1 = \frac{\gamma + \frac{1}{-i}\frac{\omega}{\omega_D}}{\gamma + \frac{1}{-i}\left(\frac{1}{\omega\tau} + \frac{\omega}{\omega_D}\right)} \mathcal{E}_1 \quad . \tag{2.103}$$

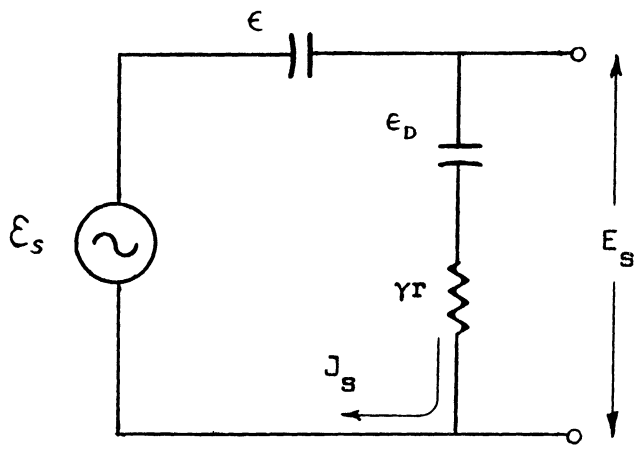

(a) Equivalent circuit.

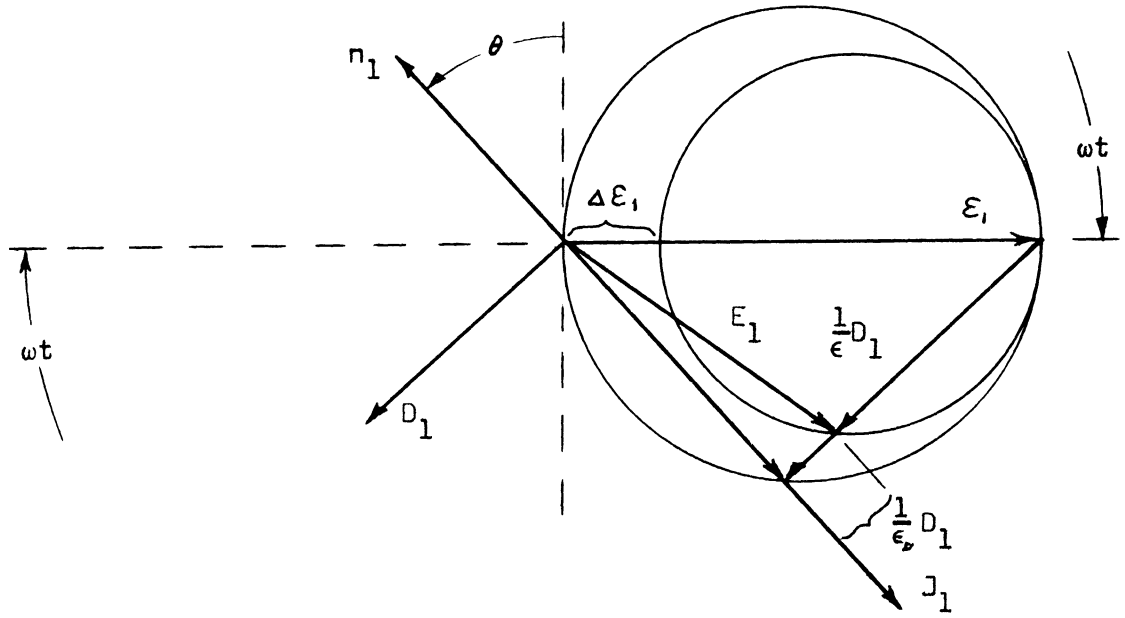

(b) Phase diagram.

Fig. 14. Equivalent circuit and phase diagram for the acoustoelectric interaction (with diffusion).

Notice that J_1 and therefore n_1 are still a maximum at $v_d = v_s$ ($\gamma = 0$), but that E_1 no longer vanishes at this point. This is because diffusion prevents charge bunching from completely neutralizing $\mathcal{E}_1$ at $v_d = v_s$.

Figure 14(b) is a phase diagram of the interaction. Here Θ is the relative phase angle by which the electron bunching n_1 lags the zeros of the piezoelectric field $\mathcal{E}_1$ and is given by

$$\Theta = \arctan \frac{\gamma}{\frac{1}{\omega\tau} + \frac{\omega}{\omega_D}}$$

In this diagram the tip of the electric field amplitude E_1 is constrained to lie on the smaller circle, and its position on this circle is determined by the point of intersection of J_1 with the larger circle. The difference in diameters between the circles is $\Delta\mathcal{E}_1$, where

$$\Delta(r,\omega) = \frac{1}{1 + \frac{\epsilon_D}{\epsilon}} = \frac{1}{1 + \left(\frac{\lambda/2\pi}{L_D}\right)^2} = \frac{1}{1 + \frac{1}{\omega\tau} \cdot \frac{\omega_D}{\omega}} \quad .$$

We may now recompute the attenuation coefficient and the expression for the acoustoelectric current. The new expressions replacing Eqs. (2.73) and (2.87) are

$$\alpha = \frac{K^2}{v_s \tau} \frac{\mathrm{Re}[\Gamma]}{\left|\Gamma + \frac{1}{-i\omega\tau}\right|^2} \tag{2.104}$$

$$j = -\mu W \frac{K^2}{v_s \tau} \frac{\mathrm{Re}[\Gamma]}{\left|\Gamma + \frac{1}{-i\omega\tau}\right|^2} \quad . \tag{2.105}$$

After substitution of Eq. (2.95) these expressions take the form

$$-\frac{1}{\mu W} j = \alpha = \frac{K^2}{v_s \tau} \frac{\gamma}{\gamma + \frac{1}{-i}\left(\frac{1}{\omega\tau} + \frac{\omega}{\omega_D}\right)} . \qquad (2.106)$$

Figure 15 is a plot of α vs. v_d from Eq. (2.106). The cross-over voltage (value of E for $\gamma = 0$) is unchanged, but the displacement of the peaks of maximum and minimum α from this point is increased to

$$\gamma = \pm \left(\frac{1}{\omega\tau} + \frac{\omega}{\omega_D}\right) , \qquad (2.107)$$

while the height of these peaks is reduced to

$$\alpha = \pm \frac{K^2 \pi}{\lambda} \cdot \frac{1}{1 + \omega\tau \frac{\omega}{\omega_D}} . \qquad (2.108)$$

If there is no externally applied drift field, then $\gamma = 1$ and Eq. (2.106) becomes

$$\alpha = \frac{K^2}{v_s \tau} \cdot \frac{1}{1 + \left(\frac{1}{\omega\tau} + \frac{\omega}{\omega_D}\right)^2} \qquad (2.109)$$

or

$$\alpha = \frac{K^2 \pi}{\lambda} \cdot \frac{2}{[1 + (\frac{\omega}{\omega_D})^2]\omega\tau + 2\frac{\omega}{\omega_D} + \frac{1}{\omega\tau}} \qquad (2.110)$$

It is clear from Eq. (2.110) that the influence of diffusion is strongest at high resistivity and becomes negligible in the limit of very low resistivity. If we further define

$$b = \frac{1}{\sqrt{1 + (\frac{\omega}{\omega_D})^2}} , \qquad (2.111)$$

then Eq. (2.110) may be written as

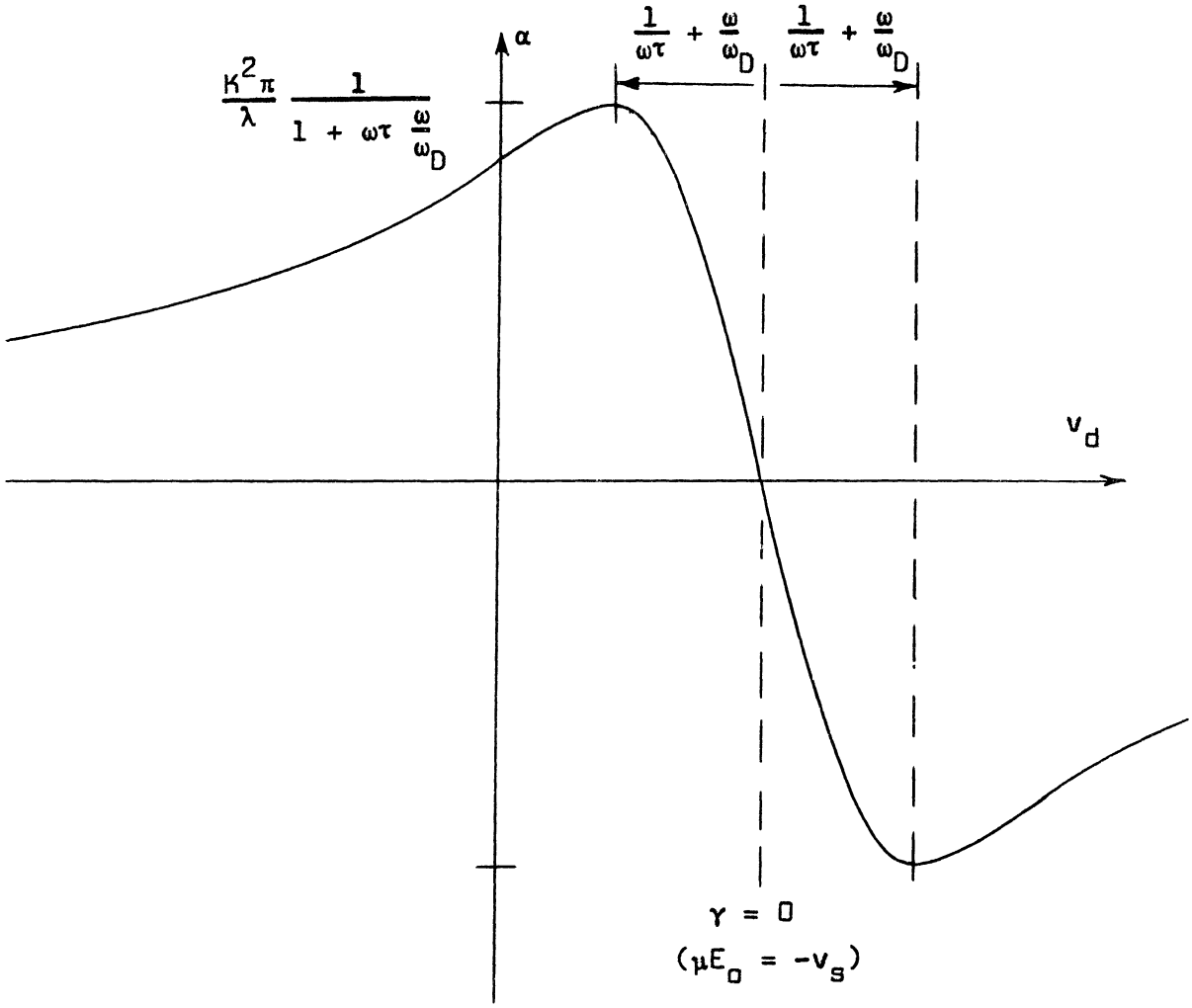

Fig. 15. Plot of α vs. v_d including the influence of diffusion.

$$\alpha = \frac{K^2\pi}{\lambda}\frac{2b}{\frac{\omega\tau}{b}+2b\frac{\omega}{\omega_D}+\frac{b}{\omega\tau}} \qquad (2.112)$$

α is therefore symmetric on a logarithmic scale about $\omega\tau = b$. If we now let

$$a = \log_e \omega\tau \qquad (2.113a)$$

$$a_o = \log_e b \quad , \qquad (2.113b)$$

then the analytic form of Eq. (2.112) will be explicitly displayed as

$$\alpha = \frac{K^2\pi}{\lambda} \frac{b}{\cosh (a-a_o) + b \frac{\omega}{\omega_D}} \quad . \qquad (2.114)$$

Figure 16 is a plot of α vs. $\omega\tau$ (assuming ω constant) as given by Eq. (2.112). The numerical value taken for ω/ω_D is that given by Hutson and White.[5] Equation (2.78) for α vs. $\omega\tau$ in the absence of diffusion is also plotted for comparison.

2.6 ACOUSTIC GAIN

The possibility of using the acoustoelectric interaction to acheive traveling wave amplification was proposed by Weinreich[1] in 1956. He proved that the application of a longitudinal electric field large enough to cause the electrons to drift faster than the propagation velocity of the acoustic wave could result in a negative attenuation coefficient. The experiments of interest at that time[3] were concerned with the acoustoelectric effect in n-type germanium, an interaction so weak as to make experimental observation of acoustic attenuation extremely difficult, and studies of acoustic amplification were not attempted.

Experimental observation of acoustic gain in cadmium sulfide was first reported by Hutson, McFee, and White.[6] Except for the additional apparatus required to impress a drift field across the crystal, the experimental arrangement they used was essentially the same as that outlined in Chapter I and discussed in detail in Chapter IV. These investigators observed maximum acoustic gains of about 18 db at 15 Mc and 38 db at 45 Mc for shear waves in a 7 mm crystal. These maxima were not sharply defined and occured at about 1050 v/cm for both frequencies. The agreement with theory was only qualitatively correct, and the experimentally determined plots of α vs. E did not have the nice inverse symmetry about the point $\gamma = 0$ predicted by theory.

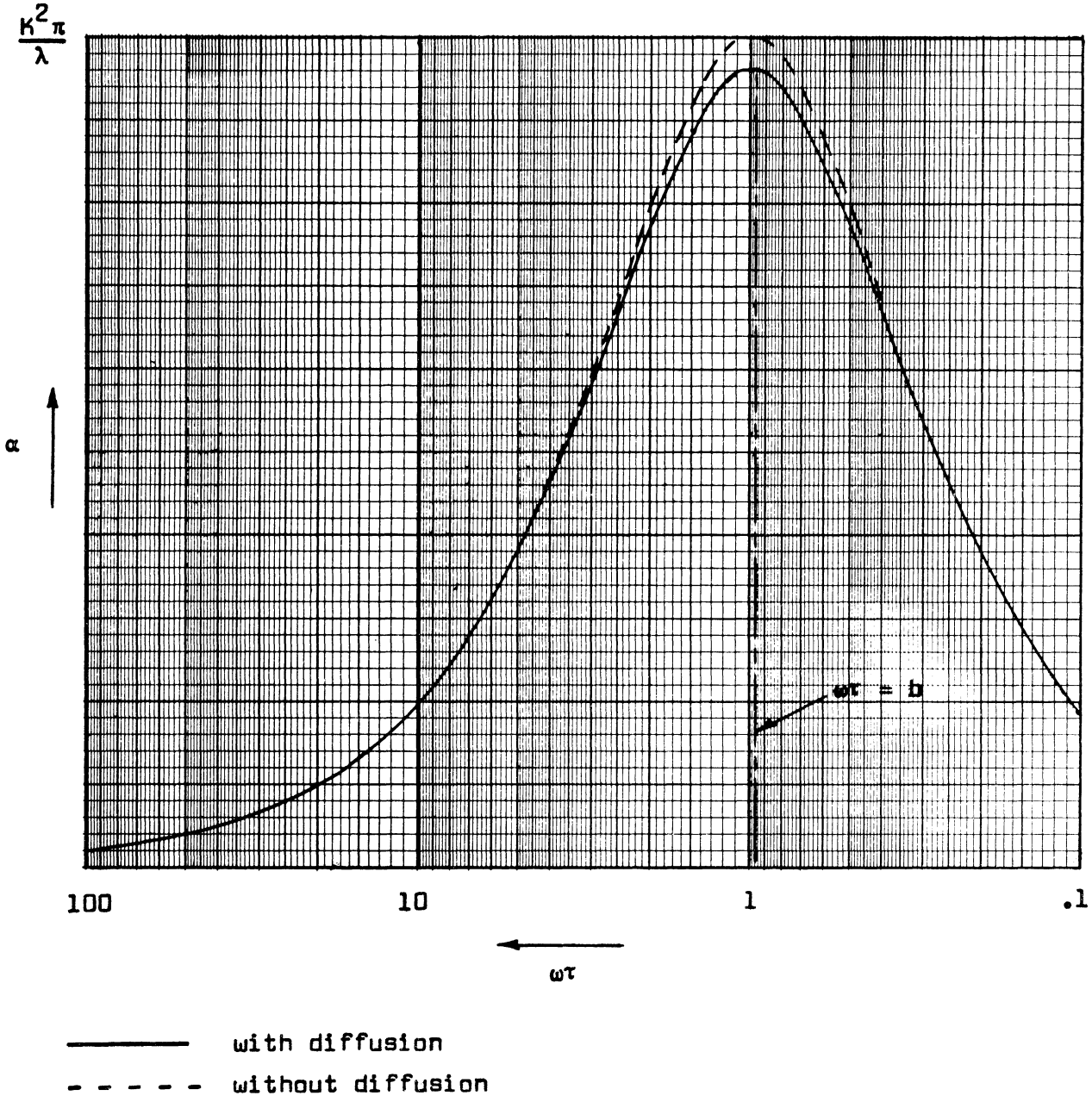

Fig. 16. Plot of α vs. $\omega\tau$ at zero drift field showing the influence of diffusion.

These authors also detected a buildup of noise at the output transducer each time an amplifying drift field (a drift field large enough for the production of acoustic gain) was applied across the crystal in the absence of an input signal. This buildup occurred over a period equal to several acoustic transit times within the crystal. They concluded that they were seeing an ultrasonic flux of amplified background noise. The round trip gain, including reflection losses, was greater than unity, so this flux buildup was able to occur over several passes as the noise bounced back and forth within the crystal.

This phenomenon was further investigated by McFee,[12] who was pursuing the noise seen by Hutson, McFee, and White[6] and also seeking an explanation for the current saturation reported by Smith.[10] Smith had observed that the crystal current produced by an amplifying drift field always decayed to a steady-state saturation value which could be calculated by assuming that the carrier drift velocity was the same as the sound velocity in the crystal. McFee's results supported the theory of Hutson[11] that the acoustoelectric current generated by the flux was responsible for the apparent current saturation.

At the end of Section 2.4 we showed that the acoustoelectric current generated under amplifying conditions must be experimentally observed as a reduction in the drift current produced by the applied electric field. This is what finally limits the growth of ultrasonic flux amplified from the background noise in the crystal. The reverse acoustoelectric current grows in intensity with the ultrasonic flux until the carrier drift velocity matches the propagation velocity of the wave. This is the saturation value of the crystal current, and at this point there is no further amplification of the ultrasonic flux.

This reverse acoustoelectric current makes accurate experimental study of acoustic amplification extremely difficult, and it probably contributed to the asymmetry of the experimental α vs. E plots published by Hutson, McFee, and White.[6] It might seem possible to avoid this complication by transmitting a relatively weak acoustic wave packet down the crystal during the first few microseconds that the drift field is turned on. This unfortunately does not entirely solve the problem. Rapid application of the drift field results in the generation of shock-excited noise within the crystal, and gradual application leaves too much time for current saturation to begin.

This is not to say that such studies are impossible; they are merely beset with vexing experimental problems. It has been the practical experience of this investigator that the difficulties associated with the experimental study of the acoustoelectric effect in CdS seem to increase in direct proportion to the magnitude of the externally applied drift field. Fortunately the acoustoelectric interaction in CdS contains a wealth of experimental information for the case of no externally applied drift field. For example, under large input signal conditions the acoustoelectric current accompanying a propagating wave may be large enough to effectively modify rates of acoustic attenuation and acoustoelectric current production. It is this phenomenon which will occupy our attention in the remaining chapters, where we shall show that it is possible to predict the results of this interaction of the wave with itself and to verify these predictions by experiment.

CHAPTER III

THE ACOUSTOELECTRIC FEEDBACK EFFECT

We have proven (a) that acoustic attenuation will produce a direct current in an external wire joining the end faces of the crystal, and (b) that an externally applied drift field will influence acoustic attenuation within the crystal. We shall now show that these cannot be independent effects.

In Section 1.2 we devised a simple equivalent circuit model (Fig. 8) which showed every region of the crystal crossed by the total acoustoelectric current $J(t)$. According to this model the direct current crossing the ith crystal segment is carried in part by the local acoustoelectric interaction $j_i(t)$, and the remaining current $J(t)-j_i(t)$ is carried by the conduction electrons. The conduction electrons therefore have a local average drift velocity

$$(v_d)_i = -\mu E_i \ ,$$

where $E_i \delta x$ is the potential drop across the ith segment. But this conduction electron drift is locally indistinguishable from the drift produced by an external electric field applied across the crystal to control acoustic attenuation. The acoustoelectric current must therefore influence acoustic attenuation. We have an <u>acoustoelectric feedback effect</u>.

The concept of an acoustoelectric feedback effect (although not so named) was first proposed by Carleton, Kroger, and Prohofsky.[9] These authors concluded that the acoustoelectric current would have no observable influence on

the overall acoustic attenuation, but their calculation was based on an oversimplified model of the acoustoelectric interaction and also assumed the special case of a cw (continuous wave) input wave train. In a later paper Prohofsky[22] once more mentioned the influence of the acoustoelectric current on the attenuation, this time including dielectric relaxation effects. However, his calculations were again for the cw case, and he was interested only in using the local acoustoelectric field as an explanation for nonlinear mixing and the production of collective waves of second sound.

The drift current density will vary from one region to another in the crystal, depending upon local rates of acoustoelectric current production. From the continuity equation we know that linear divergences in the drift current must produce local accumulations or depletions of the free electrons. This must also affect acoustic attenuation. Thus there are two ways in which the acoustoelectric current may contribute to the acoustoelectric feedback effect; they are (1) through the local carrier drifts which transport the circulating current, and (2) through local changes in the conductivity resulting from divergences in these drifts.

These are essentially large-signal effects. The drift currents and divergences depend upon local current densities which in turn are proportional to power dissipation from the acoustic wave. These electronic effects are therefore unobservable for acoustic waves of small amplitude.

A complete large-signal theory for the acoustoelectric effect in CdS does not exist at present. Such a theory was attempted in 1964 by Beale,[23] but he was forced to neglect the very important influence of space charge in order to

reach a solution, thus rendering his theory useless for application to the work described here.

Lacking an adequate large-signal theory, it might be hoped that an extension of the small-signal theory to include the acoustoelectric feedback effect would be useful for predicting acoustoelectric effects at high acoustic energy densities. This is the approach we shall take. In this chapter we shall treat the acoustoelectric feedback effect (including both of the electronic effects described above) as a perturbation upon the small-signal theory of Chapter II, and we shall use the perturbed theory to compute the acoustoelectric currents generated by acoustic waves of large amplitude.

We recognize that there eventually comes a limit beyond which it must be hopeless to expect a small-signal theory to make accurate predictions of large-signal effects. For example, our physical intuition tells us that at sufficiently large sound amplitudes all of the conduction electrons must be trapped within the piezoelectric potential wells of the traveling wave and thus be constrained to move at the propagation velocity of the wave. To the extent that the total number of conduction electrons is conserved at such amplitudes, there is then an upper limit to the acoustoelectric current density, this limit being

$$j^{max} = qn_o v_s \quad .$$

Proper accounting of this effect and the intermediate cases leading to it must await the development of a complete large-signal theory. In the absence of such a theory we shall show that extension of the small-signal theory to include the acoustoelectric feedback effect does yield meaningful predictions which may be verified by experiment.

3.1 COMPUTER PROGRAM OUTLINE

We shall set as our goal the development of a computer program for the prediction of the total circulating current J(t) generated by an acoustic wave of large amplitude as it traverses the crystal. With this aim we see our task to be the derivation of an iterated series of computational steps which may eventually be assembled into a complete program for machine calculation of acoustoelectric current traces for direct comparison with experimental oscilloscope photographs. In this section we present an outline of such a program.

We schematically divide the crystal into N segments, each of length δx. The transit time across one such segment is $\delta t = \delta x/v_s$. We then bring the traveling wave into the crystal, successively advancing it by increments δx at time intervals δt. During each time interval δt we do the following:

a. Using local values of conductivity and electric field, compute an attenuation coefficient α in each segment of the crystal where the wave is passing.

b. From the results of (a) compute the rate of acoustoelectric current generation at each point on the wave.

c. Compute the circulating current J(t). Plot this point on a graph.

d. From the results of (b) and (c) calculate the electric field intensity and local conductivity in each crystal segment for use in the computation of step (a) the next time through the program.

e. Advance the wave by an amount δx while attenuating each portion of it according to the local attenuation coefficients computed in step (a).

f. Return to step (a) and repeat the cycle.

Certain practical considerations govern the selection of δt and δx. The experimental crystal is 7 mm long, resulting in a transit time of 4.0 μsec for shear waves. The program makes N points available for plotting J(t) before the wave reaches the end of the crystal, so a choice of N = 80 will give a plot of 80 points at intervals δt = .05 μsec. These are certainly enough to accurately fix the shape of J(t). Although it might seem that greater theoretical accuracy should result from a choice of even finer spatial division, this is not the case. The period of the 30 Mc acoustic wave is .033 μsec, and it is this interval which effectively limits the experimental resolution and makes finer theoretical resolution devoid of physical meaning.

Except for the computations of steps (c) and (d) we already have all of the formulae necessary for the writing of this program. For step (a) we shall use the results of the small-signal theory, and for step (b) we need only the Weinreich relation. Step (c) requires that we derive an expression for the circulating current which includes the influence of the acoustoelectric feedback effect; we shall do this in Section 3.2.

Several formulae are needed for step (d). These are most easily developed with the aid of an equivalent circuit model. In Chapter I we assumed a simple crystal model of fixed resistors and constant current generators to help us understand the time-dependent behavior of the circulating current produced by a uniformly attenuated acoustic wave. This model is not adequate for our present purposes. In Section 3.3 we shall use the macroscopic electronic equations

of the crystal to derive an equivalent circuit model which is more accurate and complete, and in Section 3.4 we shall use this model to analyze the time-dependent behavior of the electric fields and currents in the crystal.

3.2 FINDING THE CIRCULATING CURRENT J(t)

The electric fields and currents within the crystal are locally related by the following set of four equations

$$D = \epsilon E \tag{3.1}$$

$$\frac{\partial D}{\partial x} = -q\,(n_c - n_o) \tag{3.2}$$

$$\frac{\partial}{\partial t}\,(qn_c) = \frac{\partial}{\partial x}\,(j^c + j) \tag{3.3}$$

$$j^c = \sigma E = qn_c \mu E \ , \tag{3.4}$$

where

n_c = instantaneous local density of free electrons

n_o = quiescent density of free electrons (for charge neutrality)

j = local rate of acoustoelectric current generation

j^c = local drift (conduction) current density.

We may combine Eqs. (3.1) and (3.2) to eliminate D:

$$\epsilon \frac{\partial E}{\partial x} = -qn' \tag{3.5}$$

where

$$n' = n_c - n_o \tag{3.6}$$

is the local density of electrons in excess of that required for charge neutrality. Equation (3.3) is therefore

$$\frac{\partial}{\partial t}(qn') = \frac{\partial}{\partial x}(j^c + j) \quad . \tag{3.7}$$

We may substitute Eq. (3.5) into Eq. (3.7) to eliminate qn':

$$-\epsilon \frac{\partial^2 E}{\partial x \partial t} = \frac{\partial}{\partial x}(j^c + j) \tag{3.8}$$

or

$$\frac{\partial}{\partial x}[\epsilon \frac{\partial}{\partial t} E(x,t) + j^c(x,t) + j(x,t)] = 0 \quad . \tag{3.9}$$

Satisfaction of Eq. (3.9) requires that the bracketed quantity be a function of the time only, that is

$$\epsilon \frac{\partial}{\partial t} E(x,t) + j^c(x,t) + j(x,t) = J(t) \quad . \tag{3.10}$$

We identify J(t) as the circulating current.

We may show for a short-circuit boundary condition that Eq. (3.10) gives exactly the same expression for the circulating current as did Eq. (1.16) of Chapter I. We prove this by integrating Eq. (3.10) over the length of the crystal:

$$J(t) = \frac{1}{L}\int_o^L j(x,t)\,dx + \frac{1}{L}\int_o^L j^c(x,t)\,dx + \epsilon \frac{1}{L}\frac{\partial}{\partial t}\int_o^L E(x,t)\,dx. \tag{3.11}$$

The short-circuit boundary condition requires that

$$\int_o^L E(x,t)\, dx = 0 \quad , \tag{3.12}$$

so the last term of Eq. (3.11) must vanish. We may show that the term in j^c also vanishes. From the constitutive Eq. (3.4) we have

$$\mathbf{j}^c = \sigma E = \sigma_o E + \mu q n' E \quad . \tag{3.13}$$

We may substitute Eq. (3.5) into Eq. (3.13), obtaining

$$j^c = \sigma_o E - \mu\epsilon \frac{1}{2} \frac{\partial}{\partial x} (E^2) \quad , \tag{3.14}$$

so that

$$\int_o^L j^c\, dx = \sigma_o \int_o^L E\, dx - \mu\epsilon \frac{1}{2} [E^2(L) - E^2(0)] \quad . \tag{3.15}$$

The first right-hand term of Eq. (3.15) vanishes because of the short-circuit boundary condition. The remaining term will also vanish if we require that the number of free electrons in the crystal (at a given illumination) be conserved, i.e., if

$$\frac{1}{L} \int_o^L q n_c\, dx = q n_o \quad , \tag{3.16}$$

so that

$$\frac{1}{L} \int_o^L q n'\, dx = 0 \quad . \tag{3.17}$$

Substitution of Eq. (3.5) into Eq. (3.16) gives

$$- \frac{1}{L} \epsilon \int_o^L \frac{\partial E}{\partial x}\, dx = - \frac{1}{L} \epsilon [E(L) - E(0)] = 0 \quad . \tag{3.18}$$

Thus Eq. (3.15) vanishes, and Eq. (3.11) finally becomes

$$J(t) = \frac{1}{L}\int_0^L j(x,t)\,dx \quad , \tag{3.19}$$

which is identical with Eq. (1.16) of Chapter I. Therefore, to do step (c) of the computer program outline, we need only apply Eq. (3.19).

3.3 THE EQUIVALENT CIRCUIT MODEL OF THE CRYSTAL

Equation (3.10) has a simple equivalent circuit representation. If we conceptually divide the crystal into N segments and within each segment represent the local conductivity, capacitivity, and rate of acoustoelectric current generation by idealized lumped elements, then the equivalent circuit for the ith segment is just that of Fig. 17. That this is the correct representation may be easily shown. At either node we must have

$$\dot{Q}_i + j_i^c + j_i = J \quad . \tag{3.20}$$

If each segment is of length

$$\delta x = \frac{L}{N} \quad , \tag{3.21}$$

then the voltage drop V_i across the ith segment is

$$V_i = E_i \delta x \quad , \tag{3.22}$$

and the capacitance C_i is

$$C_i = \frac{\epsilon}{\delta x} \quad . \tag{3.23}$$

Thus the charge Q_i stored on capacitance C_i is just

$$Q_i = C_i V_i = \epsilon E_i \quad , \tag{3.24}$$

so Eq. (3.20) may be written as

$$\epsilon \dot{E}_i + j_i{}^c + j_i = J \quad , \tag{3.25}$$

which is just the iterated form of Eq. (3.10). The circuit model is indeed a valid representation of Eq. (3.10). If we use the constitutive Eq. (3.4) to eliminate the $j_i{}^c$, we have finally

$$\epsilon \dot{E}_i + \sigma_i E_i = J - j_i \quad . \tag{3.26}$$

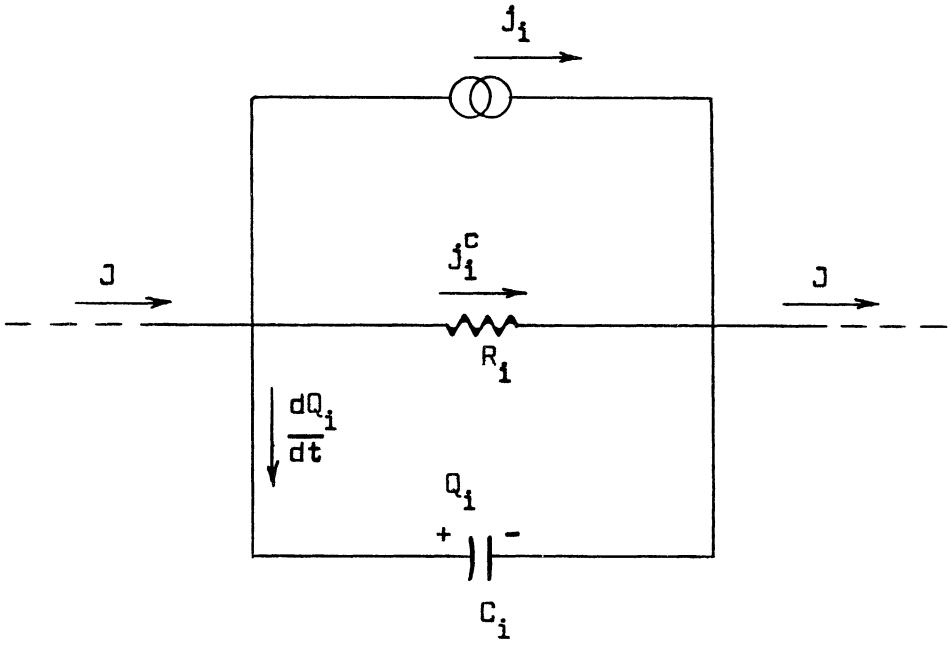

Fig. 17. Equivalent circuit model of the ith crystal segment.

3.4 SOLVING FOR THE ELECTRIC FIELDS AND CONDUCTIVITIES

Having derived the equivalent circuit model and found an expression for the circulating current J(t), we are in principle now prepared to do step (d) of the computer program outline. It is now apparent that this computational step involves finding a solution to the set of simultaneous differential Eqs. (3.26) within each successive interval δt. Unfortunately the calculation is more difficult than is perhaps indicated by the deceptively simple appearance of the circuit model, since the "resistor" representing the local conductivity σ_i of Eq. (3.26) is also a variable. We may display the true complexity of the problem by using Eqs. (3.4), (3.5), and (3.6) to eliminate j^c in Eq. (3.10), obtaining

$$\frac{\partial E}{\partial t} + (\sigma_o - \mu\epsilon \frac{\partial E}{\partial x}) E = J(t) - j(x,t) \quad . \tag{3.27}$$

Neither this nonlinear differential equation for the continuous crystal nor the equivalent set of N simultaneous nonlinear differential equations for the circuit model has an easy solution in closed form. But we are under no obligation to seek a purely analytic solution. We are attacking the entire problem of wave propagation and current generation in the crystal by iterative calculation, and there is no reason why this particular iterative step cannot be further divided into easily handled computational parts.

Let us do this. We further divide time interval δt into subintervals dt, with dt taken small enough that all of the variables of Eq. (3.26) change only slightly within each sub-interval. This will be the case if dt satisfies

$$s_i dt \ll 1 \quad . \tag{3.28}$$

for all i = 1,...N, where the local dielectric relaxation rate s_i is given by

$$s_i = \frac{1}{\tau_i} = \frac{\sigma_i}{\epsilon} \quad . \tag{3.29}$$

Within dt let us try changing only one variable at a time while holding all other variables constant. We may start by holding j_i and σ_i constant and studying the variation in E_i. Working under this assumption, we multiply both sides of Eq. (3.26) by $e^{s_i t'}$, where t' is the time measured from the beginning of the subinterval dt. We obtain:

$$(\dot{E}_i + s_i E_i)\, e^{s_i t'} = \frac{1}{\epsilon} (J - j_i)\, e^{s_i t'} \quad .$$

The left side of this equation is a total differential, so the expression may be rewritten as

$$\frac{d}{dt} (E_i e^{s_i t'} - B_i) = \frac{1}{\epsilon} (J - j_i)\, e^{s_i t'} \,, \tag{3.30}$$

where B_i is the constant of integration. The solution for $E_i(t')$ is therefore

$$E_i(t') = B_i e^{-s_i t'} + \frac{1}{\epsilon} e^{-s_i t'} \int_0^{t'} (J - j_i)\, e^{s_i t''}\, dt'' \quad . \tag{3.31}$$

B_i may be evaluated by noting that at the beginning of the interval we have t' = 0, and Eq. (3.31) reduces to

$$E_i(0) = B_i \quad . \tag{3.32}$$

We have assumed that all of the j_i are constant during sub-interval dt. From Eq. (3.19) we know that we may also take J(t) as constant. The factor $(J - j_i)$ may therefore be taken outside the integral, and we have

$$E_i(t') = E_i(0)\, e^{-s_i t'} + \frac{1}{\epsilon}(J - j_i)\,\frac{1 - e^{-s_i t'}}{s_i} \quad . \qquad (3.33)$$

Let us assume that the set $E_i(0)$ satisfies the short-circuit boundary condition. We would like the new set $E_i(dt)$ also to satisfy this condition, but Eq. (3.33) offers us no assurance that this will be the case. In general we may expect that the new set $E_i(dt)$ will <u>not</u> meet the boundary condition, i.e., that

$$\bar{E}(dt) = \frac{1}{N}\sum_{i=1}^{N} E_i(dt) \neq 0 \quad . \qquad (3.34)$$

However, if we have been careful to take dt small enough, then each of the $E_i(dt)$ will not be greatly different from the $E_i(0)$, and as a result $\bar{E}(dt)$ will be small. We may therefore specify a new set of electric field values

$$E_i'(dt) = E_i(dt) - \bar{E}(dt) \qquad (3.35)$$

which <u>will</u> satisfy the boundary condition. It is this set that we shall take as representing the electric field distribution in the crystal at the end of the interval dt.

Our calculation of the new electric field values is therefore a two step process. We first compute those changes due to local relaxation processes (first term of Eq. (3.33)) and due to the charge redistribution caused by divergences in the current (second term of Eq. (3.33)); then we adjust the new values of the field to conform to the short-circuit boundary condition.

We may now compute the local conductivity changes caused by the charge redistribution. Combining Eqs. (3.4), (3.5), and (3.6) we have

$$\sigma(x) = \sigma_o - \mu\epsilon \frac{\partial E}{\partial x} \quad . \tag{3.36}$$

To use Eq. (3.36) we must know how to express the electric field gradient in terms applicable to the equivalent circuit model. One possibility is to write the symmetric expression

$$\left.\frac{\partial E}{\partial x}\right)_i = \frac{E_{i+1} - E_{i-1}}{2\delta x} \quad ,$$

but this approach invites trouble. It divides the crystal into the two sub-sets of odd and even segments with the sub-sets coupled to each other only through the expression for the electric field gradient. The computer is in effect asked to solve the problem of two coupled large systems, a situation which of course does not exist in the real crystal. We may avoid this pitfall by writing the gradient as

$$\left.\frac{\partial E}{\partial x}\right)_i = \frac{E_i - E_{i-1}}{\delta x} \quad . \tag{3.37}$$

The expression for the conductivity therefore becomes

$$\sigma_i = \sigma_o - \mu\epsilon \frac{E_i - E_{i-1}}{\delta x} \quad . \tag{3.38}$$

Notice that Eq. (3.38) may be evaluate using either the set $E_i(dt)$ or the set $E'(dt)$. The computed values for the local conductivity are unaffected by the adjustment of electric field terms necessitated by the short-circuit boundary condition.

3.5 REVISED OUTLINE

We now have all of the formulae needed to do step (d) of the computer program outline. We must first divide δt into sub-intervals dt small enough to satisfy Eq. (3.28). Let P be the number of these sub-intervals within δt. Then each time we encounter step (d), we must perform P times the computational sequence described by Eqs. (3.33), (3.34), (3.35), and (3.38), where each equation (except (3.34)) is evaluated for all segments i = 1,...N before going on to the next.

But this program does not really abide by the rules we laid down in developing the iterated solution to Eq. (3.26); that within the sub-interval dt we would separately adjust each variable of the equation while holding the remaining variables constant. The rate of acoustoelectric current generation $j_i(t)$ and the circulating current $J(t)$ are also variables of Eq. (3.26) and should therefore be recomputed as many times as are the electric field and the conductivity. We should therefore include steps (a), (b), and (c) within the loop of computations repeated P times over each interval δt.

This is not the same as increasing the number of spatial divisions N of the crystal, an idea we rejected in Section 3.1 because it produced a finer spatial resolution than was physically meaningful for the 30 Mc wave. Instead we have chosen to sub-divide the transit time δt of the segment δx without sub-dividing the segment itself, the sub-division of the time being necessitated by the iterated solution to Eq. (3.26).

There is another very practical reason for sub-dividing only δt and not δx. If P is the number of sub-intervals dt within δt, then we are increasing

by a factor P the number of computations we must do in a practical computer program, thereby multiplying by P the running time of such a program. For N = 80 and P = 1 a practical program will take about 10 sec of machine time. Thus N = 80 and P = 10 gives a running time of about 100 sec. If, however, we had taken N = 800 (and P = 1), then we would have increased by 10^2 the number of calculations, thereby raising the running time to about 1000 sec or 18 min of computer time for each set of data.

We now present a revised outline for the computer program based on our new technique for sub-division of the interval δt.

I. Do parts A through E for p = 1,...P, where P is the number of subintervals into which δt is divided.

A. Using local values of conductivity and electric field, compute an attenuation coefficient α in each segment of the crystal where the wave is passing.

B. From the results of (A) compute the rate of acoustoelectric current generation at each point on the wave.

C. Compute the instantaneous circulating current $J_p(t)$.

D. From the results of (B) and (C) calculate the electric field intensity and local conductivity in each crystal segment.

E. Locally attenuate each portion of the wave by multiplying by the factor $e^{-\alpha v_s dt}$, where α is the local attenuation coefficient computed in (A).

II. Do each of the following steps in sequence.

F. Compute the average circulating current over the inverval δt.

$$J(t) = \frac{1}{P} \sum_{p=1}^{P} J_p(t)$$

Plot the point J(t).

G. Advance the wave by an amount δx.

H. Increase the time by an amount δt and transfer to I.

3.6 MACHINE COMPUTATION

The computer used was an IBM 7090 on The University of Michigan campus. The program was presented to the machine in MAD (Michigan Algorithm Decoder), a compiler language written at the University.

It is not necessary to sift through all of the step-by-step details of the machine calculation in order to be able to evaluate the computer program in its final form. It is important, however, that we define and explain a few basic rules of machine computation.

The computer treats names of variables as labels for locations in its memory. Subscripted variables are labels for individual locations within an array of locations. Thus E_{23} is a label for a particular location in the memory, and the numerical value of E_{23} is the number currently stored in that location.

The computer memory is characterized by destructive read-in and nondestructive read-out. By the latter we mean that we may at any time obtain from any memory location the number contained within, and this "read-out" operation does not change the number stored or in any way jeopardize our ability to obtain that same number again when the occasion demands. By destructive read-in we mean that whenever we wish to enter a new number at a given memory location,

the "read-in" operation causes the number previously stored at that memory location to be erased and therefore no longer accessible; the location is in-effect "set" to the new number. For example, consider the following machine instruction:

$$E_4 \leftarrow C_4 - E_4 + 6 \quad .$$

Here the machine is instructed to take the number stored in location C_4, subtract from it the number stored in E_4, add to the difference the number 6, and finally to store the result of the computation in location E_4. If before the computation E_4 had contained the number 3, and C_4 had contained the number 4, then after the computation E_4 would contain the number 7, but C_4 would still contain the number 4.

The computer can perform repeated operations over a running index, i.e., it can be instructed to successively do the computations

$$E_i \leftarrow C_i - E_i + 6$$

for all values of i ranging from i = 1, 2,...N.

In Section 3.7 we show the final form of the program as it is presented to the computer. In each step the computation to the right of the arrow is performed using numbers obtained from memory locations labeled by the variable names shown, and the result of the computation is then stored in the memory location indicated to the left of the arrow, the new number displacing (and therefore erasing) whatever number that location previously contained.

A succession of steps involving an iterated subscript is performed in its entirety before advancing the running index, for example in part A all steps 1 through 4 are performed first for i = t, then again for i = t-1, etc.

The quantities contained in round brackets are calculated before the program is begun, and each round-bracketed quantity is then treated as a single constant within the program.

For our purpose the conductivity σ_i, the dielectric relaxation rate s_i, and the dielectric relaxation time τ_i are merely different ways of writing a single physical quantity, and it would be redundant to calculate more than one of them. We shall therefore compute and use only s_i.

3.7 THE COMPUTER PROGRAM

I. Do parts A through E for p = 1,...P, where P is the number of sub-intervals dt into which the interval δt is divided.

A. Do steps 1 through 4 for i = t, t-1,...t-T, where T is the length of the wave inside the crystal

1. $\Gamma_i \leftarrow 1 + \left(\frac{\mu}{v_s}\right) E_i + \frac{1}{-i}\left[\frac{s_i}{\omega} + \left(\frac{\omega}{\omega_D}\right)\right]$

2. $\alpha_i \leftarrow \left(\frac{K^2}{v_s}\right) s_i \frac{\mathrm{Re}[\Gamma_i]}{\left|\Gamma_i + \frac{s_i}{-i\omega}\right|^2}$

3. $j_i \leftarrow -\mu\alpha_i W_i$

4. $W_i \leftarrow W_i\, e^{-\alpha_i(\delta x/P)}$

B. Compute the instantaneous circulating current J_p.

$$J_p \leftarrow \frac{1}{N} \sum_{i=1}^{N} j_i$$

C. Do the following computation for all i = 1,...N

$$E_i \leftarrow E_i e^{-s_i dt} + \frac{1}{\epsilon} [J_p - j_i] \frac{1 - e^{-s_i dt}}{s_i}$$

D. Compute the average electric field

$$\bar{E} \leftarrow \frac{1}{N} \sum_{i=1}^{N} E_i$$

E. Correct for the short-circuit boundary condition and find the dielectric relaxation rates by doing the following steps for all i = 1,...N.

1. $E_i \leftarrow E_i - \bar{E}$

2. $s_i \leftarrow s_o - (\frac{\mu}{\delta x}) [E_i - E_{i-1}]$

II. Do each of the following steps

F. Compute the average circulating current over the interval δt.

$J(t) \leftarrow \frac{1}{P} \sum_{p=1}^{P} J_p$, and plot this point on a graph.

G. Advance the wave by doing the following steps

1. If the wave is not entirely within the crystal, then admit the next portion of the input wave by setting $W_o \leftarrow A^2(t)$, where A(t) is the amplitude of the input wave.

2. Do the following for i = t, t-1,...t-T.

$$W_i \leftarrow W_{i-1}$$

H. Set $t \leftarrow t + \delta t$, return to the beginning of the program, and repeat the entire sequence.

CHAPTER IV

THE EXPERIMENT

The experimental arrangement was similar to that used by Hutson, McFee, and White[6] and also by Henrich[13] with whom this author shared equipment, crystals, and an experimental setup. There was one important difference which will be discussed in Section 4.3.

4.1 THE ACOUSTIC ASSEMBLY

The basic experimental arrangement was outlined in Chapter I. The acoustic system (see Fig. 2) consisted of (a) a transmitting transducer, (b) a fused silica buffer, (c) the photoconducting CdS crystal, (d) another fused silica buffer, and finally (e) a receiving transducer. The transducers were 3/8 in. diameter quartz platelets y-cut for half-wave resonance at 27.3 Mc.[24] The fused silica buffers were cylinders 1/2 in. in diameter and 1 in. long. The CdS crystal[25] was a cube 7 mm on a side oriented with the c-axis in the direction of the polarization vector of the propagating wave.

There are two reasons for using the buffers:

(1) They provide electrical insulation. This is absolutely necessary for those experiments requiring the application of a large drift field (around 1000 v) across the crystal for the purpose of studying ultrasonic gain. In other experiments (such as this one) not requiring a drift field it is still imperative that at least one end of the crystal not be grounded. But the inboard faces of the transducers must be grounded, thus the need for the insulating property.

(2) The buffers permit a convenient separation in time between the excitation of the input transducer and the occurrence of acoustoelectric phenomena in the CdS crystal, and again between these phenomena and the appearance of the acoustic wave at the receiving transducer. Capacitively-coupled electrical feedthrough effects are thus prevented from interfering with observations. This may be clarified by a study of the times involved. Typically the input transducer was excited by a 1.5-2.5 μsec burst of 30 Mc rf. For shear waves and a 7 mm CdS crystal the relationships are:

	Length	Velocity	Transit Time
CdS	7 mm	1.75×10^5 cm/sec	4.0 μsec
Fused silica	1 in.	3.8×10^5 cm/sec	6.41 μsec

All four end faces of the buffers were coated with a brushed-on layer of Hanovia liquid bright platinum. Individual wire leads were wrapped tightly around the ends of the buffers and brought into electrical contact with the end faces by painting on a slender ring of silver paste to bridge the space between them. The two outside faces of the buffers provided electrical contact to the inside (grounded) surfaces of the transmitting and receiving transducers (the transducers were not plated). The platinum layers on the inside faces of the buffers enabled electrical contact to the ends of the CdS crystal which were coated with an evaporated layer of indium. This was necessary in order that the contacts be ohmic, that is possess a linear volt-ampere characteristic.[13,26-28]

The illumination source was a General Electric H-100-A4T 100 watt mercury discharge lamp. A Kodak No. 8 Wratten filter was used to pass only the 577-9 and 546 mμ lines of Hg. These lines are weakly absorbed in cadmium sulfide, thus guaranteeing homogeneous generation of photoelectrons throughout the crystal volume.[6] Illumination intensity was adjusted by placing Wratten neutral density gelatin filters in front of the lamp.

All elements of the acoustic system were bonded together with poly-alpha methyl styrene (Dow resin V-276-9), an extremely viscous liquid (4800 poise at 25°C) which may be readily softened with a heat gun. This substance was the best available bonding material which also afforded relative ease of repeated disassembly and reassembly of the components of the acoustic system. Unfortunately it provided a poor acoustic impedance match to the elements of the system; reflection coefficients were in the neighborhood of .8 at the interfaces between elements. This condition is illustrated in Fig. 18(a), where we see an oscilloscope trace recorded at the receiving transducer of the transmitted sound pulse and its many echoes. Figure 18(b) shows the acoustoelectric current produced over an extended period of time (50 μsec) by the transmitted sound and its echoes. The echoes were in themselves no problem, since observations of the acoustoelectric current were usually confined to that brief time interval during which the [directly transmitted] sound pulse (but none of its echoes) traversed the crystal, enough time being allowed between excitations of the input transducer to permit the echoes to die away.

However, the poor transmission efficiency of the acoustic bonds was a cause for worry; there were two reasons: (1) The bonds were erratic in the

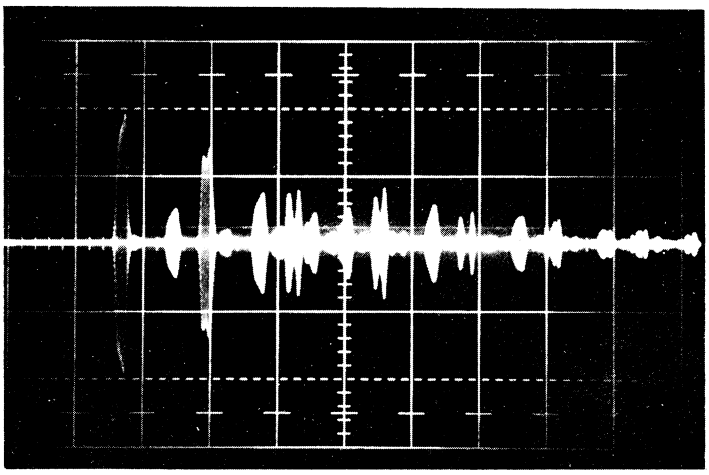

(a) Transmitted sound pulse and its echoes as detected at the output transducer. Time base = 10 μsec/cm. The crystal is in the dark.

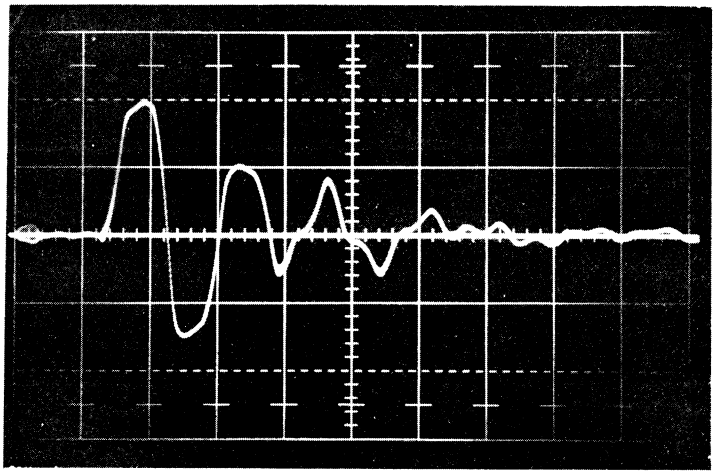

(b) Acoustoelectric current trace for a crystal resistivity of 1.35 megohm-cm. Time base = 5 μsec/cm.

Fig. 18. Illustrations demonstrating the high acoustic reflectivity of the bonds between elements of the acoustic assembly. In each photograph the sweep starts as excitation is applied to the input transducer.

sense that there was variation in their transmission efficiency from one assembly of the acoustic system to the next. Furthermore, since the mercury vapor lamp generated considerable heat, it was necessary to keep a stream of air continuously flowing across the acoustic assembly in order that the transmission efficiency of the bonds be reasonably stable during a single experimental run. (2) This poor transmission efficiency at first crippled chances for the observation of power-dependent acoustoelectric effects, since we were unable to deliver enough acoustic energy to the crystal to allow these effects to be seen. The solution to this problem is discussed in Section 4.3.

The acoustic assembly was mounted in a sample holder (see Fig. 1), a copper box partitioned into three chambers. The CdS crystal occupied the central chamber. Electric contacts to the end faces of the crystal were brought out through ceramic insulators.

The end chambers housed the transducers and the terminating impedances of the rf feed lines. The outboard faces of the transducers were electrically driven through spring-loaded polished brass buttons. The grounded partitions between chambers provided electrical screening and also offered some mechanical support to the acoustic assembly. The tunable inductors (visible in the end chambers in Fig. 1) were connected across the transducers to null their capacitance. In practice these adjustments had little influence on transducer conversion efficiency.

A series of lenses and mirrors served to deliver the light to the crystal through two rectangular openings machined into opposite faces of the sample holder. Uniformity of the illumination over the two crystal faces receiving

the light was mapped with a Texas Instruments H-11 photo device. The sensitive surface of this device was approximately 1.5 mm in diameter. By adjusting the lenses, mirrors, and the position of the light source it was possible to make the illumination uniform to within 5% across each crystal face. The problems of illumination uniformity and the optical arrangement used in this experiment are treated extensively in Ref. 13.

4.2 ELECTRONICS

In Fig. 19 there is presented a block diagram of the arrangement of electronic equipment used in the experiment. An Arenberg PG-650-C pulsed oscillator generated the excitation voltage for the input transducer. Excitation amplitude was controlled and adjusted by a pair of Hewlett-Pakcard model 355 attenuators inserted into the 30 Mc rf feed line. A Tektronix model 547 oscilloscope was used for display of acoustoelectric current waveforms. The oscilloscope triggered sweep was internally locked to the 60 cps power line frequency, and a gating signal from the oscilloscope was fed through a divider circuit to trigger the pulsed oscillator. The divider put out one sync pulse for each two it received, so the pulsed oscillator was triggered only on alternate sweeps of the electron beam across the oscilloscope face, thus providing a base line for the acoustoelectric current waveforms.

The acoustoelectric current was usually measured in terms of the voltage drop across a 200 ohm resistor shunting the current output terminals of the sample holder. This particular resistance represented the best compromise between the need to approximate a short-circuit boundary condition and the re-

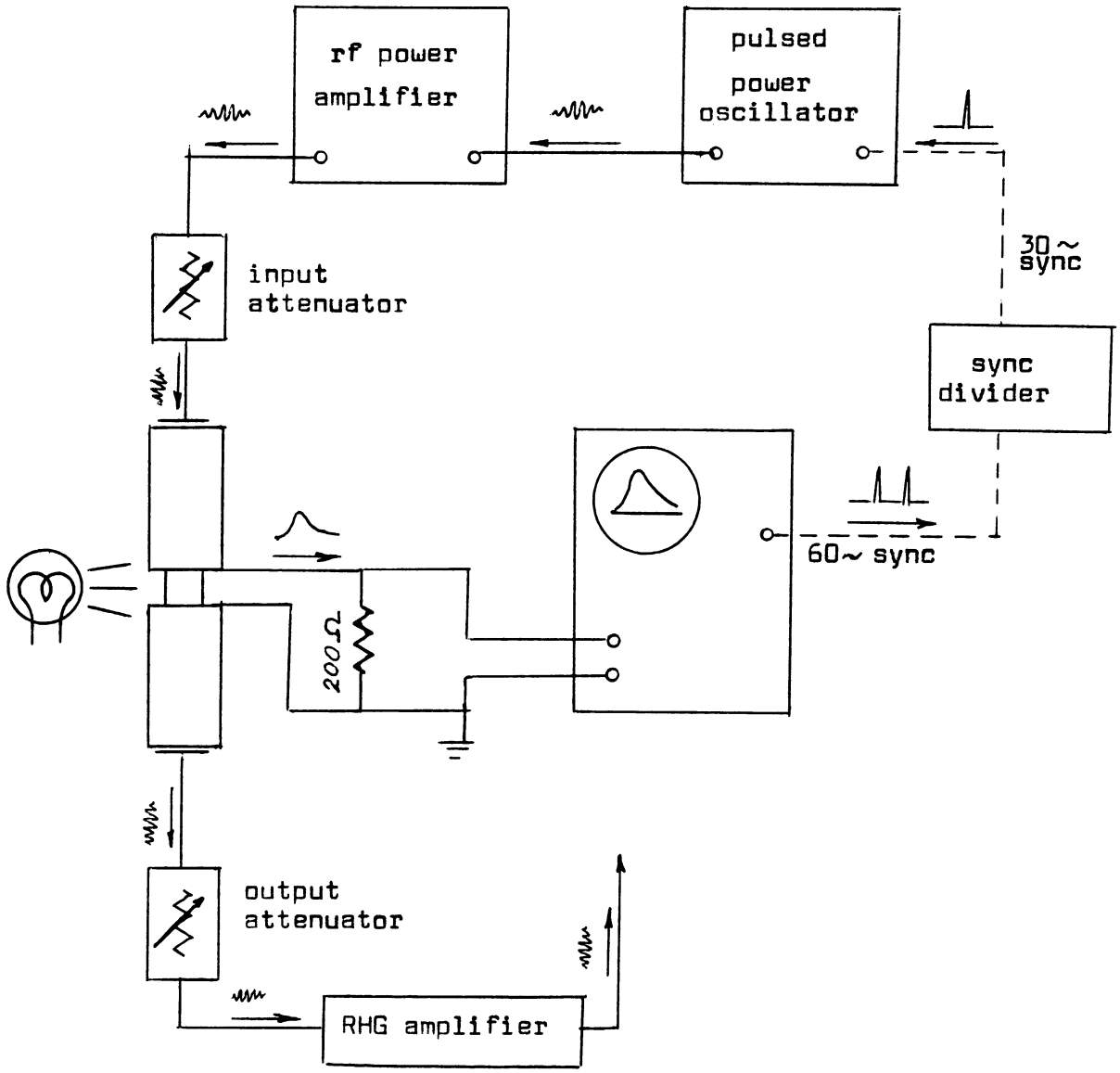

Fig. 19. Block diagram of the arrangement of electronic equipment used in the experiment.

quirement that there be enough output signal at most crystal resistivities to permit observation of the acoustoelectric current over a wide range of input acoustic energy densities.

At very high crystal resistivity ($r > 5 \times 10^4$ ohm-cm) it was necessary to substitute a 2000 ohm resistor in order that there be enough voltage drop for acoustoelectric current measurements in the small-signal region. When this resistor was first installed, capacitive loading by the oscilloscope and the connecting cable caused appreciable distortion of the trace. In Section 1.4 we showed that the rate of change of the observed current J(t) was limited by the "low pass filter" time constant

$$\tau_e = \frac{1}{\alpha v_s} .$$

In our experimental crystal the maximum value of α was 65 db/cm. Thus τ_e was never less than .62 μsec. Therefore, for accurate reproduction of acoustoelectric current waveforms (we neglect the 30 Mc ripple component), the current sampling circuit had to have a time constant short compared to 620 nanoseconds.

Capacitive loading of the 2000 ohm resistor was limited by placing a cathode follower immediately adjacent to the current output terminals of the sample holder. The cathode follower was a single 6AK5 vacuum tube connected with the screen grid driven by the cathode. This arrangement shunted the crystal with a measured capacitance less then 7 pf, giving a time constant smaller than 14 nanoseconds. It is thus apparent that the measuring circuit should not distort the acoustoelectric current pulse. That it did not was

experimentally verified by substituting much smaller resistors and carefully comparing the observed current traces.

All observations of acoustoelectric waveforms were taken directly from the oscilloscope screen as recorded by a Tektronix C-12 camera with a Polaroid roll film back. This permitted convenient recording on a single photograph (with appropriate adjustments of the oscilloscope vertical sensitivity switch) of acoustoelectric current traces taken at two or more different acoustic input power levels. The usefulness of this technique in displaying and studying power-dependent effects will be shown in Section 5.1.

There were times during the experiment when it was necessary to view the transmitted acoustic wave as it appeared at the output transducer. At those times the output transducer was coupled through a Telonic TG-950 attenuator to a RHG model E3010 30 Mc broadband tuned amplifier, and the amplified signal was then available for display on the oscilloscope screen.

4.3 MODIFICATION FOR HIGH ACOUSTIC POWER

At 30 Mc the Arenberg pulsed oscillator was capable of a maximum output of about 90 v peak across 50 ohm. Trial experimentation revealed this level of excitation to be insufficient for observation of power-dependent acoustoelectric effects. This was in large part due to the poor transmission efficiency of the poly-alpha methyl styrene acoustic bonds (Section 4.1). Comparison of observed acoustoelectric current levels with results generated by machine computation verified that additional excitation was needed for the production of power-dependent effects. This was achieved by feeding the

pulsed oscillator output through a Heathkit HA-10 linear rf power amplifier (a 1 kw grounded-grid amplifier designed primarily for class-B amplification of radio amateur single sideband signals) to boost the excitation voltage to an amplitude of 350 v peak across 50 ohms, a gain of 12 db. Power-dependent effects were then clearly evident.

The power amplifier did distort the envelope of the rf excitation pulse. This in no way upset the accuracy of the experiment, as it was only necessary to record the shape of the excitation envelope as it appeared at the input transducer in order to properly include it in the computer program.

CHAPTER V

COMPARISON OF RESULTS

As has been mentioned in other chapters, the experimental data were collected on a 7 mm CdS crystal oriented for use with shear waves. The shear mode was chosen because the relatively longer transit time (4.0 μsec vs. 1.63 μsec for the longitudinal mode) produces longer acoustoelectric current traces for study.

Certain physical constants of the crystal are needed as input data for the computer program. They are

$$\mu = 315 \frac{\text{cm/sec}}{\text{v/cm}}$$

$$K^2 = .0284$$

$$v_s = 1.75 \times 10^5 \text{ cm/sec}$$

$$\omega/\omega_D = .0393$$

Numerical values for the mobility and the electromechanical coupling coefficient in this experimental sample are due to Henrich.[13] The mobility was determined from Hall measurements on the crystal, and K^2 was chosen by Henrich to give the best fit of a theoretical curve (computed from the small-signal theory of Hutson and White) to an experimental plot of attenuation as a function of conductivity. These curves are reproduced in Fig. 20. Incidentally, the fact that the fitted curve tends to zero in the high resistivity limit indicates that nonelectronic losses in the crystal (see Section 1.5) are small enough to be neglected.

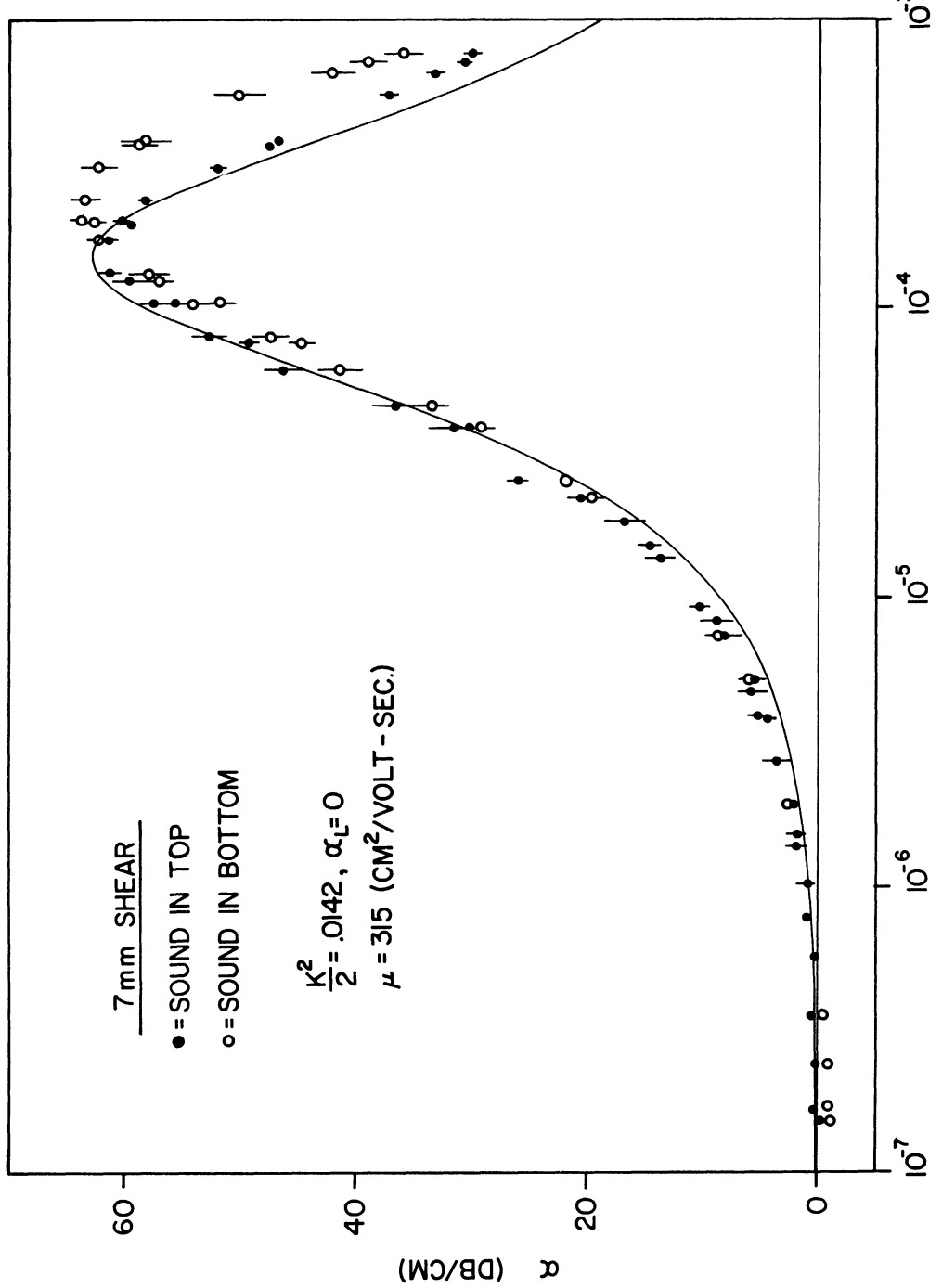

Fig. 20. Experimental data and fitted theoretical curve for attenuation as a function of crystal conductivity for our experimental sample. The two sets of data points are for the two directions of sound propagation in the crystal. The data and the fitted curve are the work of Henrich.[12]

Numerical values for v_s and ω_D are those given by Hutson and White. No attempt has been made to adjust ω_D for the slight differences in mobility or ambient temperature in our particular experiment, since such corrections would be too small to influence significantly the final form of the computer-generated acoustoelectric current traces.

This crystal was one of several reported on by Henrich and was the only one of that group which had a mobility independent of photoconductivity and at the same time did not exhibit a large first-order (linear) conductivity gradient in the direction of acoustic propagation. None of the crystals examined by Henrich was homogeneous in its photoconductivity (presumably due to a nonuniform distribution of impurities), but this one was at least a little better than the others. As we shall see later in the chapter, the inhomogeneity ultimately limits our ability to make quantitative comparisons between the predictions of the acoustoelectric feedback theory and the results of experiment.

5.1 DIRECT COMPARISON OF WAVEFORMS

The most striking verification of the acoustoelectric feedback theory comes from a comparison of oscilloscope traces of the acoustoelectric current with computer-generated predictions of those traces. For this comparison the experimental data were recorded by a method especially suited to the display of power-dependent effects. At a given crystal resistivity acoustoelectric current traces produced for several different settings of the input attenuator were superimposed (by multiple exposure) on a single oscilloscope

photograph. Each of these traces was normalized with respect to the acoustic input power by compensating every adjustment of the input attenuator with an opposite adjustment of the oscilloscope vertical sensitivity switch. Had there been only a simple linear relationship between acoustoelectric current and input acoustic power (as is predicted by the basic small-signal theory), then the traces for the different levels of input acoustic energy would have coincided exactly, as in Fig. 6(b). The fact that they did not is clear evidence that power-dependent effects were indeed present.

The 30 Mc ripple component (due to the boundary condition; Section 1.3) permits us to easily distinguish which trace is which on an oscilloscope photograph. The ripple is proportional to the input acoustic amplitude, whereas the acoustoelectric current is proportional to the input acoustic energy. Since all traces on a photograph are normalized with respect to the acoustic input power, the trace with the <u>smaller</u> ripple is the one produced by the <u>higher</u> energy input wave. (The amplitude of the ripple component is also proportional to the crystal conductivity, so traces generated at low crystal resistivity have a larger ripple than those generated at high.)

Application of the full amplified rf excitation (described in Section 4.3) to the input transducer produced a maximum mechanical strain amplitude (at the peak of the wave) of about 6.4×10^{-5} at the input face of the CdS crystal. This corresponds to a local acoustic energy density of 150 ergs/cm^3 (the measurement of which will be discussed in Section 5.2), and all settings of the input attenuator are referred to this level. These settings serve as a convenient way of specifying the acoustic input energy used to produce the oscilloscope traces.

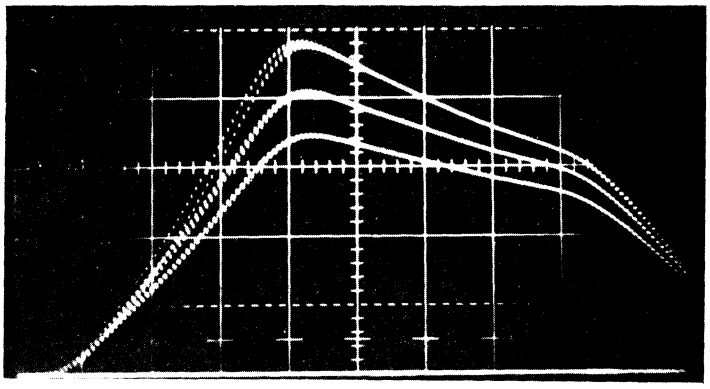

(a) Sound in "A" direction.

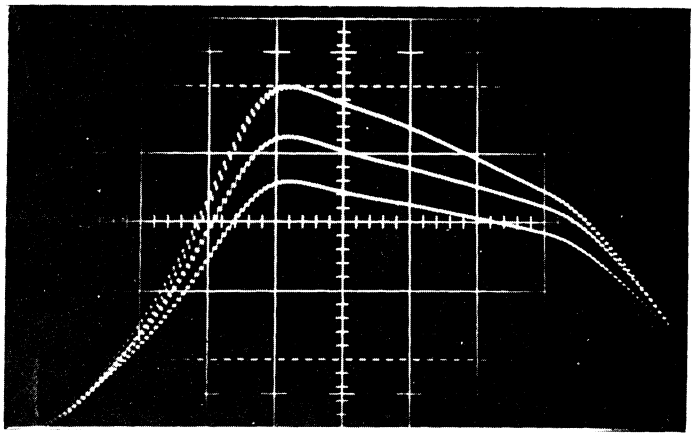

(b) Sound in "B" direction.

Fig. 21. Power-dependent acoustoelectric waveforms for crystal resistivity of 1.80×10^5 ohm-cm. Time base = .5 μsec/cm. Ext. resistor = 2000 ohm. Listed according to peak height, the traces on each photograph are:

Trace	Attenuator	Vertical Scale
Top	-10 db	.02 v/cm
Center	-3 db	.1 v/cm
Bottom	0 db	.2 v/cm

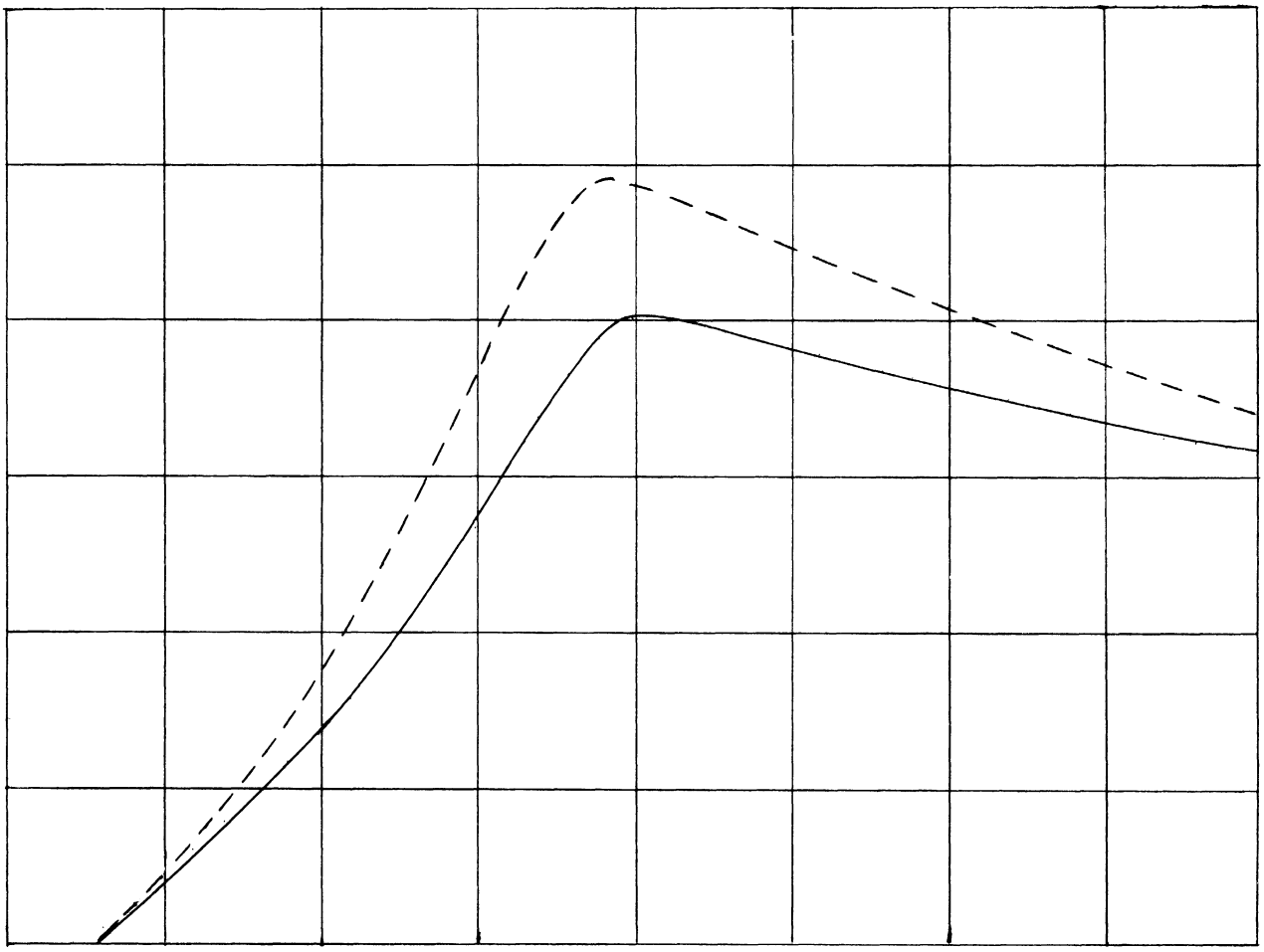

Fig. 22. Computer-generated acoustoelectric waveforms for resistivity of 1.80×10^5 ohm-cm. Time base = .5 μsec/division. External resistor = 2000 ohm. The traces shown are:

Trace	Acoustic Input Energy	Vertical Scale
- - -	-10 db	.02 v/division
———	0 db	.2 v/division

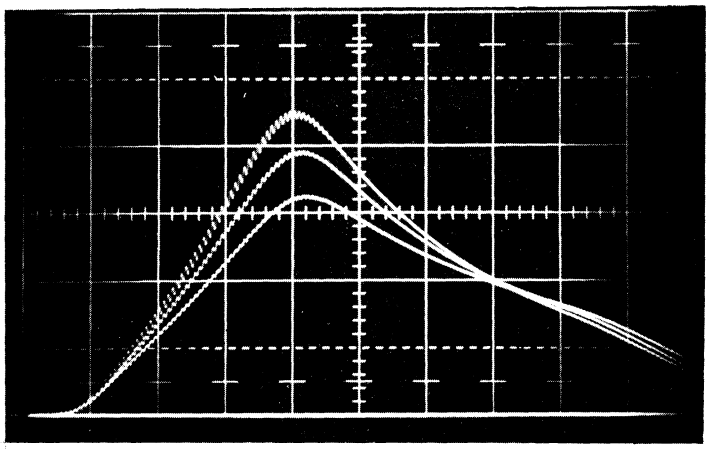

(a) Sound in "A" direction

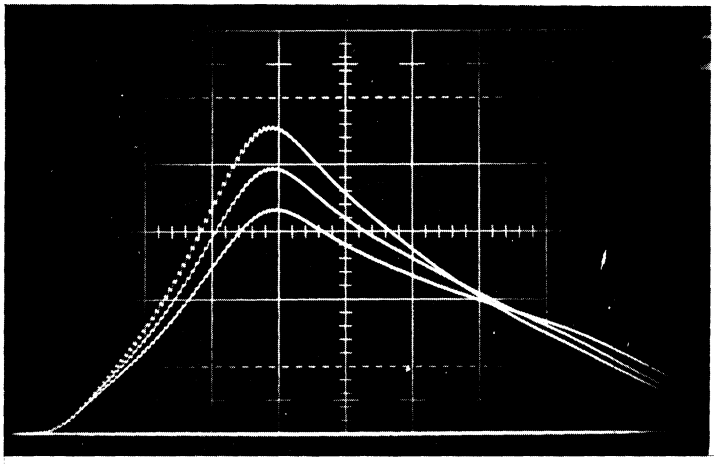

(b) Sound in "B" direction.

Fig. 23. Power-dependent acoustoelectric waveforms for crystal resistivity of 6.12 x 10^4 ohm-cm. Time base = .5 μsec/cm. External resistor = 2000 ohm. Listed according to peak height, the traces on each photograph are:

Trace	Attenuator	Vertical Scale
Top	-10 db	.05 v/cm
Center	- 4 db	.2 v/cm
Bottom	0 db	.5 v/cm

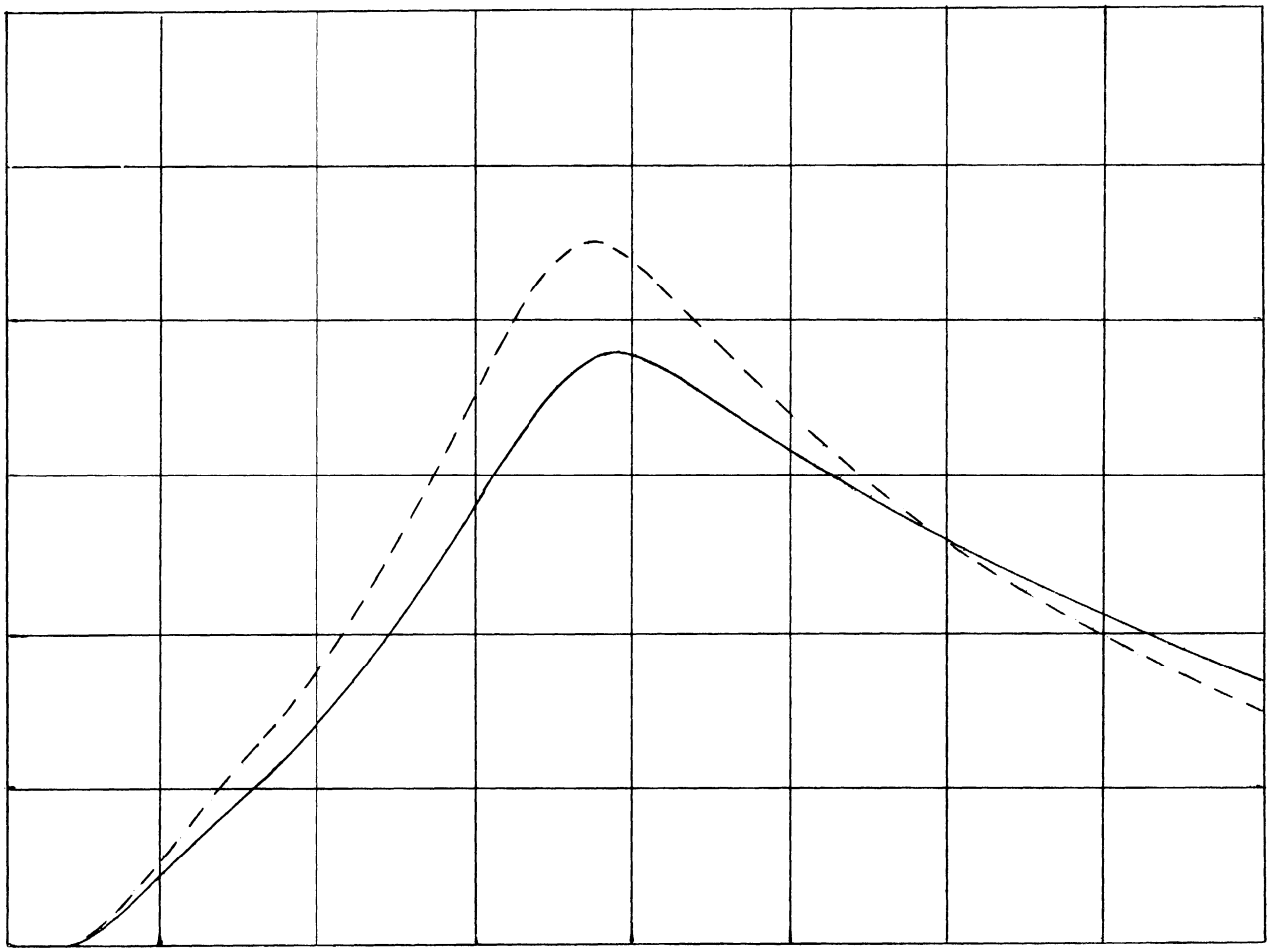

Fig. 24. Computer-generated acoustoelectric waveforms for resistivity of 6.12×10^4 ohm-cm. Time base = .5 μsec/division. External resistor = 2000 ohm. The traces shown are:

Trace	Acoustic Input Energy	Vertical Scale
- - -	-10 db	.05 v/division
———	0 db	.5 v/division

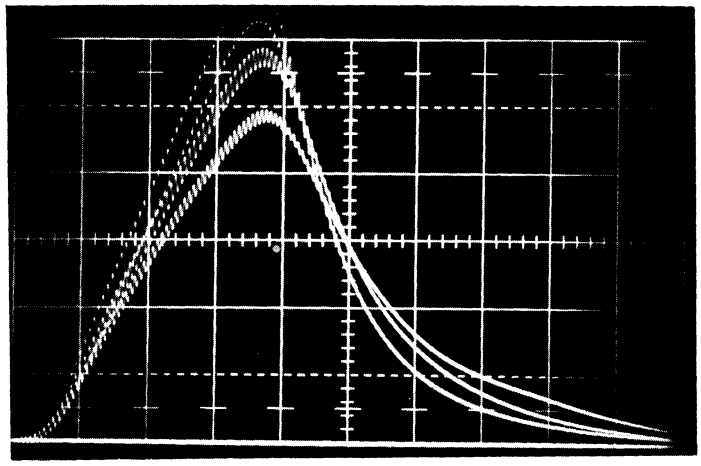

(a) Sound in "A" direction.

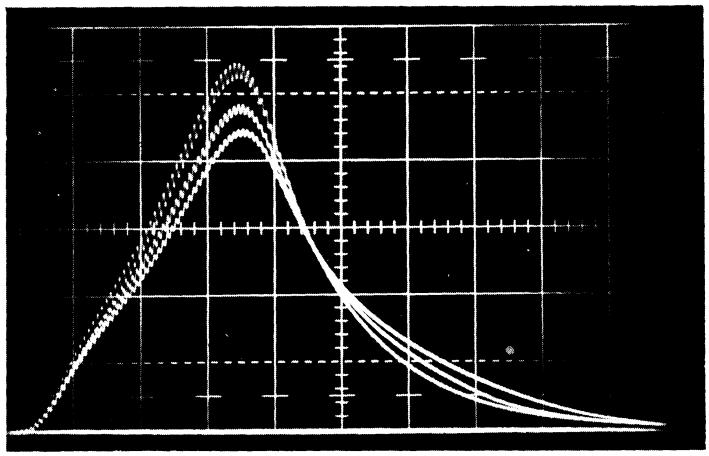

(b) Sound in "B" direction

Fig. 25. Power-dependent acoustoelectric waveforms for crystal resistivity of 1.27×10^4 ohm-cm. Time base = .5 μsec/cm. Ext. resistor = 200 ohm. Listed according to peak height, the traces on each photograph are:

Trace	Attenuator	Vertical Scale
Top	-10 db	.01 v/cm
Center	-3 db	.05 v/cm
Bottom	0 db	.1 v/cm

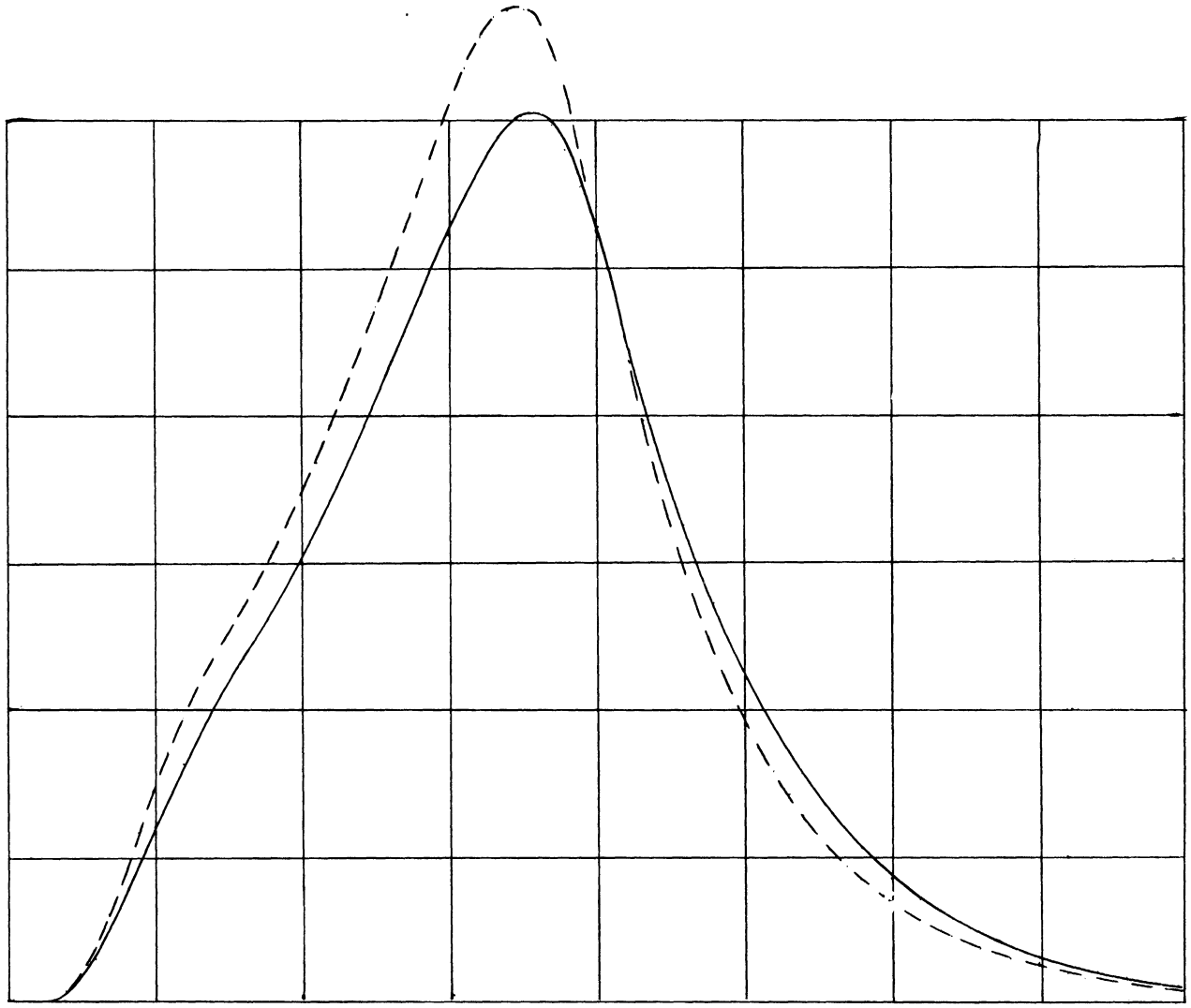

Fig. 26. Computer-generated acoustoelectric waveforms for resistivity of 1.27×10^4 ohm-cm. Time base = .5 μsec/division. External resistor = 200 ohm. The traces shown are:

Trace	Acoustic Input Energy	Vertical Scale
- - -	-10 db	.01 v/division
———	0 db	.1 v/division

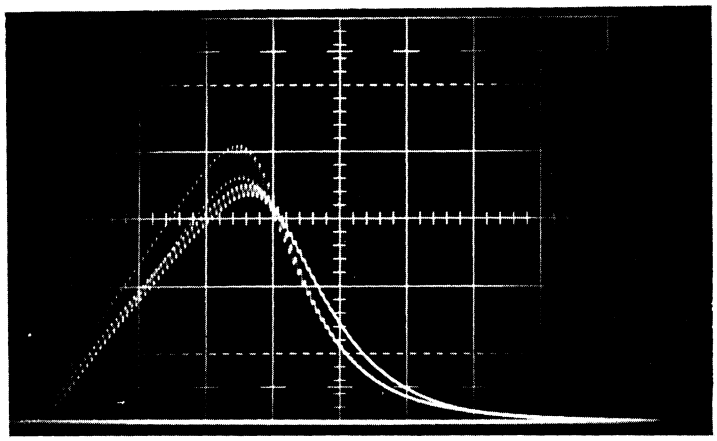

(a) Sound in "A" direction.

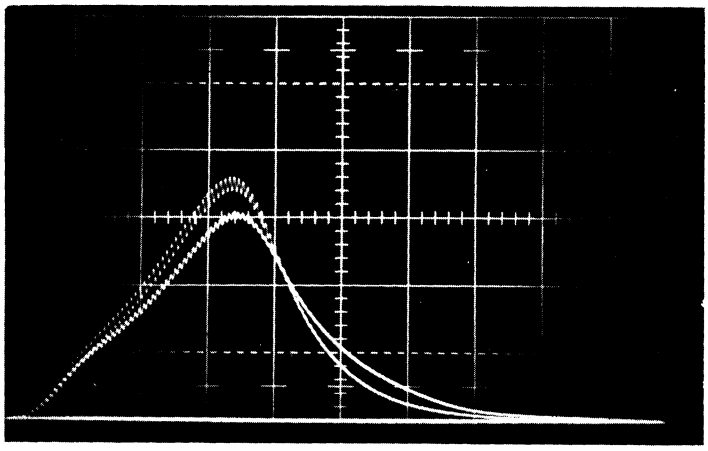

(b) Sound in "B" direction.

Fig. 27. Power-dependent acoustoelectric waveforms for crystal resistivity of 4.46×10^3 ohm-cm. Time base = .5 μsec/cm. Ext. resistor = 200 ohm. Listed according to peak height, the traces on each photograph are:

Trace	Attenuator	Vertical Scale
Top	-10 db	.02 v/cm
Bottom	0 db	.2 v/cm

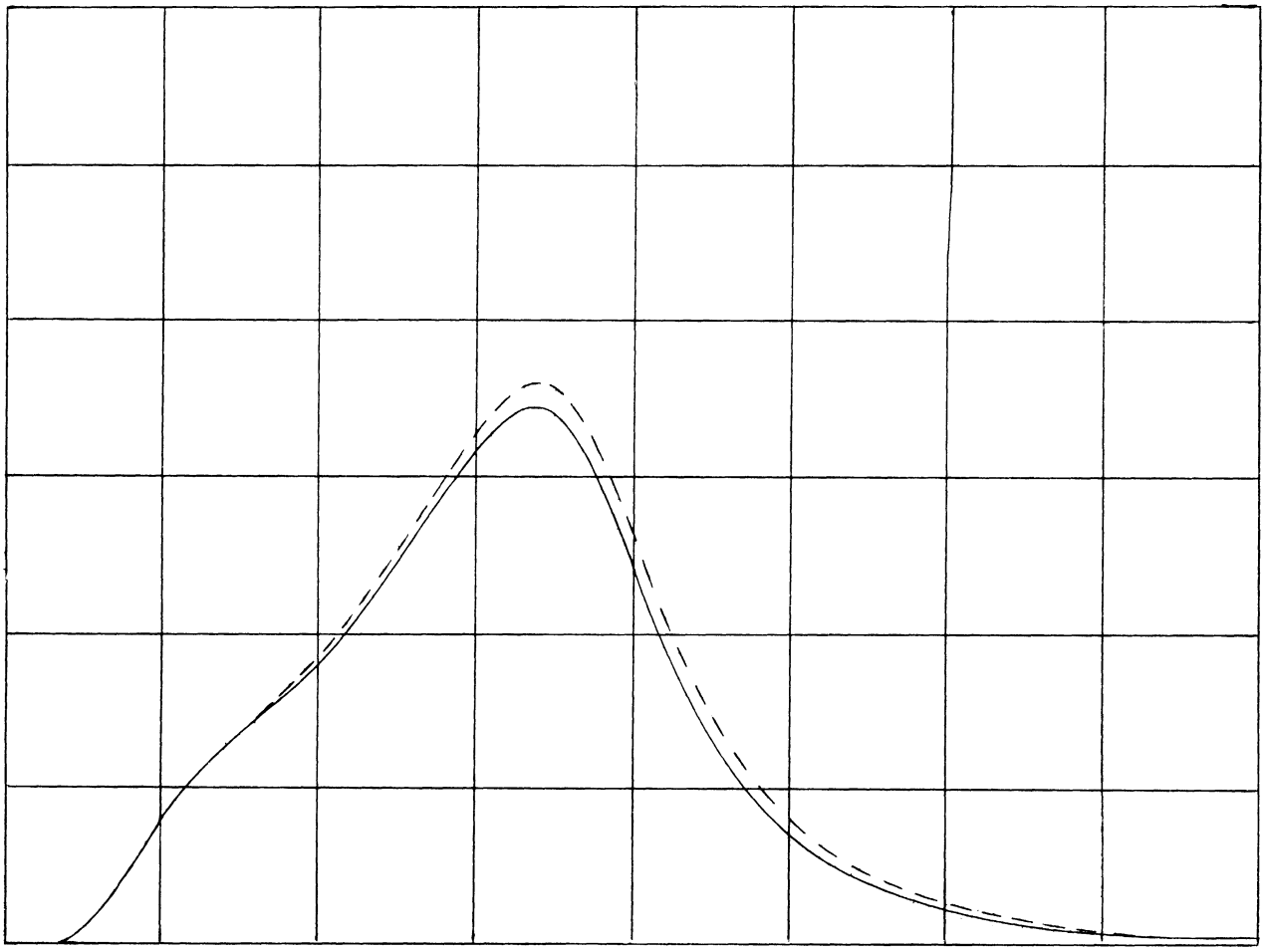

Fig. 28. Computer-generated acoustoelectric waveforms for resistivity of 4.46×10^3 ohm-cm. Time base = .5 μsec/division. External resistor = 200 ohm. The traces shown are:

Trace	Acoustic Input Energy	Vertical Scale
- - -	-10 db	.02 v/division
———	0 db	.2 v/division

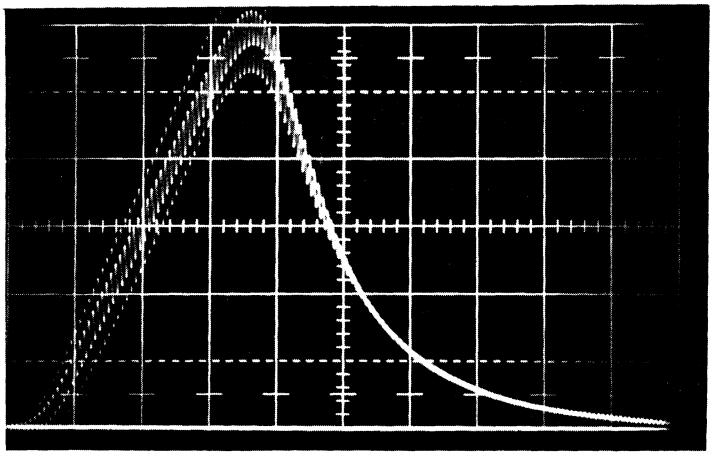

(a) Sound in "A" direction.

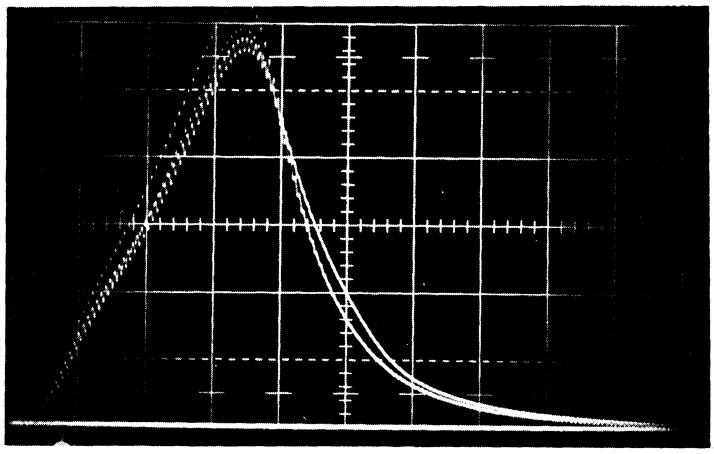

(b) Sound in "B" direction.

Fig. 29. Power-dependent acoustoelectric waveforms for crystal resistivity of 2.08 x 10^3 ohm-cm. Time base = .5 μsec/cm. Ext. resistor = 200 ohm. Listed according to peak height, the traces on each photograph are:

Trace	Attenuator	Vertical Scale
Top	-10 db.	.01 v/cm
Bottom	0 db	.1 v/cm

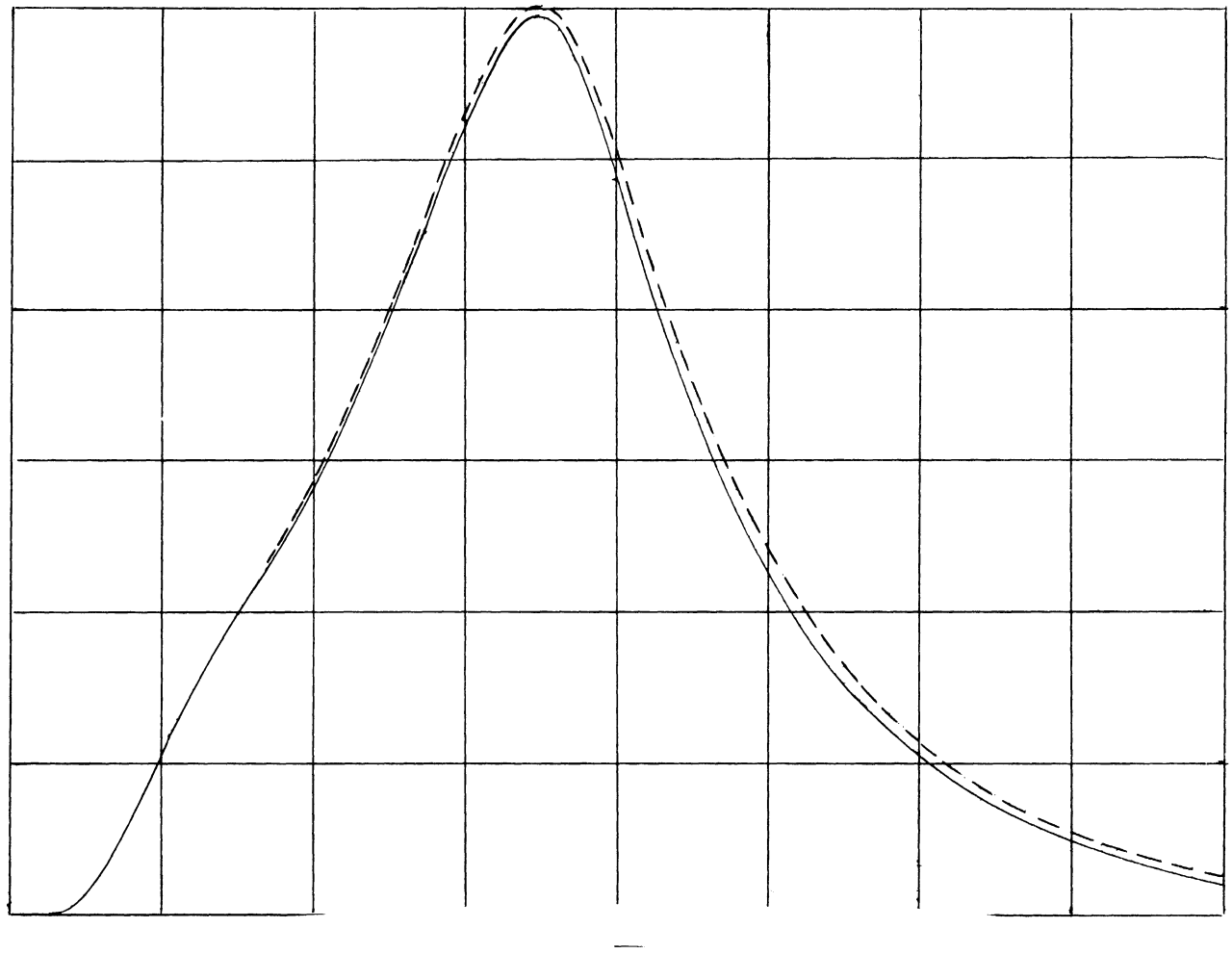

Fig. 30. Computer-generated acoustoelectric waveforms for resistivity of 2.08×10^3 ohm-cm. Time base = .5 μsec/division. External resistor = 200 ohm. The traces shown are:

Trace	Acoustic Input Energy	Vertical Scale
- - -	-10 db	.01 v/division
———	0 db	.1 v/division

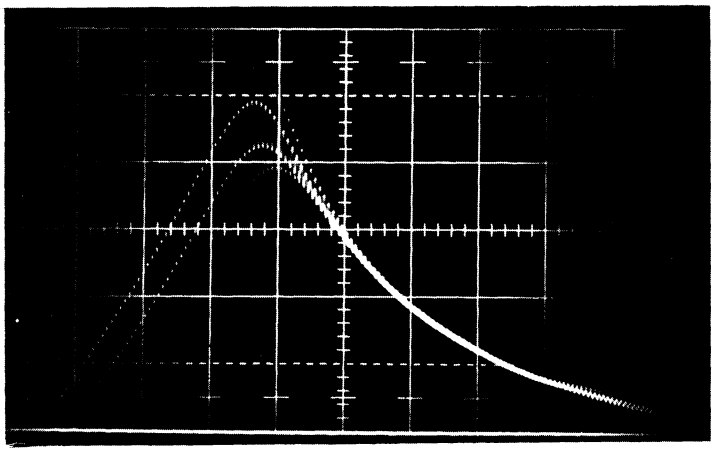

(a) Sound in "A" direction.

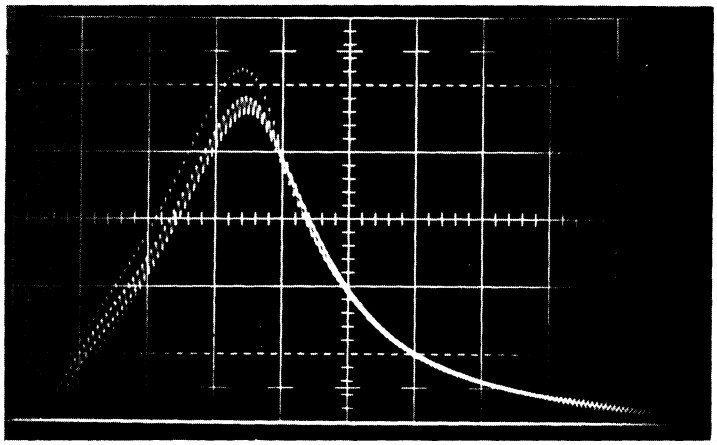

(b) Sound in "B" direction.

Fig. 31. Power-dependent acoustoelectric waveforms for crystal resistivity of 1.01 x 10^3 ohm-cm. Time base = .5 μsec/cm. Ext. resistor = 200 ohm. Listed according to peak height, the traces on each photograph are:

Trace	Attenuator	Vertical Scale
Top	-10 db	.01 v/cm
Bottom	0 db	.1 v/cm

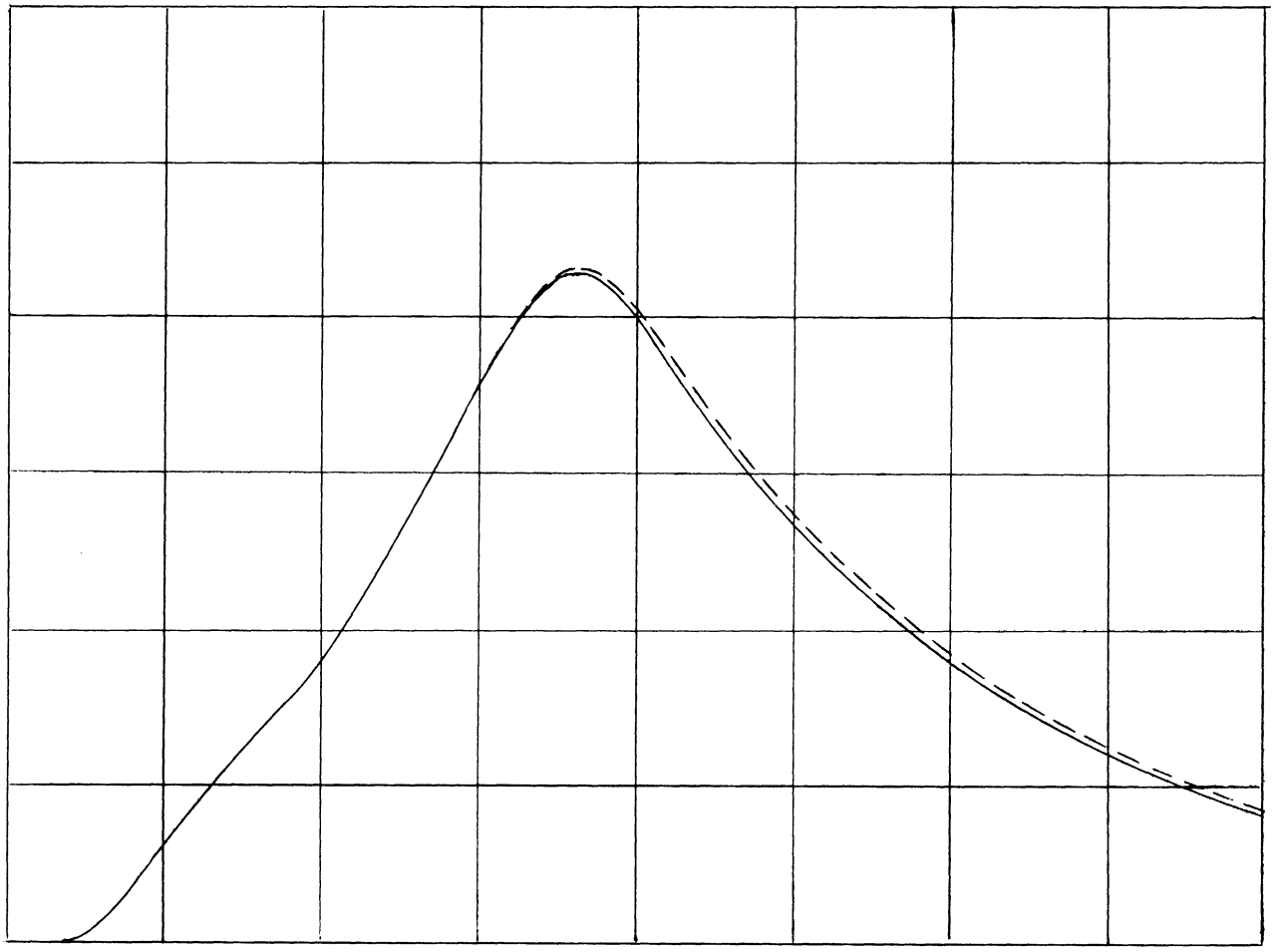

Fig. 32. Computer-generated acoustoelectric waveforms for resistivity of 1.01 x 10^3 ohm-cm. Time base = .5 μsec/division. External resistor = 200 ohm. The traces shown are:

Trace	Acoustic Input Energy	Vertical Scale
- - -	-10 db	.01 v/division
———	0 db	.1 v/division

The computer-generated plots of the acoustoelectric current may be compared directly with the oscilloscope traces (Figs. 21-32). To aid the comparison, acoustic input energies for the computed traces are also given in db referred to 150 ergs/cm^3 at the peak of the wave. For the high resistivity cases ($\frac{1}{\omega\tau} < 1$) we immediately notice three areas of agreement between theory and experiment (Figs. 21-26). With increasing acoustic input energy we observe (1) a relative decrease in the peak height of the trace, (2) a slight delay in time of the occurrence of this peak, and (3) a slowed rate of decay of the current following the peak.

For the low resistivity cases ($\frac{1}{\omega\tau} > 1$) there is much less high power distortion of the acoustoelectric current trace (Figs. 27-32), at least with the acoustic power level achievable in this experiment. This is apparent in both the experimental and the computer-generated traces (the 4.5×10^3 ohm-cm experimental case of Fig. 27 needs special consideration and will be discussed later). In comparing other details of this generally diminished power-dependent effect, we see that both theory and experiment show a reduced relative peak height at high acoustic input power, but there otherwise is not the satisfying overall agreement evident in the high resistivity case.

We must ask whether these are the results we expected. We know that the attenuation coefficient can be modified either through local changes in the crystal conductivity or by local electric fields. These two influences are best understood by studying their behavior on a plot of α vs. $-\mu E$ (Fig. 33). On such a plot the conductivity determines the displacement of the peaks of maximum and minimum α from the point $\gamma = 0$:

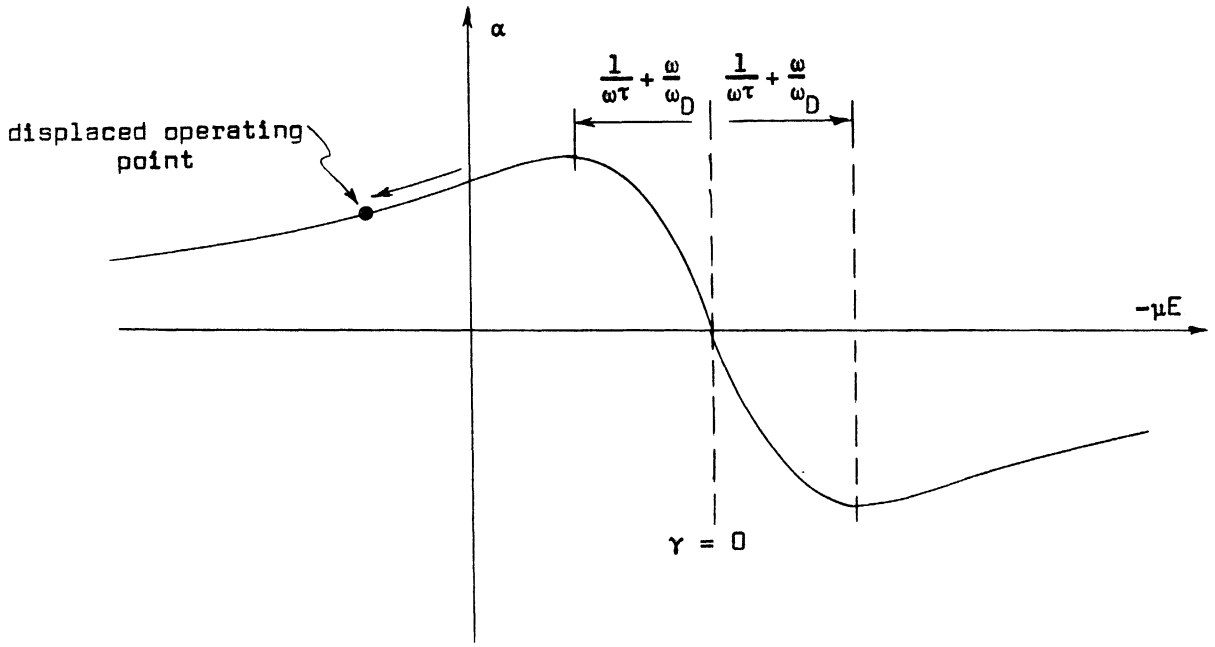

(a) The high resistivity case ($\frac{1}{\omega\tau} < 1$).

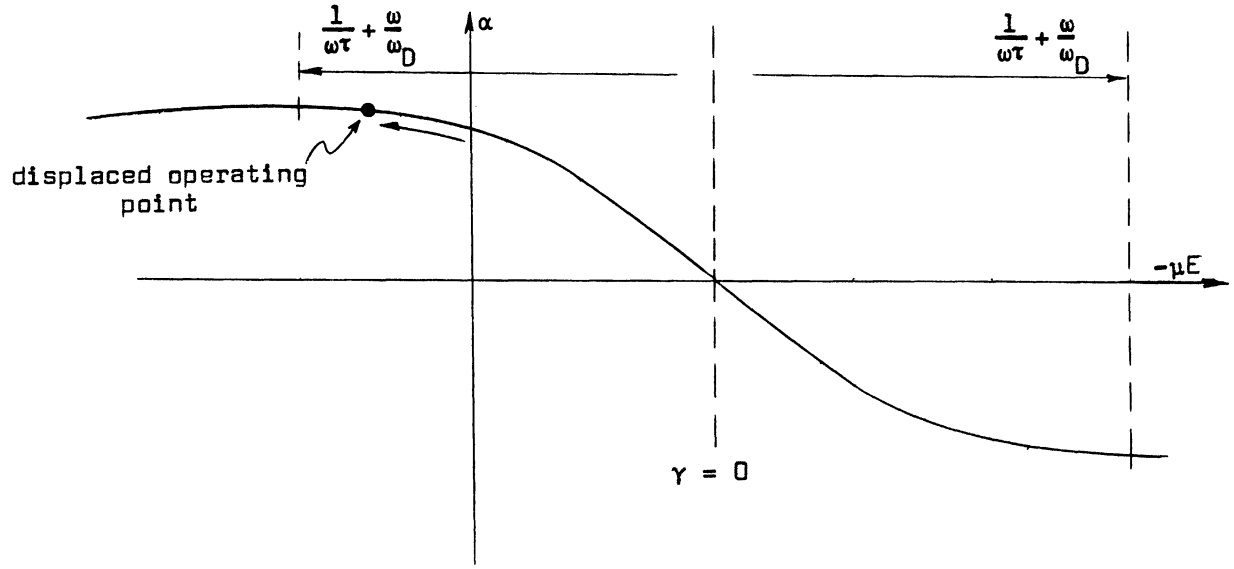

(b) The low resistivity case ($\frac{1}{\omega\tau} > 1$).

Fig. 33. Illustration showing how the local electric field influences the attenuation coefficient by displacing the operating point.

$$\gamma_{\min}^{\max} = \pm \frac{1}{\omega\tau} , \tag{5.1}$$

whereas the local electric field fixes the position of the operating point on this curve:

$$\gamma = 1 + \frac{\mu E}{v_s} . \tag{5.2}$$

The influence of the local electric field is relatively easy to predict. In general, the electric field will be largest in the region of highest acoustic energy density, and its sign will be positive (see Eq. (3.26)). It therefore displaces the operating point to the left on a plot of α vs. $-\mu E$.

To estimate the influence of local conductivity changes we notice that, because the electric field is a maximum near the peak of the wave, the average value of its slope is zero in the immediate neighborhood of this maximum. From Eq. (3.5) it follows that the average conductivity change near the peak of the wave should be small, since

$$qn' = -\epsilon \frac{\partial E}{\partial x} . \tag{5.3}$$

Therefore, to first approximation any changes in the acoustic attenuation rate at the peak of the wave may be attributed to the influence of the electric field alone.

At high crystal resistivity ($\frac{1}{\omega\tau} < 1$) the peak of maximum α falls to the right of the vertical axis, and the local electric field produces a reduced attenuation coefficient in regions of high acoustic energy density (Fig. 33(a)). The effect is to some degree self-sustaining, since the high acoustic

energy density causes a local reduction in the acoustic attenuation rate which in turn helps maintain the high acoustic energy density.

In Section 1.4 we developed an equivalent circuit model for predicting the detailed shape of the acoustoelectric current trace produced by a uniformly attenuated wave. According to the model a decrease in the attenuation rate will cause the peak of the circulating current to be reduced in amplitude and delayed in time and be followed by a more slowly decaying tail. For the case of high crystal resistivity we have shown that a propagating acoustic wave of large amplitude encounters a (nonuniformly) reduced attenuation rate. These generalized predictions for the changed shape of the observed current trace should therefore be valid. That they do apply is verified both by the output of the computer program and by the results of experiment.

At low crystal resistivity ($\frac{1}{\omega\tau} > 1$) the peak of maximum α falls to the left of the vertical axis (see Fig. 33(b)). Again the trend is for the local electric field to move the operating point to the left, but the operating point is now being pushed <u>toward</u> the peak. If it does not pass the peak (this is something about which we cannot accurately guess), then large amplitude regions of the wave should see an enhanced acoustic attenuation rate. According to the model of Section 1.4, this should cause the peak of the observed current to occur slightly earlier, be a little higher, and be followed by a more rapidly decaying tail. However, the increased dissipation will also more rapidly consume the acoustic energy, thereby diminishing the power-dependent effect and making changes in the acoustoelectric current trace less pronounced than they were for the high resistivity case.

The observable effect is much milder, as we have already noted. The computer-generated traces (Figs. 28, 30, and 32) also show a slightly earlier peak and an almost infinitesimally enhanced decay rate following the peak, but they predict a reduced rather than an increased peak height. Since our informal estimate was based on only a perfunctory consideration of electric field and conductivity behavior which is treated in detail by the computer program, the computer-generated results must of course take precedence. The computer program also accounts for the possibility that the peak and the operating point may cross. The important question is whether or not the computer-generated traces agree with the results of experiment.

There is little agreement where there is a significant power-dependent effect, as may be seen by comparing the experimental and theoretical results of Figs. 27-32. In fact, the experimentally recorded traces for the two directions of propagation do not even look alike. These experimental discrepencies are at least partially explained by a peculiarity of our CdS crystal. In Section 2.3 we observed that the point of maximum height on a plot of α vs. $\omega\tau$ (Fig. 13) occurs at the conductivity value for which the peak of maximum attenuation falls exactly on the vertical axis on a plot of α vs. E_o (Fig. 12). But the experimental plots of Fig. 20 are split at high conductivity (because of inhomogeneous crystal conductivity, as we shall explain shortly). It is therefore not surprising that the low resistivity experimental data recorded for the two directions of propagation agree neither with the theory nor with each other. This explains the serious discrepancy between theory and experiment for the 4.5×10^3 ohm-cm case (Figs. 27 and 28),

since this particular value of the conductivity (2.2×10^{-4} ohm/cm) falls between the two experimental peaks.

5.2 QUANTITATIVE COMPARISONS

We have not yet said how we experimentally determine the input acoustic energy so that we may have this data for use in the computer program. Ideally we should know exactly the acoustic strain amplitude $S(0,t)$ at the input face of the CdS crystal. The envelope shape of the acoustic wave packet is easily measured by placing a low-capacitance oscilloscope probe at the input transducer, but, since the transmission efficiency of the bonds is unknown, this is of value as a relative measurement only.

For absolute determination of the acoustic input power we must resort to the following indirect technique: We choose a crystal resistivity for which there is good agreement between experimental and theoretical values of the attenuation coefficient as determined by the crystal conductivity. For our particular experimental sample (see Fig. 20) it is clear that this will have to be a resistivity for which $1/\omega\tau < 1$. Then, by using the measured shape of the acoustic wave as input to the computer program and scaling it up and down over a wide range of closely spaced input power levels, we generate a family of theoretical acoustoelectric current plots. These may be compared with an experimentally-generated family of oscilloscope traces produced at the same crystal resistivity. The computer plots may then be paired with the oscilloscope traces by equating peak heights. The pairing must be done in the small-signal region where there is a linear relationship between peak current and

acoustic input power. Then, if all goes well, the matching should be consistent into the large-signal region where power-dependent effects occur.

The matching is not exact, as may be seen by careful study of experimental and computer-generated traces for the high-resistivity case (Figs. 21-26). In general the observed power-dependent effect is stronger than that predicted by the computer program, that is the difference in peak heights is greater for the observed than for the computed traces. There is therefore a discrepancy between the predictions of the acoustoelectric feedback theory and the results of experiment.

Let us first criticize the theory. Perhaps the most serious deficiency of the acoustoelectric feedback theory is a failure to account for the influence of the second harmonic component of the acoustoelectric current (see Section 2.4) on the local charge densities and velocities which control acoustic attenuation. Because of its large amplitude (equal to the local dc value of the acoustoelectric current) this influence must be considerable. But it would have been extremely difficult to include this effect in the acoustoelectric feedback theory, since it lies outside the scope of the small-signal theory of Hutson and White on which it is based. The small-signal theory treats the influence of "dc" electric fields and conductivities on the local attenuation experienced by a propagating acoustic wave and in its present form cannot account for the interaction of the wave with oscillatory currents of frequency 2ω.

We would have been surprised indeed had our perturbation extension of the small-signal theory been capable of accounting entirely for the changed

shape of the acoustoelectric current trace generated under large-signal conditions. At the beginning of Chapter III we claimed that, in the absence of an adequate large-signal theory, the acoustoelectric feedback theory would make meaningful predictions of large-signal effects. This much we have certainly done, as is shown by the very gratifying qualitative agreement between the experimental photographs and the computer-generated traces for the high resistivity case (the only case where we can also get low power agreement). But it would be foolish to insist that all large-signal distortions of the observed current trace could be explained in terms of the influence of local "dc" electric fields and charge densities on the small-signal interaction. What we can claim is that this influence most assuredly contributes heavily to the changed shape of the observed current trace, as we have demonstrated by the experimental and theoretical results of Figs. 21-26.

Now let us criticize the experiment. For the low resistivity case we have seen that the observed current traces recorded for opposite directions of propagation at a given crystal resistivity not only do not match the computer-generated plots; they also do not match each other. For the high resistivity case we already know that there is some disagreement between computed and measured heights of the trace under large-signal conditions. What about other details of the changed shape of acoustoelectric current traces generated by acoustic waves of large amplitude?

The most meaningful comparison of shapes is between slopes of that part of the acoustoelectric current trace produced while the wave is entirely within the crystal. It is this portion of the trace which should be a perfect

decaying exponential under the ideal small-signal condition of uniform acoustic attenuation. The method of comparing these slopes need not be elaborate or sophisticated, providing we consistently use the same technique for both the observed and the computed waveforms, e.g., we can simply measure the height of each trace at the same two points in time and then compute an "average" attenuation coefficient from the formula

$$\alpha_{db} = \frac{1}{(t_2-t_1)v_s} 10 \log_{10} \frac{j(t_1)}{j(t_2)} . \qquad (5.4)$$

The results of such a comparison are plotted in Fig. 34 for two different crystal resistivities. It is apparent that the experimental and theoretical plots show the proper qualitative behavior, i.e., they all tend toward a reduced acoustic attenuation rate with increasing input acoustic power, but it is disturbing to observe the poor quantitative agreement. For neither resistivity do the experimental plots (for the two directions of propagation) coincide with the theoretical curve or with each other. This discrepancy extends even into the low acoustic power (small-signal) region where power-dependent effects must vanish. In fact, the two cases shown were chosen for illustration because their low power agreement was better than that attainable at other resistivities. This low power disagreement is clear evidence that the attenuation is not uniform throughout the crystal and is a direct consequence of inhomogeneity in the crystal conductivity.

This inhomogeneity may be "mapped" by studying the acoustoelectric current traces generated by short, low energy acoustic wave packets. Figure 35 shows traces generated by a low power wave packet propagating in either direc-

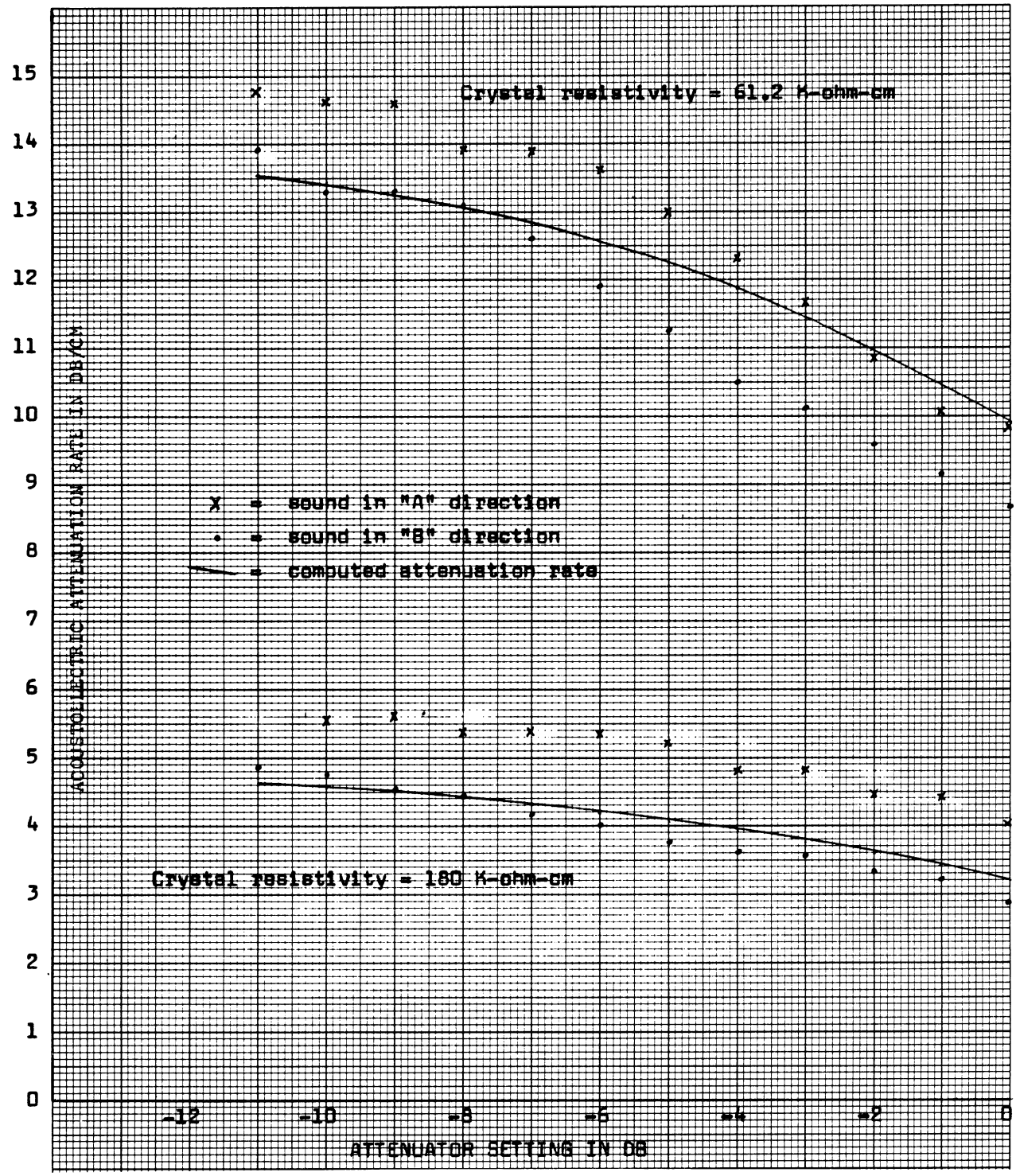

Fig. 34. Plot of slope of the tail of the acoustoelectric current trace as a function of attenuator setting.

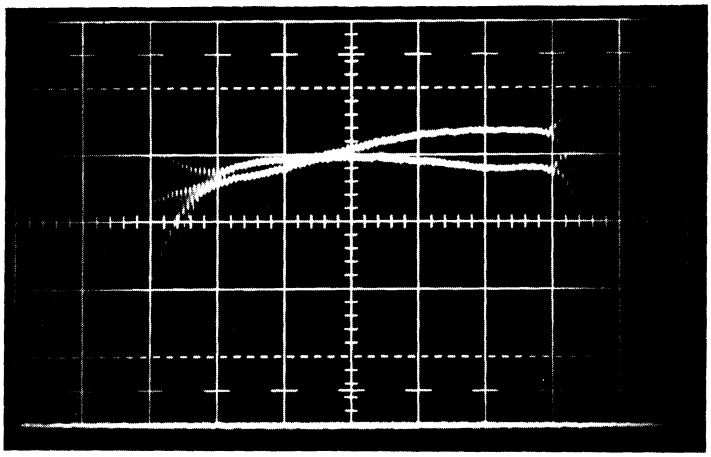

(a) Crystal resistivity = 4.4×10^6 ohm-cm.

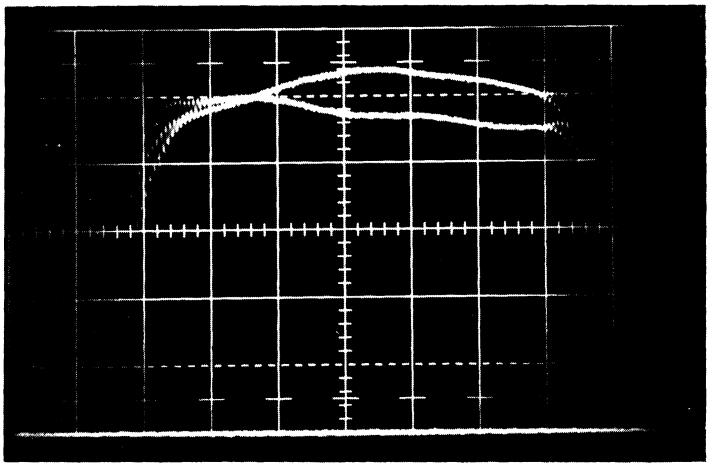

(b) Crystal resistivity = 1.0×10^6 ohm-cm.

Fig. 35. Acoustoelectric current traces generated by a 1.5 μsec input wave. Traces shown are for both directions of propagation. Vertical scale = .002 v/cm. Time base = .5 μsec/cm. Ext. resistor = 2000 ohm. The input attenuator was adjusted at each crystal resistivity to keep the traces on scale.

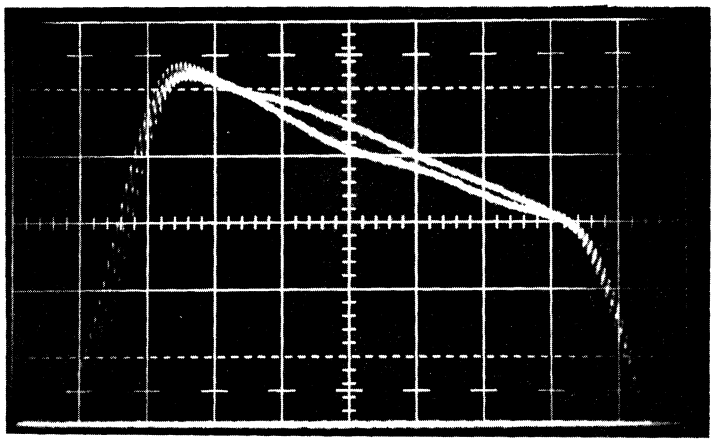

(c) Crystal resistivity = 2.2 x 10^5 ohm-cm.

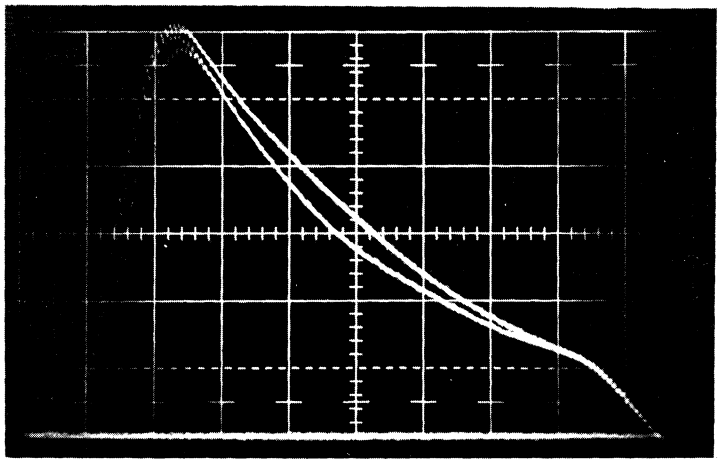

(d) Crystal resistivity = 7.0 x 10^4 ohm-cm.

tion in the crystal. These rough and irregular traces clearly illustrate how much our experimental crystal deviates from the ideal homogeneous model we implicitly assumed while writing the computer program.

Computer-predicted acoustoelectric current traces based on a single external measurement of the crystal resistance cannot hope to agree with this data. Under small-signal conditions the computer program simulating a homogeneous crystal will generate an acoustoelectric current trace identical to that predicted by the model of Section 1.4, but traces experimentally recorded from an inhomogeneous crystal will differ in both height and shape from that ideal result. Quantitative comparisons of height and shape for high acoustic input power therefore become impossibly difficult, particularly since the calibration of acoustic input power levels by pairing of experimental and theoretical traces at low power levels cannot be trusted. Quantitative comparison of the slopes of the tails of these traces is also hindered, since it is not possible to judge how much of the slope is truly a measure of the attenuation coefficient and how much merely reflects a conductivity gradient.

How can we minimize these difficulties? We can begin by selecting an experimental sample which is as nearly homogeneous as is possible to obtain. This selection was discussed at the beginning of the chapter. We can also smooth out the current traces by using longer acoustic wave trains, thereby physically integrating out some of the roughness due to the irregular conductivity. This has been done for data presented here in support of the acoustoelectric feedback theory. Such a technique certainly gives better-

looking experimental results but unfortunately still does not allow quantitative comparison between a computer program which assumes homogeneity and a real crystal which is not so simple.

We may ask whether it is possible to develop a program for treating the inhomogeneous crystal. One approach would be to enter local conductivity values point-by-point into our present one-dimensional program, providing it were possible to collect such information from photographs of the acousto-electric current traces generated by very short acoustic wave packets. This scheme would be successful if the conductivity variation occurred only in the direction of the wave's propagation vector, but the irregularity of the traces displayed in Fig. 35 leads us to suspect that this is not the case, and we at present have neither the theory nor the experimental technique to treat an irregular, three-dimensional conductivity variation. Furthermore, the fact that the experimental plots of α vs. σ in Fig. 20 agree at low conductivity but split at high conductivity indicates that the crystal's inhomogeneity pattern may shift with changing photoconductivity, so that a "map" made at one conductivity would not be correct for another. In any event, rather than burden this computer program with the corrections and adjustments needed to compensate for an unsatisfactory experimental situation, the better approach would be to seek future improvement in the quality of experimental samples available for study.

5.3 DISTORTION OF THE WAVE PACKET

All of our discussion so far has been concerned with the detailed shape

of the observed current trace with little attention being given to the acoustic wave packet itself. What observable changes take place in the wave packet as a result of the acoustoelectric feedback effect? Is it possible to make predictions about these changes which may be verified by experiment?

In Section 5.1 we showed that qualitative interpretation of the altered shape of the observed current trace was relatively straightforward in the case of high resistivity, that is, that the local electric field produces a locally diminished acoustic attenuation coefficient in regions of high acoustic energy density. Different regions of the wave packet will therefore experience different acoustic attenuation rates. The sign of the effect is unambiguous for the high resistivity case; regions of higher acoustic energy density will suffer less attenuation than those of lower. The observable result will be distortion of the wave packet envelope, with irregularities in the envelope shape being emphasized so that a high region becomes relatively higher still.

The effect is dramatically illustrated in the experimental photographs of Fig. 36. Here we see signals taken from the output transducer which resulted from input signals of identical shape but differing in amplitude by 20 db. The output signals have been normalized with respect to the input acoustic amplitudes, and the larger signal is that produced by the high power input signal. We can clearly see that the irregularities in the wave packet envelope have been greatly emphasized for the high power case. For the photograph taken at a crystal resistivity of 6.21×10^4 ohm-cm, that region of the wave packet which initially had the largest amplitude experiences about 6 db

less total attenuation for the high power case than for the low power case, whereas a region of initially small amplitude suffers about the same attenuation in both cases.

The distortion of the wave packet is correctly predicted by the computer program, the results of which are shown in Fig. 37 for a crystal resistivity of 6.21×10^4 ohm-cm. The wave packet unfortunately suffers some distortion in traversing the acoustic system, even when the crystal is in the dark (condition of no acoustoelectric interaction), so accurate quantitative comparison of output wave shapes is not possible, but the strong qualitative agreement gives additional support to the validity of our acoustoelectric feedback theory.

7.4 SUMMARY

We have shown that it is possible to make meaningful predictions of large-signal distortion of the acoustoelectric current waveform by extending the small-signal theory of Hutson and White to account for the self-interaction of a decaying acoustic wave. This self-interaction occurs because the local charge velocities and changes in charge density brought about by the acoustoelectric interaction must also influence the attenuation, just as if these conditions were imposed upon the carriers from outside the crystal.

The extended small-signal theory does not completely describe the interaction of a large-amplitude acoustic wave with the electrons (as was discussed in Section 5.2), so we do not expect that such a theoretical treatment can completely explain the changed shape of the acoustoelectric current trace generated under this condition. Accordingly, we have not attempted a detailed

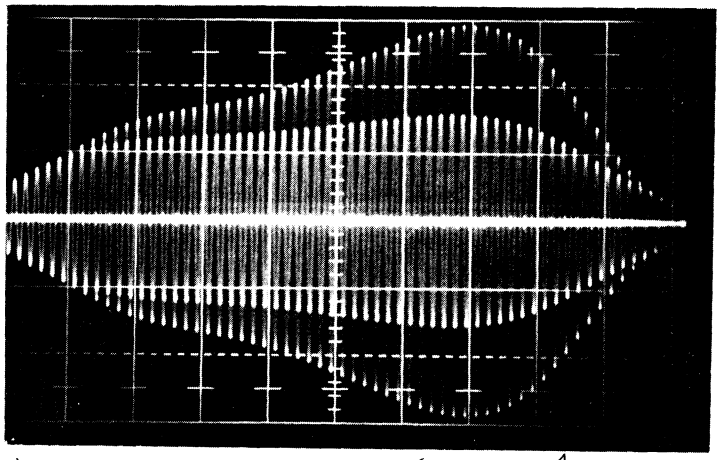

(a) Crystal resistivity = 6.21×10^4 ohm-cm.

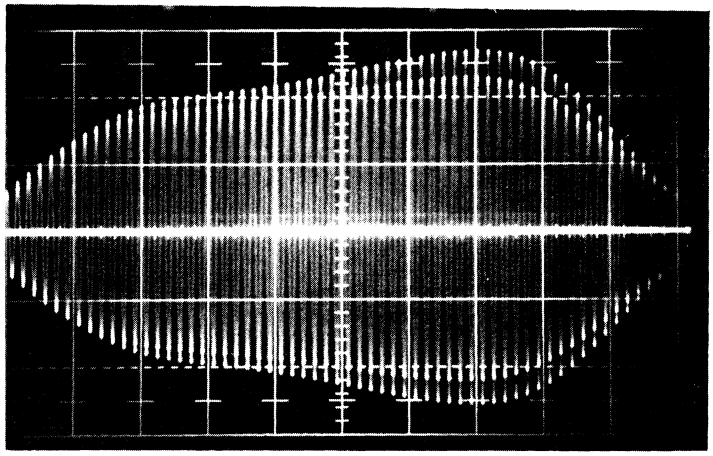

(b) Crystal resistivity = 1.80×10^5 ohm-cm.

Fig. 36. Comparison of output signals produced for input excitation levels of 0 and -20 db. In each case the larger amplitude output signal corresponds to the higher power input wave. On both photographs the output signals have been normalized with respect to the input wave, that is the vertical scale for the high power case is 10x that for the low power case.

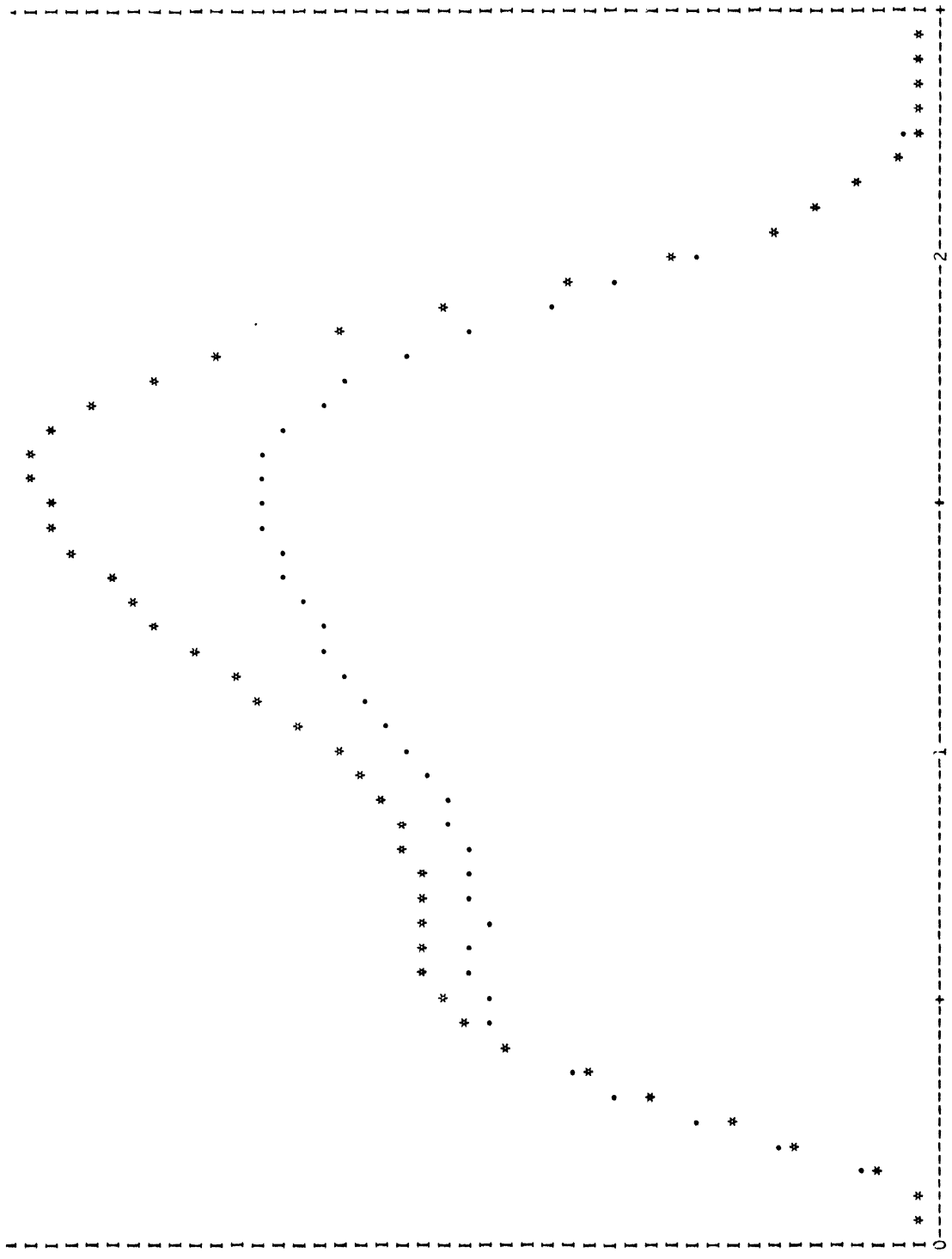

Fig. 37. Computer-calculated output signal produced for input excitation levels of 0 and -20 db. The vertical scale for the high power case is 10x that for the low power case. Crystal resistivity = 6.21 x 10^4 ohm-cm.

quantitative comparison. However, the very satisfying qualitative agreement obtained at high crystal resistivity ($\frac{1}{\omega\tau} < 1$) indicates that this self-interaction phenomenon must contribute heavily to the changed attenuation, distorted wave packet envelope, and altered acoustoelectric current trace which are experimentally observed under large-signal conditions.

APPENDIX

REDUCTION TO THE ONE-DIMENSIONAL PROBLEM

We shall sketch here the derivation of expressions for the electric fields which may accompany a propagating acoustic plane wave of any mode in a three-dimensional piezoelectric conducting medium. Our approach is basically that used by Hutson and White[5] when they re-derived with some corrections and simplifying assumptions the results of Kyame.[15,16] In his attack upon the problem Kyame derived the fifth-order secular determinant for the phase velocities of acousto-electromagnetic waves propagating in a conductive piezoelectric crystal. The solutions of this determinant correspond to two transverse electromagnetic waves traveling at nearly the speed of light in the medium and three acoustic waves traveling at approximately the speed of sound, where, depending upon the direction of propagation and the piezoelectric tensor, the acoustic waves could be accompanied by longitudinal electric fields which effectively modify the elastic constants of the medium. Kyame then showed that to a good approximation the secular determinant may be separated into a third-order acoustic wave determinant and a second-order electromagnetic wave determinant, with the two sub-determinants weakly coupled to each other through matrix elements of order $v/c\ e$; where v is the velocity of sound and c is the velocity of light in the crystal, and e is the appropriate component of the piezoelectric tensor. He thereby demonstrated that by ignoring the influence of the electromagnetic waves in his solution of the acoustic wave determinant, he was neglecting corrections to the acoustic phase velocity of order $v/c\ e$.

Our goal is less ambitious. We wish merely to show that of all possible polarizations of the electric field which may accompany a propagating acoustic wave, only the longitudinal component can be large enough to significantly influence acoustic attenuation. We shall derive this result under the same assumption used for the small-signal theory development of Chapter II, namely that the attenuation over one wavelength of the sound is so small, that for the purpose of computing local relationships among the components of the traveling wave we are justified in taking the propagation vector as being entirely real. The derivation then goes as follows:

Let x_1, x_2, and x_3 be orthogonal axes arbitrarily oriented with respect to the crystal axes and consider the propagation of plane waves in the x_1 direction. Under adiabatic conditions the piezoelectric equations of state for the medium are

$$T_{ij} = c_{ijkm}S_{km} - e_{kij}E_k \tag{A.1}$$

$$D_k = e_{kij}S_{ij} + \epsilon_{ik}E_i \ , \tag{A.2}$$

where repeated indicies indicate summation. Here

c_{ijkm} = short-circuit adiabatic elastic tensor

e_{kij} = adiabatic piezoelectric tensor

ϵ_{ik} = clamped adiabatic dielectric permitivity tensor

The constitutive equations for the medium are

$$B_i = \mu_o H_i \tag{A.3}$$

$$J_k = \sigma_{ik} E_i \tag{A.4}$$

The electromagnetic field quantities must also satisfy the Maxwell equations. The equations of particular interest to this derivation are

$$\{\text{curl } H\}_k = \frac{\partial D_k}{\partial t} + J_k \tag{A.5}$$

$$\{\text{curl } E\}_k = -\frac{\partial B_k}{\partial t} \quad . \tag{A.6}$$

We shall also define the piezoelectromotive field vector

$$\mathcal{E}_k = -\frac{e_{kij}}{\epsilon_{11}} S_{ij} \quad . \tag{A.7}$$

$\mathcal{E}_k$ approximates the kth component of the total piezoelectric driving field produced by all directions and polarizations of acoustic plane waves propagating in the medium (for k = 1 and i or j = 1 the relationship is exact). The second piezoelectric equation of state (Eq. (A.2)) may therefore be written as

$$D_k = -\epsilon_{11} \mathcal{E}_k + \epsilon_{ik} E_i \quad . \tag{A.8}$$

If we substitute Eqs. (A.4) and (A.8) into Eq. (A.5) we obtain

$$\{\text{curl } H\}_k = -\epsilon_{11} \frac{\partial \mathcal{E}_k}{\partial t} + \left(\epsilon_{ik} \frac{\partial}{\partial t} + \sigma_{ik}\right) E_i \quad . \tag{A.9}$$

We are interested only in the propagation of plane waves sinusoidal in the time. We may therefore everywhere replace $\partial/\partial t$ with $-i\omega$, with the result that

$$\{\text{curl } H\}_k = -i\omega \left(-\epsilon_{11} \mathcal{E}_k + \epsilon'_{ik} E_i\right) \quad . \tag{A.10}$$

where the relaxed dielectric permitivity tensor ϵ'_{ik} is defined by

$$\epsilon'_{ik} = \epsilon_{ik} + \frac{\sigma_{ik}}{-i\omega} \quad . \tag{A.11}$$

Equation (A.10) may be solved for two cases. For the first case we take k = 1; we are interested in the component along the propagation vector of the plane wave. The left side of Eq. (A.10) vanishes, leaving:

$$\epsilon'_{11}E_1 = \epsilon_{11}\mathcal{E}_1 - \epsilon'_{p1}E_p \quad , \tag{A.12}$$

where p = 2, 3 labels the two transverse modes of the electric field polarization. If we solve for E_1, the result is

$$E_1 = \frac{\epsilon_{11}\mathcal{E}_1 - \epsilon'_{p1}E_p}{\epsilon'_{11}} \quad . \tag{A.13}$$

For the second case we take k = p = 2, 3. The left side of Eq. (A.10) does not vanish. Following the usual program for the treatment of electromagnetic plane wave propagation we substitute Eq. (A.3) into Eq. (A.6) and take the curl:

$$\{\text{curl curl } E\}_p = \mu_o \frac{\partial}{\partial t} \{\text{curl } H\}_p \tag{A.14}$$

We then substitute Eq. (A.10) into Eq. (A.14):

$$\{\text{curl curl } E\}_p = \mu_o\omega^2(-\epsilon_{11}\mathcal{E}_p + \epsilon'_{ip}E_i) \quad . \tag{A.15}$$

Now

$$\{\text{curl curl } E\}_i = \{\text{grad}(\text{div } E)\}_i - \nabla^2 E_i \tag{A.16}$$

$$= \frac{\partial}{\partial x_i}\left(\frac{\partial E_j}{\partial x_j} + \frac{\partial E_k}{\partial x_k}\right) - \left(\frac{\partial^2 E_i}{\partial x_j^2} + \frac{\partial^2 E_j}{\partial x_k^2}\right). \tag{A.17}$$

For a plane wave propagating in the x_1 direction, only $\partial/\partial x_1$ gives a result different from zero. $\{\text{curl curl } E\}_p$ therefore collapses to

$$\{\text{curl curl } E\}_p = -\frac{\partial^2 E_p}{\partial x_1^2} = \left(\frac{\omega}{v}\right)^2 E_p \ , \tag{A.18}$$

where v is the phase velocity of the acoustic wave (in the x_1 direction). Thus Eq. (A.15) becomes

$$E_p = \mu_o v^2(-\epsilon_{11}\mathcal{E}_p + \epsilon'_{ip}E_i) \ . \tag{A.19}$$

This may be rewritten as

$$E_p = \left(\frac{v}{c}\right)^2 \left(-\mathcal{E}_p + \frac{\epsilon'_{ip}}{\epsilon_{11}} E_i\right) \ , \tag{A.20}$$

where

$$c = \frac{1}{\sqrt{\epsilon_{11}\mu_o}} \tag{A.21}$$

is the velocity of an electromagnetic wave propagating in the same direction as the acoustic plane wave.

If the electric fields E_k accompanying the wave are to produce observable acoustic attenuation, they must be nearly as large as the piezoelectromotive fields $\mathcal{E}_k$ which are generated in the <u>piezoelectrically active</u> modes of propagation. Although Eq. (A.20) is not truly a solution for E_p (it also appears on

the right as one component of E_i), it is clear that the magnitude of E_p is down by a factor of $(v/c)^2$ from values of the transverse piezoelectromotive field component ζ_p and the longitudinal electric field E_l. Thus it is apparent that the transverse electric fields are far too weak to produce observable acoustic attenuation.

By contrast Eq. (A.13) tells us that the longitudinal electric field component E_l is approximately equal to the longitudinal piezoelectromotive field component ζ_l. (We shall drop the insignificant transverse fields E_p from Eq. (A.13)). If the direction and mode of acoustic wave propagation are such as to generate a significant longitudinal piezoelectromotive field, then Eq. (A.13) may be written

$$E_l = \frac{\zeta_l}{1 + \frac{1}{-i\omega\tau}} , \tag{A.22}$$

where the dielectric relaxation time τ is defined by

$$\tau = \frac{\epsilon_{11}}{\sigma_{11}} . \tag{A.23}$$

Equation (A.22) may be compared with Eq. (2.59) of Chapter II. Thus we see that the three-dimensional problem is essentially reduced to a problem in one-dimension, that being along the propagation vector of the acoustic wave.

FOOTNOTES AND REFERENCES

1. G. Weinreich, Phys. Rev. 104, 321 (1956).

2. G. Weinreich and H. G. White, Phys. Rev. 106, 1104 (1957).

3. G. Weinreich, T. M. Sanders, and H. G. White, Phys. Rev. 114, 33 (1959).

4. A. R. Hutson, Phys. Rev. Letters 4, 505 (1960).

5. A. R. Hutson and D. L. White, J. Appl. Phys. 33, 40 (1962).

6. A. R. Hutson, J. H. McFee, and D. L. White, Phys. Rev. Letters 7, 237 (1961).

7. D. L. White, J. Appl. Phys. 33, 2547 (1962).

8. I. Uchida, T. Ishiguro, Y. Sasaki, and T. Suzuki, J. Phys. Soc. Japan 19, 674 (1964).

9. H. R. Carleton, H. Kroger, and E. W. Prohofsky, Proc. IEEE 53, 1452 (1965). This reference contains an extensive bibliography of recent work on acousto-electric ultrasonic amplification and current saturation.

10. R. W. Smith, Phys. Rev. Letters 9, 87 (1962).

11. A. R. Hutson, Phys. Rev. Letters 9, 296 (1962).

12. J. H. McFee, J. Appl. Phys. 35, 465 (1964).

13. V. E. Henrich, Ph.D. thesis, Univ. of Mich. (1967). This reference contains an extensive discussion of experimental technique with cadmium sulfide and the acoustoelectric effect.

14. G. Weinreich, Phys. Rev. 107, 317 (1957).

15. J. J. Kyame, J. Acoust. Soc. Am. 21, 159 (1949).

16. J. J. Kyame, J. Acoust. Soc. Am. 26, 990 (1954).

17. See for example W. P. Mason, Physical Acoustics and the Properties of Solids (D. van Nostrand Co., Inc., Princeton, New Jersey 1958), Appendix A.3.

18. Ibid., Appendix A.2.

19. D. Berlincourt, H. Jaffe, and L. R. Shiozawa, Phys. Rev. 129, 1009 (1963).

20. Our time convention is $e^{-i\omega t}$; hence the minus sign attached to i.

21. B. Tell, Phys. Rev. 136, A772 (1964).

22. E. W. Prohofsky, J. Appl. Phys. 37, 4729 (1966).

23. J.R.A. Beale, Phys. Rev. 135, A1761 (1964).

24. For use at an operating frequency of 30 Mc the transducers are actually cut for half-wave resonance at 29.2 Mc, this being the condition for maximum acoustic radiation when they are lightly loaded. For a further explanation see W. P. Mason, Physical Acoustics and the Properties of Solids, page 99.

25. This crystal was given to us by Dr. B. Tell.

26. R. W. Smith, Phys. Rev. 97, 1525 (1955).

27. A. M. Goodman, J. Appl. Phys. 35, 573 (1964).

28. F. A. Kroger, G. Diemer, and H. A. Klasens, Phys. Rev. 103, 279 (1956).